_____

INSTABILITY OF EXCITATION WAVES
INDUCED BY ELECTRICAL FIELDS

D i s s e r t a t i o n

zur Erlangung des akademischen Grades

doctor rerum naturalium

(Dr. rer. nat.)

genehmigt durch der Fakultät für Naturwissenschaften

der Otto-von-Guericke-Universität Magdeburg

von   M. Sc. (Phys. Chem.) Methasit Pornprompanya

geboren am 4 Februar 1972 in Bangkok, Thailand

Gutachter: Prof. Dr. Stefan C. Müller (Magdeburg)

Dr. Ing.   Hana Ševčíková (Prag)

Prof. Dr. Helmut Weiß (Magdeburg)

Eingereicht am   4 August 2004

Verteidigung am   28 Januar 2005

ZUSAMMENFASSUNG

Durch elektrische Felder induzierte Instabilitäten von Erregungsfronten

Chemische Wellen sind ein faszinierendes Phänomen, das in reagierenden Systemen auftreten kann, die sich weit entfernt vom Gleichgewicht entwickeln. Beispiele hierfür sind Pulswellen, die sich in sogenannten erregbaren Medien ausbreiten. In solchen Medien stehen die nichtlinearen Reaktionen lokal miteinander in Kontakt durch den Transport ihrer Reaktionen, z.B. durch Diffusion. Nach der Erregung werden diese Elemente unempfänglich für Reize, solange bis sie allmählich wieder in den erregbaren Zustand zurückkehren.

Belousov-Zhabotinsky Wellen (BZ Wellen) sind ein bekanntes Beispiel für Reaktions-Diffusionswellen, die in räumlich verteilten chemischen Systemen mit autokatalytischen Reaktionen auftreten können. Ebenso ist bekannt, dass die Einwirkung von elektrischen Feldern, durch die Elektromigration der ionischen Reaktionspartner sowohl die Wellenform als auch die Ausbreitungsgeschwindigkeit wesentlich beeinflussen kann. BZ-Wellen breiten sich schneller gegen einen Gradienten des elektrischen Potentials aus und langsamer in Richtung des Gradienten. Bei der Ausbreitung in einem Gradienten des elektrischen Potentials von überkritischer Größe treten bei BZ-Wellen Phänomene auf, die durch das globale elektrische Feld induziert werden. Darunter fallen (i) die Abspaltung neuer Wellen von der Rückseite der existierenden Welle, (ii) die Umkehrung der Richtung der Wellenausbreitung und (iii) Auslöschung von Wellen.

Das Malonsäure-Ferroin-Schwefelsäure-Bromat-System (oder das klassische BZ-System) ist das verbreitetste System für Untersuchungen der Effekte von elektrischen Feldern auf chemische Wellen und Musterbildung. Ein wichtiger Nachteil dieses Systems ist jedoch die Bildung von Kohlendioxid bei der Reaktion, was die Bildung von Blasen und damit eine Störung der Reaktionsdiffusionsmuster zur Folge hat. Dadurch ist es unmöglich, das System über eine längere Zeitdauer zu untersuchen. Daher lohnt es sich, Malonsäure durch ein anderes Substrat, nämlich 1,2,3-Trihydroxybenzol (Pyrogallol, PG), zu ersetzen und damit die Blasenbildung zu vermeiden. Außerdem gehört das System ohne Ferroin zur Klasse der unkatalysierten Bromatoszillatoren (UBO), die auch Schwingungen in gut durchmischten

Systemen und Wellenausbreitung in ungerührten Systemen aufweisen. Denn Pyrogallol ist neben seiner Funktion als Substrat auch - genau wie Ferroin - an der Erzeugung von $HBrO_2$ beteiligt. Durch Zugabe von Ferroin (oder eines Metallionen-Katalysators) zum Pyrogallolsystem wird eine interne Kopplung zwischen zwei Katalysatoren hergestellt, so dass neue dynamische Phänomene erwartet werden können, die verschieden von denen im klassischen, katalysierten BZ-System sind. Daher wurde in dieser Arbeit eine genaue experimentelle Untersuchung des Wellenverhaltens in diesem System unter dem Einfluss eines elektrischen Feldes durchgeführt, die helfen soll, den chemischen Mechanismus dieses komplizierten Systems besser zu verstehen. Damit wäre ein neues Reaktions-Diffusions-System verfügbar, das gut geeignet für Untersuchungen von chemischen Schwingungen und Wellen ist.

Die Versuche werden in einem Kapillarreaktor, der in einem Bad auf 15 ^{o}C thermostatisiert wird, durchgeführt. Der Reaktor ist mit einer Lösung gefüllt, die Schwefelsäure, Natriumbromat, Pyrogallol und Ferroin enthält. Die Ausbreitung der Pulswellen durch die Kuvette mit und ohne elektrisches Feld wurde durch Ausnutzung der unterschiedlichen Absorption des sichtbaren Lichts durch Ferroin (den reduzierten Reaktionspartner) und Ferriin (den oxidierten Reaktionspartner) verfolgt. Die Untersuchungen erfolgten durch einen optischen Glasfilter bei einer Wellenlänge von 490 nm und wurden durch eine CCD (Charge Coupled Device) Kamera mit einer Auflösung von ca. 27 μm/Pixel aufgenommen. Die aufgenommenen Bilder wurden durch eine Bildaufnahmekarte (Data Translation, DT 3155) verbunden mit der LabVIEW Bilderfassungssoftware digitalisiert und weiter verarbeitet. Die Analyse erfolgte mit in IDL (Interactive Data Language) geschriebenen Programmen.

Dies ist das erste Mal, dass über Untersuchungen zum Einfluss des elektrischen Feldes auf pseudo-eindimensionale Pulswellen im BZ-System mit Pyrogallol als Substrat und Ferroin als Katalysator berichtet wird. Die globalen Tendenzen der untersuchten elektrischen Feldeffekte, die für Beschleunigung, Verlangsamung, Auslöschung und Umkehr von Wellen verantwortlich sind, entsprechen denen, die bei der klassischen BZ-Reaktion mit Malonsäure als Substrat gefunden wurden. Ihr Auftreten hängt von der Intensität des Feldes und dem Verhältnis zwischen Pyrogallol und Ferroinkonzentration ab. Im Gegensatz zur klassischen BZ-Reaktion wurde hier jedoch eine Sättigung der Ausbreitungsgeschwindigkeit in Bezug auf die Stärke des elektrischen Feldes gefunden.

Die Wellen durchlaufen auch mehrfache Umkehrungen bei Umschaltung der Polarität des elektrischen Feldes. Während dieser mehrfachen Umkehrungen treten Asymmetrien auf: und zwar in (i) in den Ausbreitungsgeschwindigkeiten der umgekehrten Wellen, (ii) in den Ferroinkonzentrationen an der Front der umgekehrten Wellen kurz vor dem Umschalten der Polarität des elektrischen Feldes und (iii) an der Stelle, an der im Gebiet der ursprünglichen eine neue Welle entsteht. Die mehrfachen Umkehrungen treten in einem begrenzten Bereich der Steuerparameter auf und hängen von der Pyrogallolkonzentration ab.

SOUHRN

Nestabilita excitabilních vln indukovaná elektrickým polem.

Chemické vlny patří mezi fascinující jevy, které nastávají v některých reakčních systémech vzdálených od termodynamické rovnováhy. Příkladem jsou pulsní vlny šířící se v tzv. excitabilních prostředích. V takových prostředích jsou lokální nelineární reakční elementy vzájemně propojeny pomocí transportních procesů, např. difúzí. Po excitaci prochází tyto elementy refakterní fází, během níž obnovují své excitabilní vlastnosti.

Předložená práce se zabývá experimentálním studiem vlivů vloženého stejnosměrného elektrického pole na pseudo-jednorozměrné pulsní vlny šířící se podélně v tenké kapiláře naplněné Bělousov-Žabotinského (BŽ) reakční směsí obsahující pyrogalol jako substrát a ferroin jako katalyzátor. Některé pozorované vlivy elektrického pole, zejména zrychlení či zpomalení šíření vln, anihilace a obrácení pohybu vlny, jsou v souladu s efekty pozorovanými v klasické BŽ reakční směsi s kyselinou malonovou jako substrátem. Novým jevem, nezjištěným v klasickém BŽ systému, je tzv. saturační průběh závislosti rychlosti šíření vlny na intenzitě elektrického pole. Bylo také zjištěno, že intenzita elektrického pole, při níž lze dosáhnout obrácení směru pohybu vlny, je závislá na koncentraci pyrogalolu a feroinu.

Hlavním výsledkem předložené práce je zjištění, že přepínáním polarity vloženého elektrického pole opakovaně měnit směr pohybu vlny. Během opakovaného obracení směru pohybu vlny byla pozorována jistá asymetrie v následujících vlnových charakteristikách : (i) rychlosti šíření obrácených vln, (ii) koncentraci ferroinu v prostředí před obrácenou vlnou těsně před přepnutím polarity elektrického pole a (iii) ve vzdálenosti, v níž se zformuje obrácená vlna za vlnou původní. Opakované obracení směru pohybu vln se vyskytuje coby přechodový jev v omezeném rozsahu kontrolních parametrů, kterými jsou intenzita elektrického pole a interval přepínání jeho polarity. Rozsah kontrolních parametrů je závislý na koncentraci pyrogalolu.

ABSTRACT

Instability of Excitation Waves Induced by Electrical Fields

Chemical waves are a fascinating phenomenon that occurs in some reacting systems evolving far from thermodynamic equilibrium. Examples are pulse waves propagating in so-called excitable media. In such media the non-linear reactive elements are locally coupled with each other by transport processes, e.g. diffusion. These elements become refractory after excitation, slowly recovering to their receptive state, in which they can be excited again.

This work presents an experimental investigation of the effects of imposed dc electric fields on pseudo-one-dimensional pulse waves propagating in a thin capillary tube containing the Belousov–Zhabotinsky (BZ) system, with pyrogallol as substrate and ferroin as catalyst. The global tendencies of the investigated electric field effects, accounting for acceleration, deceleration, annihilation, and reversal of waves, correspond to those found in the classical BZ reaction with malonic acid as substrate. As a new result unlike the classical BZ system, a saturation-type relationship in the propagation velocity dependence on the electric field intensity has been found. The occurrence of wave reversal depends on the pyrogallol and ferroin concentrations.

The waves are also shown to undergo multiple reversals upon switching the polarity of an imposed dc electric field. During the multiple reversals an asymmetry arises in the following ways: (i) the propagation velocities of reversed waves, (ii) the ferroin concentrations in front of the reversed waves shortly before switching the electric field polarity, and (iii) the location at which a new wave emerges in the wake of the original one. Multiple reversals occur as a transient phenomenon in a limited range of control parameter values such as sizes of the medium and the electric field intensities and depend on the pyrogallol concentration.

TABLE OF CONTENTS

Publications

1 M. Pornprompanya, S.C. Müller, and H. Ševčíková

   Pulse waves under an electric field in the Belousov-Zhabotinsky reaction with pyrogallol as substrate

   Phys. Chem. Chem. Phys., **4** (2002), 3370-3375.

2 M. Pornprompanya, S.C. Müller, and H. Ševčíková

   Multiple reversals of pulse waves in an excitable medium resulting from switching the polarity of dc electric fields

   Chem. Phys. Lett., **375** (2003), 364-368.

Chapter 1

Introduction and Objective of Research

Propagating waves of chemical or biological activity [Eps98, Fie85, Mur89, Wal00] are typical examples of spontaneous pattern formation in macroscopic systems driven far from thermodynamic equilibrium [Bab86, Cro93]. They may show complex dynamics in time or both in time and in space, and they are sustained by the interplay of non-linear, self-accelerating reaction kinetics (autocatalysis), and local spatial coupling due to diffusion. Chemical reactions occurring at a particular point cause the concentrations of chemicals there to change, becoming higher or lower than they are at points nearby. At the same time, random thermal motion of molecules tends to degrade these differences by the process of diffusion. In essence, reactions build differences up, while diffusion washes them out. Waves and patterns then emerge when non-linear chemical reactions and diffusion are out of balance. Examples found in chemical systems are propagating concentration waves of intermediates in the Belousov-Zhabotinsky (BZ) reaction [Eps98, Fie85, Mur89, Pót98, Vid86] and in the catalytic oxidation of CO on single Pt crystal surfaces under high vacuum conditions [Eng96, Kap95], shrinking and expanding spots, and lamellar patterns observed in the Ferrocyanide-Iodate-Sulphite (FIS) reaction [Lee94]. Other examples in biological systems [Mur89, Wal00] are waves of electrical activity in the heart muscle and the central nervous system [Pan97], as well as waves of the signal transmitter cyclic adenosine monophosphate (cAMP) in the aggregation phase of cell colonies in the slime mold, *Dictyostelium discoideum*. Recent reviews can be found in references [Mai97, Sag03].

For decades, the BZ reaction has been widely used as an experimental system to study oscillations, waves, and patterns. In general, the BZ reaction involves the oxidation of an organic substrate by bromate under the action of a catalyst (a metal-ion of redox potential between 1.0 and 1.6 V, e.g. Ce^{3+}, Mn^{2+}, $Fe(phen)_3^{2+}$ (or ferroin), and $Ru(bipy)_3^{2+}$) in an acidified aqueous medium. The intermediate $HBrO_2$ (bromous acid) is the autocatalytic species which determines the propagation velocity of the wave according to its rate of production and its diffusivity. The recovery process in the wake of the wave front is

controlled by a reactive decrease in the bromide ion concentration, which brings the system from the oxidized or excited (i.e. refractory) state back to the reduced (i.e. excitable) state of the catalyst. In the most studied, „classical" version of the BZ reaction, malonic acid (MA) is used as a substrate. In this system, long term observations of spatial patterns and propagating waves are often damaged by CO_2 bubbles arising as a product of the oxidation of malonic acid.

Over the years, a variety of new substrates (mostly phenol or aniline based compounds [Orb78]) have been introduced to replace MA and to create a bubble-free medium. Although many substrate-analogues of the classical BZ system are known, only a few of them have been so far utilised for studies on propagating waves [Ada02, Orb80]. A system containing 1,4-cyclohexanedione (1,4-CHD) as a substrate and ferroin as a catalyst was found to exhibit interesting non-linear phenomena that account for wave stacking and merging [Ham01], which was not observed in the classical BZ system. This indicates that the investigation of wave propagation in BZ systems containing new kinds of organic substrates can reveal new dynamical phenomena not observed previously in the classical BZ system.

The variety of non-linear chemical wave phenomena largely increases when propagating waves are exposed to external forces like gravity, light, and a magnetic field or an electric field [Eps98 and references therein, Eva04, Wal00]. Under increasing gravity, the propagation velocity of the wave in 1,4-CHD system is increased by the effect of convection [Fuj01]. Furthermore, the photosensitivity of 1,4-CHD system is stronger than the $Ru(bipy)_3^{2+}$-catalyzed classical BZ system [Kur97]. In the classical BZ system, the waves under an external electric field are known to speed up when moving towards the positive electrode (in a negative field) and to slow down when moving towards the negative electrode (in a positive field). The positive field of an increasing magnitude evokes i) splitting of new waves in the wake of the existing one, ii) reversal of the direction of the wave propagation, iii) annihilation of waves. These phenomena were observed with planar waves propagating in narrow capillaries and with circular waves subjected to unidirectional dc electric fields both in liquid and gelled media [Fee81, Šev83, Šev84, Šev92, Šev96a, Šev96b, Šev99]. Spiral waves were found to drift in the electric field [Ste92] and to become distorted with respect to their original Archimedean shape [Bel95]. Under sufficiently high electric field strength, spiral pairs annihilate mutually to form target patterns [Sch92]. By using an alternating electric field of characteristic frequency and amplitude, the shape of the spiral waves becomes asymmetric

resulting in the appearance of the spiral wave of larger wavelength than the original wave (super-spirals) [Pér93], the spiral waves can be destroyed (so-called spiral break up) [Tab94], or the wave front can display fluctuating wrinkles [Sei01].

In this thesis effects of an applied dc electric field on the propagation of waves are investigated in a spatially quasi-one-dimensional BZ system containing 1,2,3-trihydroxybenzene (pyrogallol, PG) as a substrate and ferroin as a catalyst [Orb98, Sri98a] Without ferroin, this system belongs to the class of uncatalyzed bromate oscillators (UBO) that perform oscillations in well stirred systems [Orb78, Sri98b] and support propagation of waves in non-stirred media [Ada04, Orb80]. In UBO systems, an organic intermediate of a quinone structure takes the role of the metal catalyst by both promoting the autocatalysis of $HBrO_2$ [Orb79] and being recovered together with the bromide by the reaction with HOBr after the autocatalysis is terminated [Liu92a]. When a metal-ion redox catalyst is added, UBO systems become internally coupled with the classical BZ system (via oxybromine intermediates [Dut02, Gil92]), which leads to significant changes in the number and the form of oscillations in batch systems [Kör80, Tla83, Tla84]. Experimental and numerical studies of an open CSTR (Continuously Stirred Tank Reactor) pyrogallol system with ferroin [Gil92] have shown new oscillatory waveforms resulting from the internal chemical coupling. The goal of the presented thesis is to investigate whether the increased complexity of the pyrogallol system with ferroin (compared to the classical BZ system) can give rise to novel dynamical phenomena, when the propagating waves are exposed to an electric field. We expect that the application of an electric field on the waves in this system can help us to better understand the role of two catalysts (PG and ferroin) in the chemical mechanisms.

The thesis is organized as follows. Chapter 2 describes briefly literature overview on basic concepts of pattern formation in reaction-diffusion systems including the nature of chemical waves, wave reflection in excitable media, and the theory of chemical wave-electric field interactions. A review on the classical BZ system, electric field effects, and chemical mechanisms of the uncatalyzed BZ reaction mainly focused on the system with pyrogallol as substrate is also given. Chapters 3 and 4 present experimental methods and results, respectively. Attempts to explain the observed phenomena are given in the discussion part of chapter 5. Finally, the thesis is closed with chapter 6 presenting conclusions and perspectives.

The highlight of this work is the observation of multiple wave reversals being similar to wave reflection. Reflections of waves in a general reaction-diffusion system are rare due to the refractory period, i.e. the time needed to recover from an excitation, which inhibits such occurrences, i.e. excitable elements cannot be excited again within this period. The reflections occur at the interface between two excitable regions and they are numerically simulated and analysed elsewhere [Ei02, Pet94]. In their study, the propagating pulse wave slows down when approaching the "no flux" boundary and then reverses its direction of propagation. In contrast, we experimentally observed here such phenomena in the excitable BZ system with pyrogallol as substrate by means of external forcing with an applied electric field. The excitation pulse in this system actually disappears before the development of a new pulse at the tail of a parent pulse propagating to the opposite direction when approaching to the "mass-flux" boundary where the polarity of electric fields is reversed, and this process can be repeated many times.

Chapter 2

Backgrounds of Research

2.1 Basic concepts of pattern formation in reaction-diffusion systems

2.1.1 The nature of chemical waves

Chemical waves are changes in macroscopic variables (concentrations, temperature, pressure, voltage, etc.) which can propagate over long distances without attenuation. This distinguishes them from the evolution of a diffusion profile which gradually changes and loses its structure. Chemical waves involve the interaction of diffusion and some chemical reactions. Apparently, the chemical kinetic processes keep the wave profile from becoming increasingly smooth due to diffusion. These kinetic processes, which are effective in wave propagation and pattern formation, must be non-linear in the descriptive variables. In other words, they need to possess a feedback mechanism. Autocatalysis is the most common type of feedback mechanism. Generic representations of autocatalytic processes can be written in the form:

quadratic autocatalysis: $\quad\quad$ A + B $\rightarrow$ 2B $\quad\quad$ rate = $k_q$ab $\quad\quad$ or

cubic autocatalysis: $\quad\quad$ A + 2B $\rightarrow$ 3B $\quad\quad$ rate = $k_c$ab^2

where a and b are the concentrations of the reactant A and the autocatalyst B. k_q and k_c are the respective rate constants. The macroscopic description of reaction-diffusion systems is usually based on a pair of partial differential equations given by

$$\frac{\partial u}{\partial t} = e^{-1} f(u,v) + D_u \nabla^2 u$$

$$\frac{\partial v}{\partial t} = g(u,v) + D_v \nabla^2 v,$$

$$(1)$$

where u and v denote the concentrations of the activator (autocatalyst or propagator variable) and of the inhibitor (controller or recovery variable) as a function of time t and spatial coordinates, respectively. The first terms f(u,v) and g(u,v) describe non-linear reactions and the second terms arise from Fick 's 2nd law of diffusion, where ∇^2 (or also written as Δ) is

the Laplacian operator in one, two or three spatial dimensions, D_u and D_v are diffusion coefficients of the species u and v, respectively. ε is a parameter that is proportional to the ratio of the diffusion rate to the chemical reaction rate. These equations govern the dynamics of chemical wave propagation. If $D_u \geq D_v$ (or long-range activator), the system supports propagating waves. In contrast, stationary spatial patterns are found in systems with $D_u \ll D_v$ (or long-range inhibitor), e.g. Turing patterns found in the CIMA (Chlorite-Iodide-Malonic Acid) reaction [Kap95, Pót98, Sch03].

(1.1)
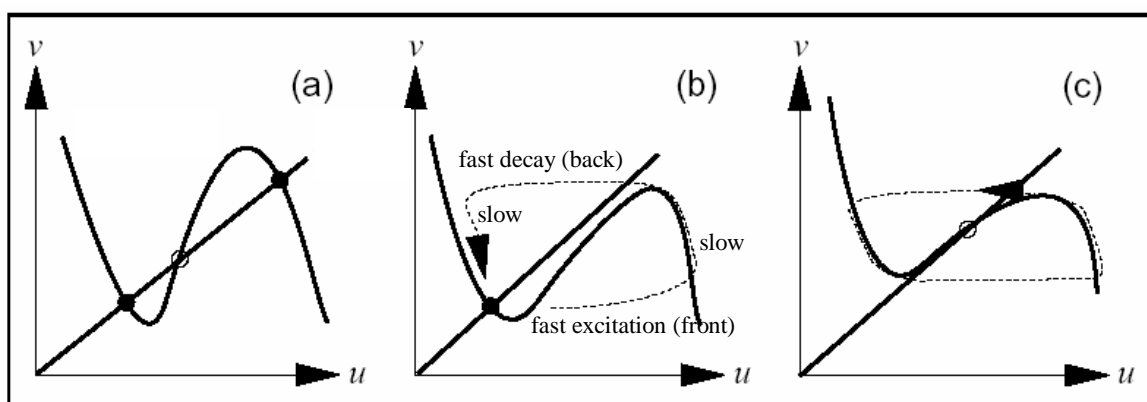
(1.2)
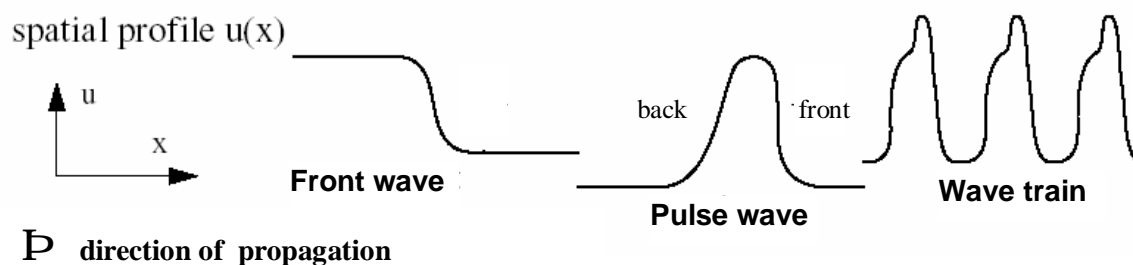
Figure 1: Three kinds of active media.

(1.1) Schematic drawings of u-v phase planes with (a) bistable, (b) excitable, and (c) oscillatory dynamics. Solid lines denote the nullclines, full (open) circles denote stable (unstable) fixed points. The dotted line illustrates in (b) a typical excitable trajectory and in (c) the limit cycle.

(1.2) Drawings showing typical spatial profiles of u in one spatial dimension (x) for each respective kind of active media: front wave-bistable media, pulse wave-excitable media, and periodic wave train-oscillatory media.

For such a two-component activator-inhibitor system, it is possible to elucidate general features of pattern-forming active media. There are two curves in a u-v phase plane called nullclines: $f(u,v) = 0$, f (or u)-nullcline having a characteristic S-shape and $g(u,v) = 0$, g (or v)-nullcline increasing (or sometimes decreasing) monotonically. The intersections of nullclines determine the stationary states of the system [Bab86, Eps98]. Active media [Cro93, Eps98] can be mainly classified as bistable, excitable, or oscillatory. Wave profile and wave velocity in a spatially extended system are uniquely determined by the properties of the active medium. In Fig. 1 the nullclines of typical bistable, excitable, and oscillatory media in the FitzHugh-Nagumo model [Cro93, Mur89] are shown.

The nullclines of a typical bistable system (Fig. 1.1a) intersect three times, giving rise to two stable and one unstable fixed points. In the spatially extended system, the typical pattern of a bistable medium is a front, i.e. an interface that separates two domains where the system resides in the two different stationary states which are stable to sufficiently small perturbations. Stronger perturbations can cause transitions between these two states.

The local dynamics of an excitable medium (Fig. 1.1b) is characterized by a stable fixed point [Mer92]. The fixed point is located at the left part of the f-nullcline. Small perturbations of that state decay immediately, while perturbations which overcome a certain threshold (the middle branch of the f-nullcline) increase and decay only after the system has performed a large loop in phase space. In this case, the system first goes to the right branch of the f-nullcline (u quickly increases corresponding to an excitation), then moves along this branch and drops for large v from large to small values of u. Then it relaxes slowly to the fixed point on the left branch of the f-nullcline via a state from which new excitations cannot be performed, even when large perturbations are applied, i.e. refractory state. In the spatially extended system such a medium supports propagation of pulses. More complex patterns such as rotating spiral waves in two spatial dimensions and scroll waves (a two-dimensional surface that rotates around a one-dimensional axis called the wave filament) [Pan97, Win74] in three spatial dimensions are possible [Win84].

Oscillatory media are characterized by a closed trajectory in phase space. In Fig. 1.1c, an unstable fixed point surrounded by a limit cycle is present. In a spatially extended medium governed by such relaxation oscillations, periodic wave trains are observed. The typical possible regular patterns in oscillatory systems are spiral waves and target patterns (expanding concentric circular waves).

2.1.2 Wave reflection in excitable media

In an excitable medium, e.g. the BZ medium, where we have separated time scales with fast activator ($\varepsilon \ll 1$, see Eqs. 1) and slow inhibitor, there is a pulse-like wave having large spatial gradients at the front and the back. The wave front is followed by a zone of excitation which is terminated by the wave back. Within the wave back, the medium is at first refractory to the propagation of another wave of excitation, but it gradually recovers excitability as it relaxes to the rest state that it can be excited again. Therefore, when two waves meet upon head-on collision, they do not reflect from each other but they do annihilate. Wave front travels into the refractory region of the other wave, where this region cannot respond to any perturbations. Hence, the propagating waves can no longer be sustained, and thus they vanish. For the same reason, they are absorbed by impermeable barriers. With this property of annihilation of chemical waves [Woo85] in active-dissipative media being due to a subtle interplay of activating and inhibiting components that may distribute in space because of diffusion and change in time, these waves differ markedly from acoustic waves, electromagnetic waves, and solitons which form in conservative (i.e. constant or not changing) media.
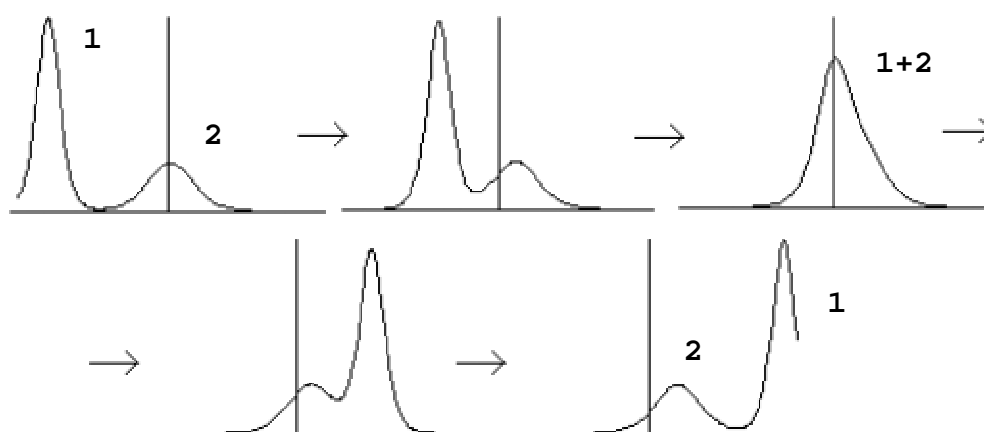
Figure 2: Solitons or stable solitary waves behave like "particles".

Solitons [Dra89, Fil00] or solitary waves are particle-like nonlinear waves, e.g. waves formed on the surface of water. In Fig. 2, there are two waves (1 and 2) located initially far apart, each of them traveling with a constant shape and propagation velocity. As two such solitary waves get closer, they gradually deform and finally merge into a single wave packet (1+2); this wave packet, however, soon splits into two solitary waves with the same shapes and velocities as they were before the "collision". The concept of a soliton has been applied to a vast and diverse range of situations, from the d.c. gas-discharge system [Bod02, Eng96] to muscle contraction [Asl99 and references therein] in animals and humans.

However recent investigations report on various cases about reflection of chemical waves [Ei02, Kos95, Mid93, Oer98, Pet94, Zha93a]. During the CO oxidation on Pt catalyst with surface defects (see Fig. 3.1) two oxygen waves were observed to pass through each other, as if they were solitons [Kap95, Oer98]. In experiments, reflection of a Belousov-Zhabotinsky (BZ) wave was found to occur at the boundary between two media with a stepwise changing thickness [Zha93a] as shown in Fig. 3.2.

Pulses travelling through chemically reacting excitable media can undergo wave splitting and reflection. In the former, the pulse proceeding in the forward direction sends out a pulse in the reverse direction, resulting in two pulses travelling in opposite directions. In the latter, the pulse, upon reaching the boundary of the reacting region, reverses its propagation direction, resulting in a single pulse travelling in the opposite direction. In a reaction-diffusion model of an excitable medium with a cubic autocatalytic reaction one wave was observed to be reflected between no-flux boundaries like an elastic object, when the diffusivity of the reactant was significantly higher than that of the autocatalyst [Pet94]. For even higher diffusivity of the reactant, the waves were formed to subject repeatedly to splitting. The interaction between split waves led finally to the formation of stationary spatial patterns [Pet94].

(3.1)
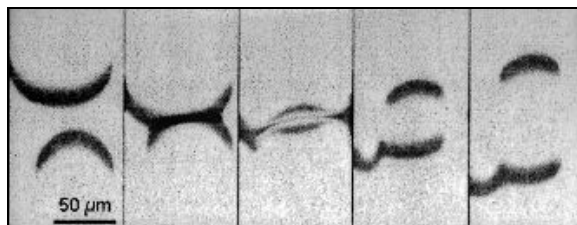
(3.2)
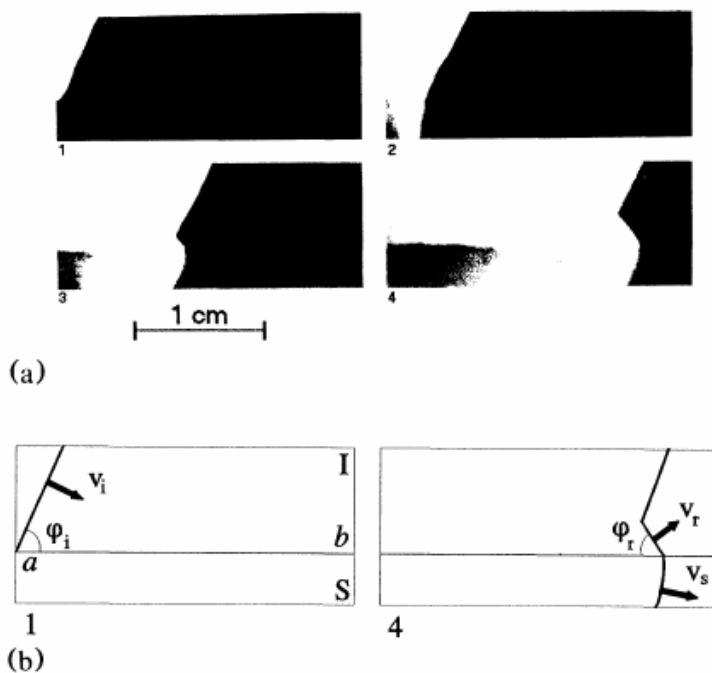
Figure 3 : Two examples of the reflection of chemical waves.

(3.1) In the CO oxidation reaction on Pt (110) (adapted from [Oer98]): Simulation of a reflective collision of two oxygen waves (black crescent waves) in the two-into-two type. Time interval between two frames is 4 s. Negative images.

(3.2) In the ferroin-catalyzed BZ-reaction (from [Zha93a]): (a) Polyacrylamide gel layer opened to air with stepwise thickness; time intervals between frames 1 and 2, 2 and 3, 3 and 4 are 75 s, 130 s, and 200 s, respectively. (b) Schematic of frames 1 and 4. ab: boundary between regions I (0.45 mm) and S (0.75 mm); v_i, v_s, and v_r are wave vectors of the incident, secondary circular, and reflected waves; $\varphi_i = 67.4^\circ \pm 3^\circ$ and $\varphi_r = 54.0^\circ \pm 2^\circ$ are angles of incidence and reflection.

The numerical simulations of the counter propagating reduction waves (i.e. a zone of a reduced catalyst (ferroin), propagating through an oxidized medium having high ferriin concentration) in the spatially one-dimensional BZ reaction [Kos95, see also Kaš95] have revealed that two waves do not annihilate but emerge after the collision with the size and shape unchanged as if they were solitons. One wave was found to reflect at zero-flux surfaces (echo waves). Back and forth movement of a temperature wave has been numerically simulated also in a model of an electrically heated catalytic ribbon [Mid93] and two waves in a model system with exothermic reaction have been theoretically found to repel one another when their velocities were very low [Ei02]. The reversal of the wave motion was experimentally observed in a homogeneous excitable BZ medium with MA as substrate [Šev92], when a perturbation in the form of a d.c. electric field was applied to the system, which we will see again in Section 2.3.4.

The following paragraphs describe in more detail some recent theoretical and numerical considerations of the reflection of chemical waves in reaction-diffusion systems.

Petrov et al. [Pet94] investigated the cubic autocatalator model in a reaction-diffusion configuration of a Continuously Fed Unstirred Reactor (CFUR),

(1) $A + 2B \rightarrow 3B$ rate = $k_1 ab^2$

(2) $B \rightarrow C$ rate = $k_2 b$.

The governing reaction-diffusion equations have the form:

$$\frac{\partial a}{\partial t} - d\nabla^2 a = g(a,b) = \frac{1-a}{t_{res}} - ab^2$$
$$\frac{\partial b}{\partial t} - \nabla^2 b = f(a,b) = \frac{b_0 - b}{t_{res}} + ab^2 - gb,$$

(2)

where α and β represent dimensionless concentrations of the reactant A and the autocatalyst B, respectively. τ and τ_{res} are dimensionless time and the residence time (the ratio of the reactor volume and the total flow rate). δ is the ratio of the diffusion coefficients, D_A/ D_B. $\beta_0 = b_0/a_0$ and $\gamma = k_2/(k_1 a_0^2)$ where a_0 and b_0 are initial concentrations of A and B. Two nullclines of the system along which $f(\alpha,\beta) = g(\alpha,\beta) = 0$ for $\tau_{res} = 315$ are shown in Fig. 4. The stable fixed point (right) and the saddle point (left) where both nullclines intersect each other, lie close to each other in the α-β phase plane.
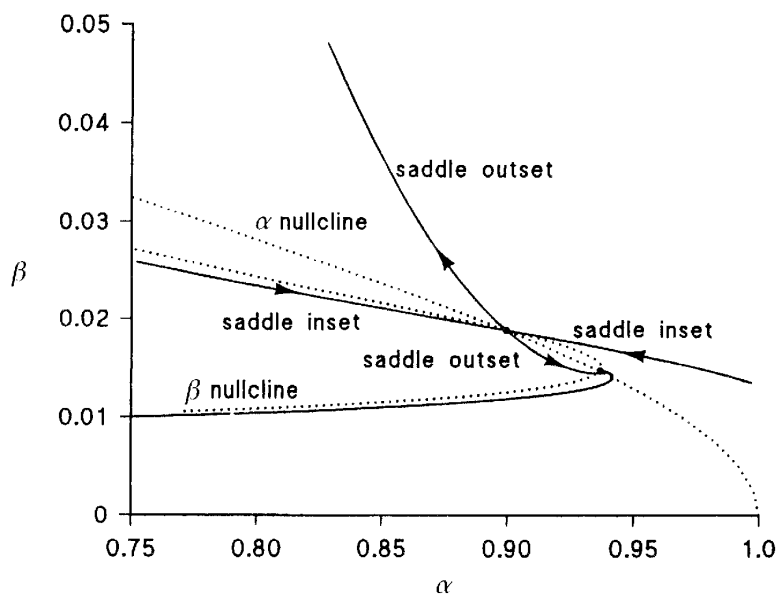
Figure 4: α-β phase plane for τ_{res} = 315 (from [Pet94]). Solid curves show inset and outset of saddle point. Dotted curves show both nullclines.

In one dimensional finite space region at the end-points of the interval for appropriate parameter values (τ_{res} = 315, β_0 = 1/15, γ = 1/40, and δ = 7) they obtained waves that started from the vicinity of one endpoint, migrated to the vicinity of the other, gradually decreased their velocity to zero and, taking an oppositely directed velocity, returned to their starting position. After this the waves moved forward again and the whole process was repeated periodically as shown in Fig. 5.1. These bouncing waves can be explained relatively easily. A spatial B-impulse will propagate through the interval investigated decreasing the concentration of A behind and in front of its instantaneous position. The inflow of A at the appropriate end-point of the interval cannot compensate the amount diffused into and consumed in the reaction front, therefore, the concentration of A will decrease in front of the wave front, the wave slows down and eventually stops (see Fig. 5.2). By this time, however, a sufficiently great amount of A will be accumulated by diffusion at the back of the standing wave front, and B starts to react with A in this direction, its production predominates its spontaneous decay. In the development of a bouncing wave the ratio of diffusion coefficients (δ) plays an important role, it must be sufficiently high. Wave splitting occurs at δ = 17.

(5.1)
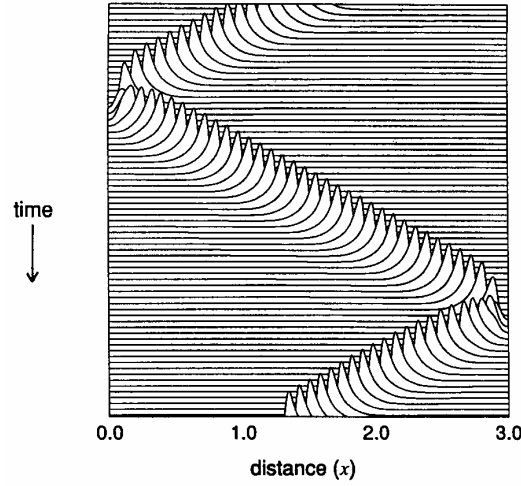
(5.2)
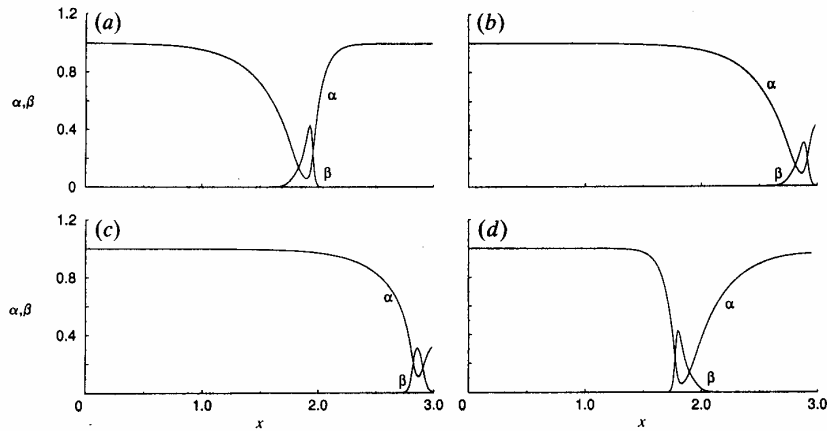
Figure 5 : Results from numerical calculations of the reflection of a chemical wave at no-flux boundaries (i.e.

$$\frac{\partial a}{\partial x} = \frac{\partial b}{\partial x} = 0 \quad \text{for } x = 0.0 \text{ and } x = 3.0) \text{ in cubic autocatalator model (from [Pet94])}.$$

(5.1) Space-time plot showing profiles of B with $\delta = 7$ and $D_B = 1.0 \times 10^{-5}$ cm^2/s. Each profile corresponds to an increment of 100 dimensionless time units.

(5.2) Profiles of A (or α) and B (or β) in wave reflected at boundary. (a) Wave propagating from left to right; (b) level of B is depleted between wave front and boundary; (c) profile of B becomes approximately symmetrical as propagation velocity reaches zero; (d) wave propagating from right to left.

Ei et al. [Ei02] considered the following two-component excitable reaction-diffusion system:

$$\frac{\partial u}{\partial t} - \Delta u = \frac{1}{e} f(u,v) = \frac{1}{e}(-au + vk(u))$$

$$\frac{\partial v}{\partial t} - d\Delta v = g(u,v) = h(v^* - v) - vk(u), \tag{3}$$

where d is the ratio of the diffusion rates of u and v, ε the time constant between the dynamics of u and v. a, h, and v^* are some positive constants. $k(u) = \exp[u/(1+(u/c))]$ with positive constant c, describes the exothermic reaction step, where u is the temperature and v the concentration of chemical reactant. The nullclines of the system are shown in Fig. 6a. They numerically showed that one-dimensional travelling pulses propagating very slowly, can repel one another when d is high enough, as shown in Fig. 6b. They also observed the same phenomenon as shown in Fig. 5.1 and they called it "rebounding".

(a)
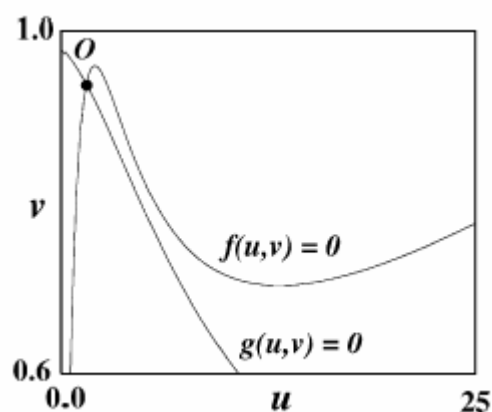
(b)
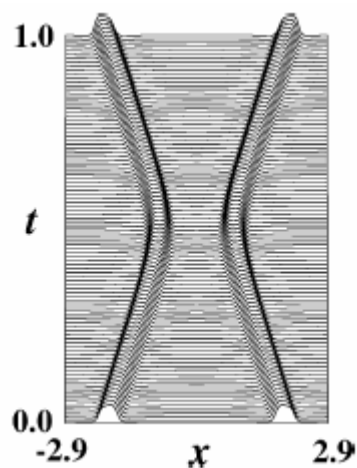
Figure 6 : Results from numerical simulations of the repulsion or reflection of two closely approaching pulses (from [Ei02]).

(a) Nullclines of f(u,v) and g(u,v) in Eqs. (3) where $\varepsilon = 0.001$, a = 2.0, c = 5.0, h = 45.0, and $v^* = 1.0$. O is a stable point.

(b) Time (t)-space (x) plot showing the repulsion of two travelling pulses where the parameters are the same as Fig. 6a with d = 4.5.

2.2 Theory of chemical wave-electric field interactions: Summary

The origin of spontaneous oscillations and spatial structures depends on the coupling between transport and transformation processes. In chemical systems, transformation processes are represented by chemical reactions which are time dependent. Transport processes are associated with change in location. Therefore coupling between the two might result in periodic oscillations in space and time. Turing [Tur52] was the first to show that coupling between autocatalytic chemical reaction and diffusion can result in oscillations and pattern formation, and this has been proposed as a key event in the evolution of biological structures. Diffusion was considered there as the only transport process. The character is broadened here in order to include electrical migration effects.

Let us consider a homogeneous system of N chemical active species, i = 1, 2, 3,…, N. All the components may diffuse, and since some of them are ionic, they may migrate under the influence of an applied electric field. We ignore any convection by assuming a stagnant solution. At every location, the chemical species obey the conservation equation [Has97, Jor74, Ort92] for the ith component:

$$\frac{\partial C_i}{\partial t} = R_i - \nabla J_i = R_i - \nabla (J_{D,i} + J_{M,i}) \,, \tag{4}$$

where C_i is the concentration of the ith species as a function of spatial coordinates and time t, R_i is the net rate of the ith species production by chemical reaction as a function of C_i and rate constants. J_i is the total flux density [§] defined by the Nernst-Planck equation [Old94]. $J_{D,i}$ is the flux density by diffusion given by Fick's 1st law:

$$J_{D,i} = -D_i \nabla C_i \,, \tag{5}$$

where D_i is the diffusivity, and $J_{M,i}$ is the flux density by electrical migration:

$$J_{M,i} = -m_i C_i \nabla U \,, \tag{6}$$

[§] The flux density or simply "flux" is a measure of the number of moles n_i of a solute species ith crossing unit area A of a specified surface in unit time, i.e. $J_i = (1/A)(dn_i/dt)$.

where U is the electrical potential and μ_i is the mobility of the ion defined by the Nernst-Einstein relation [Kuh00, Old94]:

$$m_i = \frac{|z_i|FD_i}{RT} = \frac{s_i}{E}.$$ (7)

z_i is the number of electrical charge of the ion, F is the Faraday constant, s_i is the ionic drift velocity, R is the gas constant, and T is the absolute temperature.

The electric field E can be written as a gradient of electric potential U:

$$E = -\nabla U.$$ (8)

Gauss's law of electrostatics [Ger00]: $\nabla E = j / e$, determines the medium with a dielectric constant ε and charge density j [Old94] defined as,

$$j = F \sum_{i=1}^{N} z_i C_i.$$ (9)

For processes taking place on time scales greater than a millisecond, Eq. 8 reduces to the Poisson equation (a combination of Eq. 8 and Gauss's law of electrostatics) for the voltage U, that is

$$\nabla^2 U = -\frac{j}{e} = -\nabla E.$$ (10)

For a medium containing an excess of supporting electrolyte we can assume that an applied electric field intensity E is constant, i.e. $\nabla E = 0$ [Ort92], and thus after combining Eq. 4 with Eqs. 5, 6, 8, and 10, Eq. 4 finally becomes

$$\frac{\partial C_i}{\partial t} = R_i + D_i \nabla^2 C_i + m_i (\nabla U \nabla C_i + C_i \nabla^2 U) = R_i + D_i \nabla^2 C_i - m_i E \nabla C_i.$$ (11)

An excitable activator-inhibitor reaction-diffusion system in one spatial dimension, for example, a planar chemical wave propagating parallel to an electric field, we have

$$\frac{\partial u}{\partial t} = f(u,v) + D_u \frac{\partial^2 u}{\partial x^2} - m_u E \frac{\partial u}{\partial x}$$

$$\frac{\partial v}{\partial t} = g(u,v) + D_v \frac{\partial^2 v}{\partial x^2} - m_v E \frac{\partial v}{\partial x} \quad ,$$

(12)

where D_u, D_v, and μ_u, μ_v are the diffusion coefficients and the electrical mobilities of the activator u, the inhibitor v, respectively. E is a constant electric field strength. We introduce a new spatial variable ξ into Eqs. 12 and use a cycle rule to rewrite again those equations. These are

$$\xi = x - v_E t \quad \text{and} \quad \frac{\partial u}{\partial t} = \frac{\partial u}{\partial x}(\frac{\partial x}{\partial t}) = \frac{\partial u}{\partial x}(-v_E) .$$

(13)

v_E is the wave velocity with an imposed electric field E. Finally, we obtain

$$f(u,v) + D_u \frac{\partial^2 u}{\partial x^2} + (v_E - m_u E)\frac{\partial u}{\partial x} = 0$$

$$g(u,v) + D_v \frac{\partial^2 v}{\partial x^2} + (v_E - m_v E)\frac{\partial v}{\partial x} = 0 .$$

(14)

For small magnitudes of electric field intensities $\mu_v = \mu_u = \mu$ and $v_E = v_0 + \mu E$ [Góm97, Sch79, Vié96] where v_0 is the field-free wave velocity.

The most extensively studied chemical wave medium, the BZ system, involves ionic species. The propagation of chemical signals is due to the interrelationships among the composition profiles of the participating species, and these can be dramatically affected by electric fields [Fee81, Sch81, Sch83]. Composition gradients involving ionic species may lead to local departures from charge neutrality (i.e. the charge conservation law in the course of chemical reactions: $\Sigma z_i R_i = 0$). Strong electrical forces try to minimize this charge neutrality; hence ionic migration is strongly correlated by the resulting so-called Planck fields driven by the ionic composition gradients [Ort92]. Such fields can tend to force reactants together or keep them apart, depending on ionic charges and diffusion coefficients, and hence can alter dramatically the nature of wave propagation. Since background electrolytes screen these

fields, it is quite conceivable that as ionic strength is varied [Šni98], qualitatively new phenomena could arise due to wave-electric field interactions.

In the context of the wave propagation the Planck field E_{Planck} [Ort92] is given by

$$E_{Planck} = \frac{F \sum_{i=1}^{N} |z_i| D_i \nabla C_i}{k} \quad ,$$ (15)

where κ is the electrical conductivity. It has two interesting implications:

a) A Planck field propagates along with an electrochemical wave; this field increases with ionic concentration gradients ∇C_i.

b) Planck field and through current effects are strongest in systems with small conductivity κ defined [Kuh00, Old94] by

$$k = F \sum_{i=1}^{N} |z_i| C_i m_i .$$ (16)

Electrical forces are strong and hence even small local deviations from charge neutrality lead to appreciable fields. These fields are always such as to import ions that tend to neutralize the local charge. Charge neutrality is well maintained in most experimental situations involving a BZ medium having high conductivity or ionic strength Γ given by

$$\Gamma = \frac{1}{2} \sum_{i=1}^{N} z_i^2 C_i .$$ (17)

Ortoleva et al. showed theoretically that the response of chemical waves to the through current I depends strongly on the reaction mechanism [Sch77, Sch79, Ort92]. A most interesting set of phenomena are possible. The following predictions [Ort92] are given in terms of the wave velocity as a function of an applied electric field strength E for cases in which the medium is sufficiently conducting that the Planck fields do not contribute.

1. Multiple types of waves can exist in the medium subjected to the through current ($I \cong 0$) while the current –free system has only one type of wave.
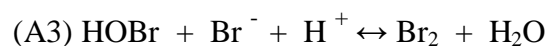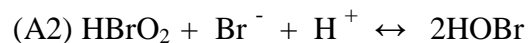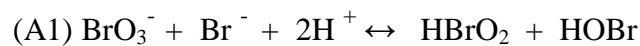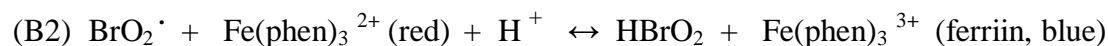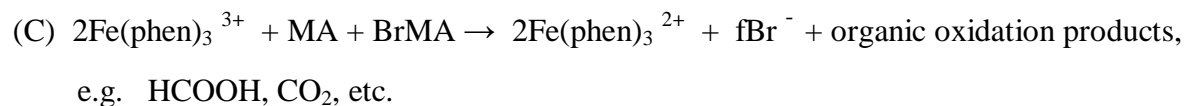
2. A cut-off field E_A may exist beyond which there are no waves; the effect is asymmetric in that waves started in the field-free system (E = 0) will be annihilated when a super-critical field is turned on only if the field and wave velocity are parallel or anti-parallel depending on the reaction mechanism.

3. The effect of an applied current on the wave velocity may saturate as I (or E) becomes large.

4. As the conductivity of the medium is reduced (by reducing the concentration of ions having higher electrical charges and/or mobility (see Eq. 16) and being not essential to the wave-driving reaction), qualitatively different types of waves may arise as the Planck field becomes important.

5. In an excitable one-dimensional medium, a pair of pulses propagating in opposite directions may be induced if a field less than the annihilation field $(E < E_A)$ is applied.

6. Static patterns may be made to propagate under an applied static electrical field. This prediction has been confirmed by experimental results in the CIMA reaction and the propagation velocity dependence on the electrical current of moving spots was found to be linear [Sch03].

Similarly, we expect that the response of reacting systems to applied electric fields should be quite interesting, since applied fields can force reactants into or away from each other. One expects that this additional transport could lead to interesting variations in the types of phenomena supported by a given reaction-diffusion system.

2.3 The Belousov-Zhabotinsky (BZ) reaction

2.3.1 FKN mechanism and Oregonator model

The mechanism of the BZ reaction was elucidated in 1972 by Field, Körös, and Noyes (FKN) [Fie72a]. The FKN mechanism is widely regarded as correct in its major features to describe this reaction. In 1974, Field and Noyes proposed a five-step, three-variable reduction of the FKN mechanism called the Oregonator [Fie74a, Fie75]. This model has been extremely successful over the years in providing a semi-quantitative description of the varied non-linear behaviour of the reaction. The basic features of the FKN mechanism are outlined below for ferroin ($Fe(phen)_3^{2+}$) as the catalyst:

PROCESS A

(A1) $BrO_3^- + Br^- + 2H^+ \leftrightarrow HBrO_2 + HOBr$

(A2) $HBrO_2 + Br^- + H^+ \leftrightarrow 2HOBr$

(A3) $HOBr + Br^- + H^+ \leftrightarrow Br_2 + H_2O$

PROCESS B

(B1) $BrO_3^- + HBrO_2 + H^+ \leftrightarrow 2BrO_2^{\cdot} + H_2O$

(B2) $BrO_2^{\cdot} + Fe(phen)_3^{2+}(red) + H^+ \leftrightarrow HBrO_2 + Fe(phen)_3^{3+}$ (ferriin, blue)

(B3) $2HBrO_2 \leftrightarrow HOBr + BrO_3^- + H^+$

PROCESS C

(C) $2Fe(phen)_3^{3+} + MA + BrMA \rightarrow 2Fe(phen)_3^{2+} + fBr^- +$ organic oxidation products,

e.g. $HCOOH$, CO_2, etc.

Oscillations in the BZ reaction can be conveniently described in terms of three composite processes, A, B, and C. Bromide is slowly oxidized by bromate in reaction A1 when its concentration is high. The products of this step rapidly undergo further reactions with bromide in steps A2 and A3 to yield bromine. The net reaction for process A is given by (A1) + (A2) +3(A3):

(A) $BrO_3^- + 5Br^- + 6H^+ \rightarrow 3Br_2 + 3H_2O$.
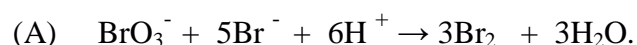
As bromide is consumed in process A, it eventually reaches a critical concentration where the rate of its oxidation by $HBrO_2$ in reaction A2 is comparable to the rate of $HBrO_2$ oxidation by bromate ion in reaction B1. The $BrO_2^{\cdot}$ product of reaction B1 is rapidly reduced in reaction B2 to generate $HBrO_2$, and the result is the autocatalytic sequence given by (B1)+2(B2):

(B2′) $BrO_3^- + HBrO_2 + 2Fe(phen)_3^{2+} + 3H^+ \rightarrow 2HBrO_2 + 2Fe(phen)_3^{3+} + H_2O$.

Thus, the quadratic autocatalysis is initiated when the production of bromous acid in the reaction B2′ is comparable in rate to its consumption in reaction A2. Bromous acid concentration increases autocatalytically with a concurrent oxidation of the catalyst. Bromide is rapidly driven to very low concentrations by its reaction with bromous acid and the rate of

process A becomes negligible. As $HBrO_2$ concentration increases, its autocatalytic growth is eventually limited by the bimolecular disproportionation reaction B3. The net reaction of process B is given by 2(B1)+4(B2)+(B3):

(B) BrO_3^- + $4Fe(phen)_3^{2+}$ + $5H^+$ → HOBr + $4Fe(phen)_3^{3+}$ + $2H_2O$.
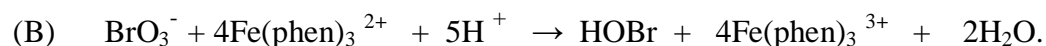
The bromine product of process A reacts with malonic acid $(CH_2(COOH)_2)$ to generate bromomalonic acid (BrMA), i.e. Br_2 + MA → BrMA (or $BrCH(COOH)_2$) + Br^- + H^+. The product HOBr of process B may brominate MA directly or react with bromide supplied later in the cycle to yield bromine, thereby also generating BrMA. This supply of BrMA is attacked by the oxidized catalyst, ferriin, to liberate bromide according to the composite reaction C. Process C is complex and not well understood, however, the net effect is the reduction of the catalyst and the regeneration of bromide. Recently, the mean rate constant value of process C at 25 ^{o}C is reported to be (3.1 ± 0.2) x 10^{-5} s^{-1} for ferroin as the catalyst [Ung97]. These general features are represented by reaction C, where f is a stoichiometric factor determining the moles of bromide generated per mole of catalyst reduced. Thus, following the rapid autocatalytic growth of $HBrO_2$ and concurrent oxidation of ferroin, bromide is generated by the ferriin catalysed oxidation of BrMA. The bromide concentration increases to a critical value where it competes for $HBrO_2$ in reaction A2, and the control of the system is switched from process B to process A. Bromide is again slowly consumed in process A, and the sequence is repeated. The switch from process A to process B occurs when reaction rates A2 and B1 are roughly equal. As the bromate concentration remains virtually constant during a given oscillation, the switch to autocatalysis occurs when the bromide concentration has been reduced by process A to the critical bromide ion concentration $[Br^-]_{crit.}$ [Fie72a, Fie86] given by

$k_{A2}[HBrO_2][Br^-][H^+]$ = $k_{B1}[BrO_3^-][HBrO_2][H^+]$

$[Br^-]_{crit.}$ = (k_{B1} / k_{A2}) $[BrO_3^-]$

$\qquad$ = $(42.0 \ M^{-2} \ s^{-1} / 3.0$ x $10^6 \ M^{-2} \ s^{-1})$ $[BrO_3^-]$

$\qquad$ ≈ 1.4 x$10^{-5}[BrO_3^-]$. $\hfill$ (18)

With a reasonable FKN mechanism and the appropriate values for the reaction rate constants [Fie86], it should be possible not only to match individual experimental observations but also to predict more generally the experimental conditions. For this, it is especially convenient to use the Oregonator model derived from the FKN scheme. This is frequently written in the

standard form of five irreversible steps, whose rate constants are assumed to incorporate proton concentrations when appropriate,

Rate constants

(O1) **slow reaction:** $\qquad$ A + Y → X + P $\qquad$ $k_1 = k_{A1}[H^+]^2 = 2\ M^{-3}s^{-1}[H^+]^2$

(O2) **fast reaction:** $\qquad$ X + Y → 2P $\qquad$ $k_2 = k_{A2}[H^+] = 3.0 \times 10^6\ M^{-2}\ s^{-1}[H^+]$

(O3) **autocatalysis HBrO$_2$:** A + X → 2X + Z $\qquad$ $k_3 = k_{B1}[H^+] = 42.0\ M^{-2}\ s^{-1}[H^+]$

(O4) **limitation HBrO$_2$:** $\qquad$ 2X → A + P $\qquad$ $k_4 = k_{B3} = 3 \times 10^3\ M^{-1}\ s^{-1}$

(O5) **regeneration Br$^-$:** $\qquad$ B + Z → fY $\qquad$ $k_5 = 1\ M^{-1}\ s^{-1}\ [B]$

, where A = BrO_3^- , B = all oxidizable organic species (MA+BrMA), P = HOBr, X = $HBrO_2$, Y = Br $^-$, and Z = $Fe(phen)_3^{3+}$. The concentrations of the major reactants, A and B, are treated as constants. The reaction rate equations for the intermediate species X, Y, and Z are

$$d[X/]dt = k_1[A][Y] - k_2[X][Y] + k_3[A][X] - 2k_4[X]^2 \qquad (19)$$

$$d[Y]/dt = -k_1[A][Y] - k_2[X][Y] + fk_5[B][Z] \qquad (20)$$

$$d[Z]/dt = k_3[A][X] - k_5[B][Z]. \qquad (21)$$

These rate equations can be simplified by transforming them to dimensionless equations given by

$$\frac{dx}{dt} = \frac{y(q-x) + x(1-x)}{e} \qquad (22)$$

$$\frac{dy}{dt} = \frac{-y(q+x) + fz}{e^*} \qquad (23)$$

$$\frac{dz}{dt} = x - z, \qquad (24)$$

where the dimensionless variables are x = $2k_4[X]/k_3[A]$, y = $k_2[Y]/k_3[A]$, z = $k_5k_4[B][Z]/(k_3[A])^2$, and τ = $t/k_5[B]$. The three dimensionless parameters that remain have typical values of ε = $k_5[B]/k_3[A] \approx 10^{-2}$, $\varepsilon^* = 2k_5k_4[B]/k_2k_3[A] \approx 10^{-5}$, and q = $2k_1k_4/k_2k_3 \approx 10^{-4}$. Note that the genuine autocatalytic non-linear term x(1-x) is clearly identified. ε^* is very small and much less than 1, thus the concentration of bromide ion (y) will change quickly in time because dy/dτ is large, so we now use the steady state approximation $\varepsilon^*(dy/d\tau) = 0$ to obtain a steady state of bromide concentration y = y_{ss} = fz/(q+x). Substituting this result into Eqs. 22 and 24, we get

$$e\frac{dx}{dt} = x(1-x) + \frac{(q-x)}{(q+x)}fz$$

$$\frac{dz}{dt} = x - z. \tag{25}$$

Written in this way, the reduced Oregonator model has the typical form of reaction rate of an activator-inhibitor model [Mur89, Pót98, Sag03, Wal00], with $x = u = HBrO_2$ the activator or autocatalytic species and $z = v = $ ferriin the consuming species (inhibitor), and the corresponding reaction-diffusion-electrical migration equations are

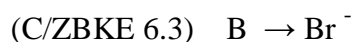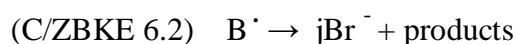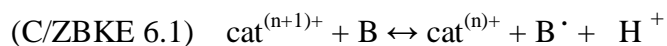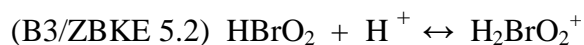$$\frac{\partial u}{\partial t} = \frac{1}{e}[u(1-u) + \frac{(q-u)}{(q+u)}fv] + D_u\Delta u - m_u E\nabla u$$

$$\frac{\partial v}{\partial t} = u - v + D_v\Delta v - m_v E\nabla v, \tag{26}$$

where D_u, μ_u and D_v, μ_v are the diffusion coefficients, the electrical mobilities of bromous acid and ferriin, respectively. E is an applied electric field intensity. Typical values of D_u and D_v [Šev96a, Šev96b] are 2.0 x 10^{-5} cm^2/s and 0.603 x 10^{-5} cm^2/s, respectively. Note that bromide ion (y) is also referred as the inhibitor species, D_y = 2.084 x 10^{-5} cm^2/s [Šev96a, Šev96b]. It may be unreasonable to use an uncharged component $HBrO_2$ to describe electrically induced flux. But in fact, because of the reaction kinetics, the dynamical behaviour of Br $^-$ is closely related to that of $HBrO_2$ [Fie85] thus we can use conventionally μ_u = μ_y = 8.096 x 10^{-4} cm^2/V.s and μ_v = 7.041 x 10^{-4} cm^2/V.s obtained from the Nernst-Einstein relation (see Eq.7). Diffusion coefficients and ion mobilities given are tabulated values at room temperature 25 ^{o}C, extreme dilution in water. Equation 26 represents generally a two-variable Oregonator model used for simulating the effect of an imposed electric field on the BZ spiral waves [Pér93, Tab94] in which diffusion and electrical migration terms of the variable v are always omitted (i.e. the catalyst is immobilized).
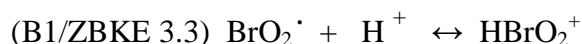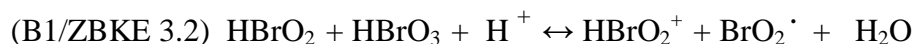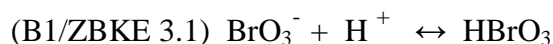
A recent extension of the Oregonator model to ZBKE (Zhabotinsky, Buchholtz, Kiyatkin, Epstein) model [Zha93b] has been proposed in order to fit experimental observations of the BZ waves for which the original Oregonator did not seem to give satisfactory results. Electric field effects on BZ oxidation waves were also successfully simulated with this model [Šev96a, Šev96b]. The general features of the ZBKE mechanism are more complicated in oxybromine species than the original FKN mechanism, as shown in the reaction schemes [Šev96a],

(A1/ZBKE 1) $HBrO_3 + Br^- + H^+ \leftrightarrow HBrO_2 + HOBr$

(A2/ZBKE 2) $HBrO_2 + Br^- + H^+ \leftrightarrow 2HOBr$

(B1/ZBKE 3.1) $BrO_3^- + H^+ \leftrightarrow HBrO_3$

(B1/ZBKE 3.2) $HBrO_2 + HBrO_3 + H^+ \leftrightarrow HBrO_2^+ + BrO_2^{\cdot} + H_2O$

(B1/ZBKE 3.3) $BrO_2^{\cdot} + H^+ \leftrightarrow HBrO_2^+$

(B2/ZBKE 4) $HBrO_2^+ + cat^{(n)+} \leftrightarrow HBrO_2 + cat^{(n+1)+}$

(B3/ZBKE 5.1) $2HBrO_2 \leftrightarrow HOBr + HBrO_3$

(B3/ZBKE 5.2) $HBrO_2 + H^+ \leftrightarrow H_2BrO_2^+$

(B3/ZBKE 5.3) $H_2BrO_2^+ + HBrO_2 \leftrightarrow HOBr + HBrO_3 + H^+$

(C/ZBKE 6.1) $cat^{(n+1)+} + B \leftrightarrow cat^{(n)+} + B^{\cdot} + H^+$

(C/ZBKE 6.2) $B^{\cdot} \rightarrow jBr^- + products$

(C/ZBKE 6.3) $B \rightarrow Br^-$
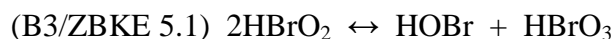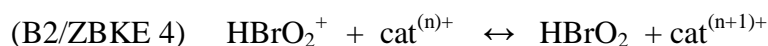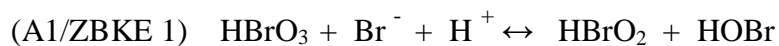
Here $cat^{(n)+}/cat^{(n+1)+}$ is reduced/oxidized form of the catalyst, $B = MA + BrMA$, and the stoichiometric factor, j, is allowed to vary from 0.5 to 1.

2.3.2 Excitability of the BZ reaction

The nature of the response of the system depends crucially on the parameter f - the number of bromide ions produced in process C. Oscillations occur for values of the parameter f specifically lying in the range $\frac{1}{2} < f < 1 + \sqrt{2}$ [Eps98]. The system switches control between the three processes (A, B and C) giving rise to periodic variations in the intermediate species (Br $^-$, HBrO$_2$, ferriin) concentrations as a function of time or space. For conditions just outside those required for spontaneous oscillatory behaviour - for instance for systems with f slightly larger than $1 + \sqrt{2}$ - the BZ system shows a property known as excitability [Eps98].
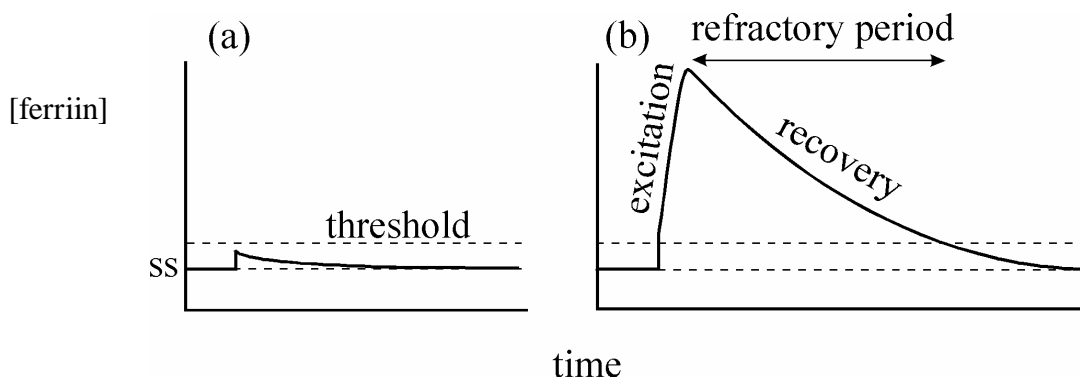
Figure 7: Schematic representation of important features of an excitable BZ system. (a) subcritical perturbation and (b) supercritical perturbation.

An excitable system is characterised by (i) having a steady state SS; (ii) the steady state is stable to small perturbations; (iii) if the perturbation exceeds some critical or threshold value, the system responds by exhibiting an excitation event. For the BZ system, this excitation event is the oxidation of the catalyst, corresponding to process B with a local colour change in the vicinity of the perturbation (initiation) site. This response is typically large compared to the critical stimulus – so the system acts as a 'non-linear amplifier' of the perturbing signal. Following the excitation, the system eventually returns to the initial steady state and recovers its excitability. There is, however, a finite period, the refractory period, between the excitation and the recovery during which the system is unresponsive to further stimuli. These basic characteristics are summarised in Fig. 7.

2.3.3 Properties and behaviour of waves

A variety of behaviour of an oxidation wave (i.e. a narrow region consisting of an oxidized form of a catalyst, propagating through a reduced medium) is exhibited by the BZ reaction in a thin film of the unstirred solution. There are three types of waves observed in such a medium [Ros88, Win74]. They are

1. Phase waves (Kinematic waves or Pseudo-waves): these are high-velocity waves little influenced by diffusion. A phase wave, however, owes its existence to a gradient in the phase (or state, in mathematical description: $\zeta = x - vt$ where ζ is phase, x is position, v is velocity, and t is time [Ros88]), i.e. from reduced phase to oxidized phase (bulk oscillations), rather than the period of oscillation. Thus, a reaction mixture of a single composition and temperature oscillating at a single period, but with the phase of oscillation as a function of

spatial coordinates, exhibits apparent wave behaviour like the moving lights of a neon advertising sign. The speed at which such waves travel is determined primarily by the underlying concentration of phase gradients and so can be tuned to almost any values.

2. Trigger waves: these waves may occur in an oscillatory reaction mixture but are usually observed in a non-oscillatory excitable medium, because the reaction mixture becomes oscillatory at the surface of a particle of dust or at a scratch on the surface of the container or by slightly tilting the silver wire, because a momentary depletion of bromide allows bromous acid autocatalysis to proceed to a sufficient extent to initiate a wave. They propagate with constant velocity. Here, reaction (autocatalysis) and diffusion are intimately linked. These waves are oxidation waves (high ferriin concentration) travelling in the reducing environment with high concentrations of bromide ions and ferroin. Trigger waves in one dimension are called pulses and a series of them is a wave train. Field and Noyes were first to semi-quantitatively explain trigger wave propagation in the BZ reaction [Fie72b, Fie74b].

3. Phase diffusion waves [Ros88]: this kind of wave occurs also in an oscillatory medium. It appears only if concentration gradients are smaller or more shallower than trigger wave. The velocity of phase diffusion wave is nearly constant for a limited time interval, when exceeds that of the trigger wave (of essentially constant velocity), then a phase wave and not a trigger wave propagates in the solution.

The trigger wave movement mechanism has been explained in the following way: the concentration of bromide ions decreases at the beginning below a critical value and the oxidation stage takes place; the leading edge of the wave or wave front (sharp blue boundary) with high concentration of bromous acid, ferriin, and low concentration of bromide ions is formed as shown in Fig. 8.
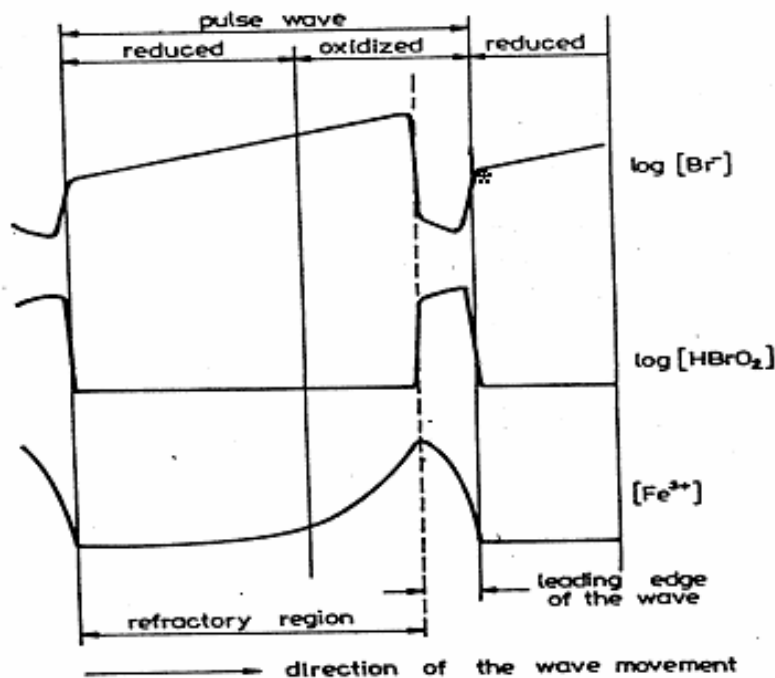
Figure 8: Schematic representation of a pulse wave in an excitable BZ system showing important intermediate concentration profiles (adapted from [Šev83]). Note that Fe^{3+} represents ferriin. A marked star (*) is the critical point of bromide ion concentration.

The reducing stage takes place behind the boundary (dashed line) and the reacting medium becomes red again due to process C. In the region with a high concentration of bromide ions a new wave cannot be initiated This region is called refractory. $HBrO_2$ diffuses in front of the wave front and consumes bromide ion in reaction A2. Bromous acid autocatalysis is initiated as the bromide ion concentration decreases below its critical value, thus a new start of the oxidation process, and the result is a wave that triggers its own propagation.

Trigger waves propagate with constant velocities, and the wave velocity v is proportional to the square root of the product of bromate and hydrogen ion concentrations expressed in the linear function defined by Tyson [Fie85, Sho87, Til74]:

$$v \geq 2(D_{HBrO_2} k_{B1}[H^+][BrO_3^-])^{\frac{1}{2}} \; . \tag{27}$$

The diffusion coefficient of bromous acid D_{HBrO2} is 2.0 x 10^{-5} cm^2/s at room temperature (25 ^{o}C) and k_{B1} is the rate constant of reaction step B1, i.e. 42 M^{-2}s^{-1} in FKN mechanism. A major approximation of Eq. 27 is the neglect of the reaction between bromous acid and bromide ions ahead of the wave (reaction step A2). The velocities predicted by this equation are compared with the experimentally measured velocities [Fie74b, Nag89a]. Quantitative studies of ferriin [Mor91] and cerium ion [Nag89b] concentration profiles and dependences of wave propagation velocities on temperature [Kuh85], depth of solution and initial reactant concentrations [Fie74b, Nag89a, Woo85] were reported. The propagation velocity was found to depend on the cerium ion concentration [Nag89a] but not depend on the MA concentration and the ferroin concentration [Fie74b, Woo85]. Generally for a given recipe of initial reactant concentrations, the increasing temperature mainly increases the value of the autocatalytic rate constant and thus the propagation velocity of trigger waves [Kuh85, Šev83]. Wave propagation velocity also depends on the catalyst type. The experimental data [Nag88a, Nag88b] have shown that the propagation velocity of the waves decreases in the order: ferroin > cerium > manganese catalysed BZ systems, respectively.

Trigger waves in two dimensional media of the BZ reaction also give rise to outward propagating target waves (a series of concentric circular waves). The larger the separation between waves in a given target pattern, the longer the solution has to recover. Rotating spiral waves (see Fig. 9) generated by mechanically shearing one or more target waves [Win74] can occur in the media.
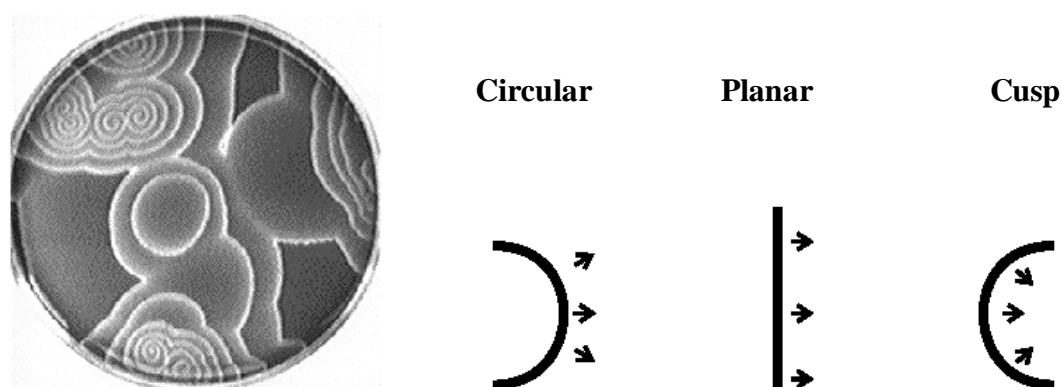
Figure 9: Left: Target waves and spiral wave pairs in the thin layer of BZ solution spread in a petri dish. White, grey, and black zones are excited (high [ferriin]), recovery, and stationary (but excitable) regions (high [ferroin]), respectively. Right: Three shapes of the wave front (see more detail in the text).

There is also a relationship between the wave velocity (speed) and the wave period or the wavelength (the spacing between successive wave fronts) of the periodic trigger waves. This is known as the dispersion relationship [Tys88]. The three quantities are related by the simple condition, i.e. velocity = (1/period) x (wavelength) = (frequency) x (wavelength). A typical dispersion relationship has the form sketched in Fig. 10.
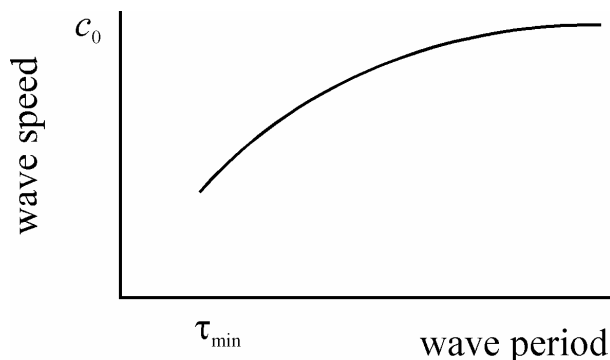
Figure 10: Drawing showing the general character of the dispersion relation curve for BZ-waves (see details in the text).

According to Fig. 10, if the wave period is too short ($< \tau_{min}$) no waves propagate. For short wave periods (high frequencies), waves can propagate, but have low velocity. As the period increases (frequency decreases), the wave speed increases, getting to a limit at very long periods. This limit corresponds to the speed c_0 of a solitary wave propagating in the solution that has completely recovered to the resting steady state composition.

Recently, there is a search for universal dispersion relationship of the BZ waves. Flesselles et al. [Fle98] obtained an approximate analytical expression linking the wave speed v(T) (mm/min) to the wave period T (min) for a given excitable medium in the following form of a hyperbolic tangent function:

$$v(T) = c_0[\tanh(T/T_*)] , \tag{28}$$

where c_0 is the speed for the solitary wave (i.e. for waves sufficiently far apart for the system to return to its steady state between oxidation events) and T_* is a characteristic period that is closely equal to the rotation period of a spiral wave in the same medium. It is clear that Eq. 28 fits well with the experimental dependence of the wave speed on the wave period [Fle98].

The velocity of a circularly curved wave front (see also Fig. 9) is lower than that of a planar wave in the same system. The dependence of the speed of a wave on the curvature ($K = 1/r$) of the front is given by the eikonal equation [Tys88, Zyk87], which has the linear form:

$$v(K) = v(0) - D_u K . \qquad (29)$$

Here $v(K)$ is the normal velocity of the curved wave front, $v(0)$ is the speed of the corresponding planar wave front, and r is the radius of curvature of the wave segment. D_u is the diffusion coefficient of the autocatalytic species, in this case, in the BZ medium, $D_u = D_{HBrO2}$.

For a circular front, the curvature is positive and its radius is simply equal to the radius of the circle. Because of this, the wave speed is reduced from the planar wave speed. Furthermore, the smaller the circle, the greater the reduction in the velocity. In fact, if equation holds for very low curvature, there will be a critical radius r_{crit} (in order of $\approx$ 20 µm for BZ-waves [Foe89]) such that $v(K) = 0$ for $r = r_{crit} = D_u /v(0)$ and a wave with this curvature would not propagate. This then predicts a minimum size for the wave initiation site (or the pacemaker), as waves will fail to propagate unless $r > r_{crit}$. Cusp-shaped regions where waves collide (see Fig. 9) are curved towards their direction of propagation and so have negative curvatures. The eikonal equation indicates that the wave speed will enhance relative to the planar wave speed in these cases. With high curvatures, the dilution due to diffusion spreading of the autocatalyst into the region ahead of the wave is much enhanced compared to the planar wave having an infinite curvature ($r = 0$).
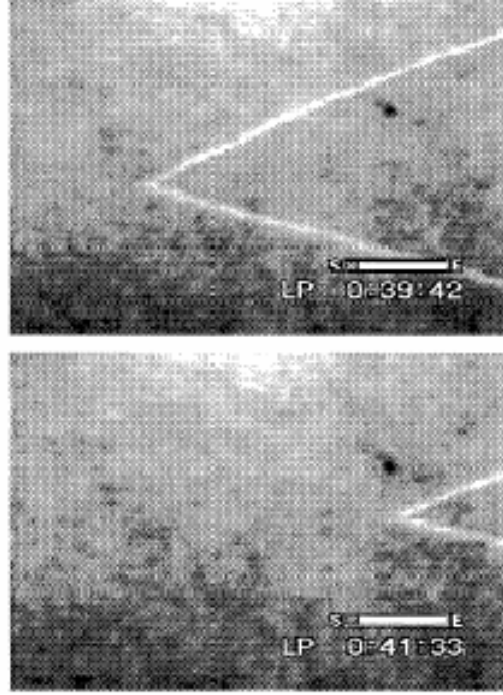
Figure 11: Two consequences in time and positions of the V-shaped wave ($\theta = 60^o$ at the vertex) moving to the right in the light sensitive BZ reaction looking through a CCD camera with the interference filter of 450.6 nm (adapted from [Bra99a]). This pattern was generated by illuminating the V –shaped light of intensity 24 W/m^2 only on a portion of the silica gel matrix including the BZ solution. White corresponds to the excited (oxidized) state of the green coloured Ru(bipy)$_3$$^{3+}$, black to the reduced state of the orange coloured Ru(bipy)$_3$$^{2+}$, and gray to the recovery state. The time between two pictures is 1 min 51 s.

Recent experimental observations of V-shaped waves in the light sensitive Ru(bipy)$_3$$^{2+}$ catalysed BZ reaction [Bra99a] have shown that these waves (see Fig. 11) appear as the result of oblique collision of two planar waves-the colliding parts of the fronts annihilate, and after a corner of an angle $\theta = 2\arcsin[v(0)_{wing}/v(K)_{vertex}]$ between the planar waves (or between two wings of V-shaped wave) becomes smooth, a stationary propagating wedge with finite negative curvature at its vertex appears. The modified eikonal equation for these V-shaped waves with small curvatures [Bra99b] is given as

$$v(K)_{vertex} = v(0)_{wing} - \frac{D_u}{\sin^2(\frac{q}{2})}K. \qquad (30)$$

2.3.4 Survey of electric field effects

The key species of the BZ reaction, identified in the Oregonator model, are $HBrO_2$, Br^-, and the metal ion catalyst. We see that these species are all of different charge types; therefore, an applied electric field should affect the propagation of BZ wave. Ortoleva and co-workers [Fee81] first recognized that the high ionic strength of the typical BZ reaction mixture would result in a large conductivity with unacceptable heating. Therefore, a modified low ionic strength recipe was developed in which bromic acid ($HBrO_3$) was substituted for the usual bromate salt and sulphuric acid. The system was studied using a reagent-saturated membrane filter between two electrodes. In Feeney's experiments [Fee81] a circular two-dimensional BZ wave showed an increased velocity with respect to the absence of a field when it propagated toward the positive electrode (that is, in the negative electric field) and a decreased velocity when it propagated toward the negative electrode (that is, in the positive electric field). The local depletion of the bromide ions in front of the wave is either enhanced in a negative field or suppressed in a positive field by the action of ionic migration. These effects are then reflected in either the increase or the decrease of the autocatalysis rate and thus the propagation velocity of the wave. Wave propagation perpendicular to the electric field was little affected. The most dramatic observation in these experiments was the formation of a crescent wave from a circular wave in the presence of the electric field. Upon switching off the field, the free ends of the crescent wave formed oppositely rotating spiral waves. Anyway, the effects observed are also due to evaporation, heating, and the presence of the products from electrolysis. More refined experiments with the same effects were done by Hasal et al. [Has97]. Application of a d.c. electric field to spiral wave structures was found to cause a drift of the spiral core toward the anode [Ste92] by action of electro-migration of bromide ion in the spiral core. It is shown in Fig. 12.1 that there is a drift component that increases the distance between the cores of a pair of spirals with opposite chirality. On the other hand, if the field direction is reversed, the same spiral pair will follow a reversed drift pattern, that is the two spirals forming the pair will be forced to collide with each other. This results in mutual annihilation [Sch92]. When a sinusoidal alternating electric field is applied perpendicularly to the membrane saturated with the ferroin catalysed-BZ reagent in an open unstirred reactor, target wave patterns undergo a transition to complex spiral wave patterns. This transition results from periodically changing excitability and the bromide ion concentration in the membrane at the reversed polarity. In addition, the number of the spiral cores depend on frequency and amplitude of the field [Sei01], as shown in Fig.12.2.

(12.1)

(-)

(+)　　　　　　　　　　　(+)

(a)　　　　　　　　　　　(b)
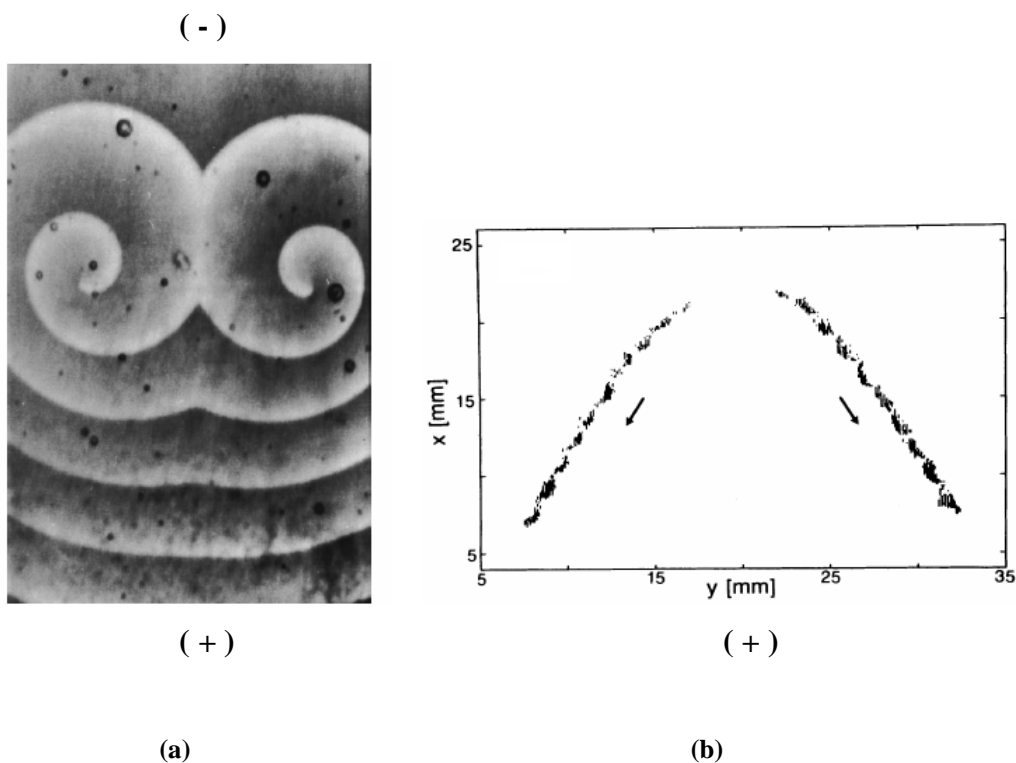
(12.2)
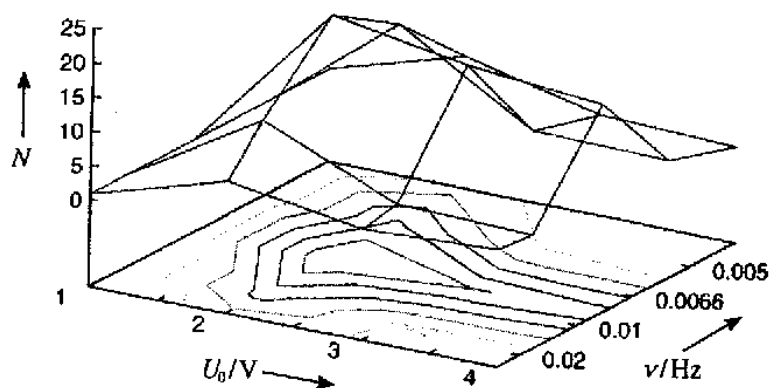
Figure 12 : BZ-spiral waves in the electric field.

(12.1) Electric field induced drift and strong deformation from Archimedean geometry of spiral waves in the agar gel BZ medium (to eliminate the role of induced hydrodynamic convective flow) at E = 5 V/cm, I = 35 mA (from [Ste92]). (a) A snap-shot of drifting spiral pair. (b) Unresolved trajectories of the spiral centres (or spiral tips). The drift direction to the positive electrode is also influenced by the sense of rotation (or chirality): in (a) clockwise for the left hand spiral wave; anticlockwise for the right hand spiral wave.

(12.2) Average number of spiral centers N depending on the alternating electric field of amplitude U_0 and frequency v (from [Sei01]). The maximum number of spiral cores is at $U_0 = 2.0$ V and $v = 8.3$ mHz.

Quantitative data on the propagation velocity in an imposed d.c. electric field have been obtained for planar BZ waves propagating along a spatially quasi-one-dimensional system [Šev83, Šev84, Šev92, Šev99]. The non-linear dependence of the propagation velocity on electric field intensity was found and depended on the polarity of the field, as shown in Fig. 13. A thermostated capillary tube was connected through membranes to two electrolytic cells as electrophoresis method, effectively eliminating undesirable effects from heating and electrolysis products.
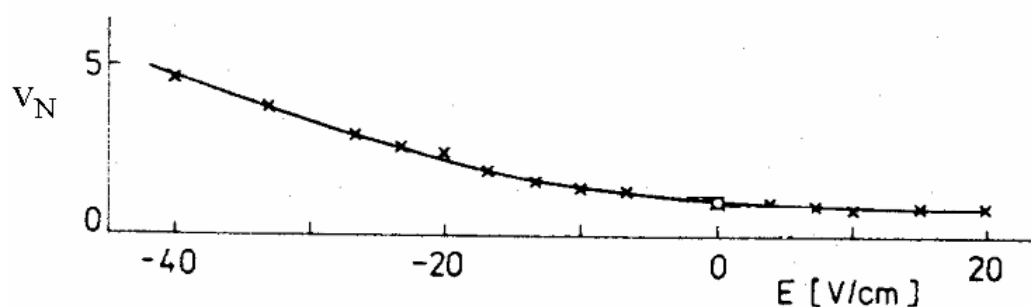
Figure 13: Dependence of the normalized wave velocity $v_N = v_E/v_0$ (where v_E and v_0 are the wave velocities with and without an electric field, respectively) on the imposed electric field intensity E for a pulse wave in the BZ medium (adapted from [Šev84]). The experiments were performed in 0.6 mm (circular diameter) capillary reactor bath thermostated at 15 ^{o}C. Initial composition ($\Gamma = 0.37$ M and $\kappa = 0.069$ S/cm at 18 ^{o}C [Šev83]): 0.05 M MA, 0.205 M bromic acid, 7 mM KBr, and 4 mM ferroin; v_0 (by average) = 2.25 ± 0.07 mm/min. The electric field is negative when the wave propagates to the positive electrode and is positive when the wave propagates to the negative electrode.

In Ševčíková experiments [Šev83] when a field of 16.7 V/cm is applied, the forward progress of a wave propagating toward the negative electrode is greatly reduced, and the wave back serves to initiate waves in the opposite direction, i.e. they observed wave splitting (so-called back firing). The new waves propagate at a higher velocity and are initiated at a higher frequency than waves in a field-free environment. The life time of this wave source (and hence the number of emitted waves) depends on the magnitude of the electric field intensity. Wave splitting occurring at high positive fields, the positively charged ferroin and ferriin migrate ahead of the wave front, and the bromide ions build up in the refractory region behind it until the low bromide ion region is spread out and wide enough for a new wave to form and propagate (see Fig. 14.1).

(14.1)

(14.2)

(a)   (b)
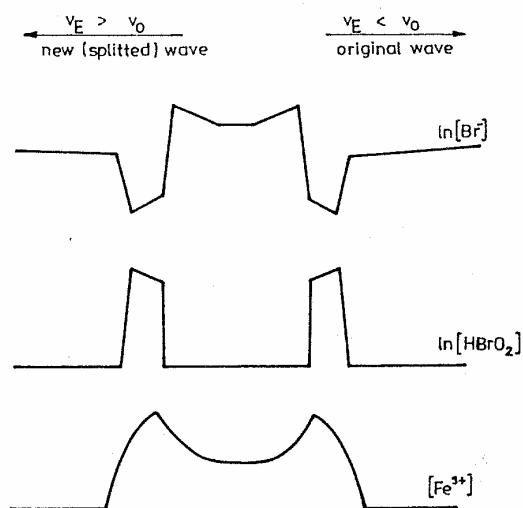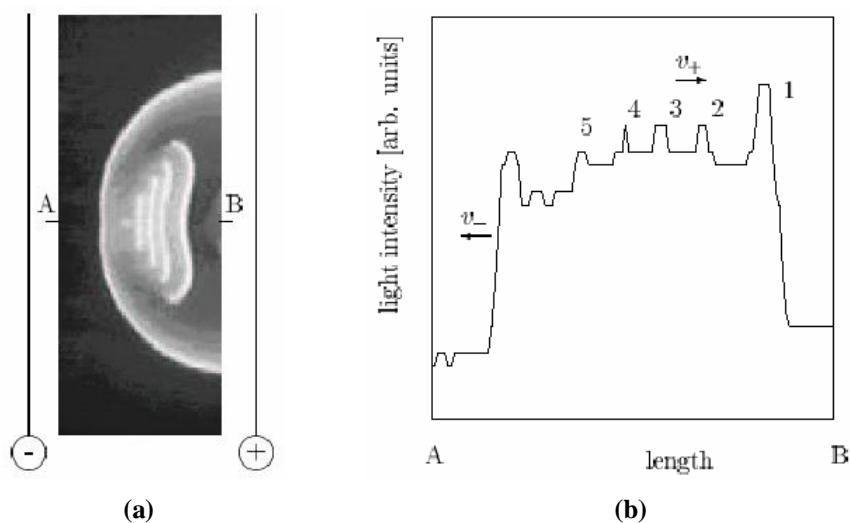
Figure 14: BZ-wave splitting.

(14.1) Schematic one-dimensional concentration profiles of three important intermediates in BZ system during the course of the wave splitting (from [Šev83]). [Fe^{3+}] represents the ferriin concentration.

(14.2) (a) Two dimensional pattern of five split waves in agar gel BZ medium after the electric field intensity E = 8.59 V/cm was switched on for 2.3 min (from [Šev96a]). Image area 1.35 x 3.16 cm^2. (b) Light intensity profile corresponding to [ferriin] along the AB line of (a). v_+ and v_- show the direction of the wave propagation toward positive and negative electrodes, respectively; $v_+ > v_-$.

At E = 20 V/cm, a wave is annihilated after initiating another wave propagating in the opposite direction. Thus, the applied electric field results in reversal propagation. Wave splitting (see Fig. 14.2) and wave reversal have also been observed in a spatially two-dimensional BZ-system [Šev96a, Šev96b]. The wave annihilation occurs at E > 20 V/cm , when a sufficient amount of bromide ion migrates into the wave front, increasing the rate of reaction step A2 (bromide-bromous acid reaction) and preventing the autocatalytic oxidation of ferroin.

In the course of the reversal, the migration of the bromide ions toward the anode-that is, in the direction opposite to that of the wave propagation, slows down the propagation of the wave front. On the other hand, it helps to decrease the bromide concentration in the refractory tail below the critical value, and consequently the wave's trailing edge turns into a sharp wave front that moves in a direction opposite to that of the original wave annihilated at the same time, as shown in Fig. 15.
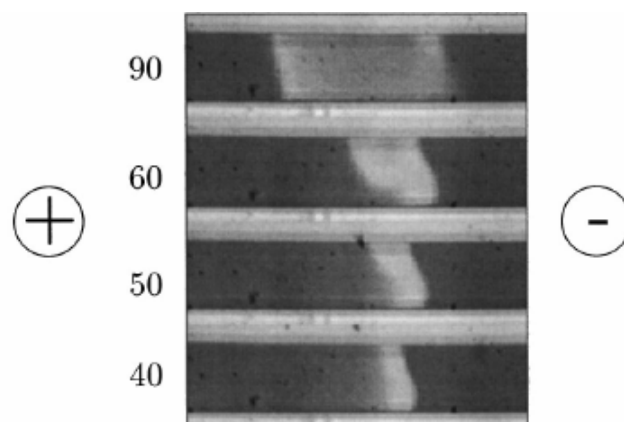
Figure 15: Electric field-induced S-shaped front deformation caused by the convective flows and wave reversal of a pulse wave in liquid BZ medium at 100 V in 0.7 mm (rectangular diameter) capillary reactor (from [Šev99]). Numbers given are the time in seconds elapsed after switching the voltage on. Figures shown are observed from the side view of the capillary. The portion of the cuvette shown is 0.85 cm in length.

One can conclude that the bromide ion is an important key reaction intermediate of the reaction to understand the electric field effects on BZ oxidation waves [Has97]. Bromide depletion leads to wave acceleration, and bromide supply to wave deceleration. The migration supply of bromide ions increases when increasing the field intensity, and implies the following sequence of phenomena: 1. deceleration of wave propagation 2. wave splitting 3.

wave reversal and 4. wave annihilation (i.e. the wave is first stopped propagating then the wave front get dispersed and the oxidation zone is finally disappeared), where the propagation velocity is parallel to the electric field.

The effects arising when the electric field is applied on propagating chemical waves can be taken as a prototype of non-linear phenomena due to applied fields. These studies (especially in one-dimensional case) are also important with respect to the fact that propagation of information along the nerve axons has both electrical and chemical nature [DeF97, Fer85].

2.4 The uncatalyzed BZ reaction with pyrogallol as substrate

2.4.1 Plausible chemical mechanisms

The oxidation of pyrogallol (PG) or 1,2,3-trihydroxybenzene [Rap03] by bromate ions is an example of an uncatalyzed bromate oscillator controlled by the concentration of bromide ions [Orb79]. The mechanism [Sha85] is not as well understood as that of the classical BZ reaction. There should, however, be many similarities, at least in the chemistry of the oxy bromine species. It can proceed by processes which are similar to the processes involved in the bromate oxidation of malonic acid in the classical BZ reaction, as described in the former parts of this chapter. When the bromide ion concentration reaches a sufficiently high level, process A (steps A1-A3) occurs (see Section 2.3.1). The bromine produced in the step A3 may react with pyrogallol, liberating bromide ions, as indicated by

(D) $\quad Br_2 + C_6H_3(OH)_3 \rightarrow BrC_6H_2(OH)_3\ (BrPG) + H^+ + Br^-$.
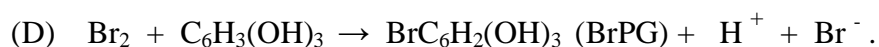
The three adjacent hydroxy groups on the benzene ring in pyrogallol (see Fig.16) activate the ring towards electrophilic attack by bromine, whereby hydrogen on the benzene ring is replaced with bromine. Actually, two of the hydrogen atoms on either side of the three hydroxy groups can be readily replaced by bromine atoms.

One of the effects of process A is a reduction in the concentration of bromide ion. As the concentration of the bromide ion decreases, the rate of process A diminishes, and process B takes over.

PROCESS B:

(B1) $BrO_3^- + HBrO_2 + H^+ \rightarrow 2BrO_2^{\cdot} + H_2O$

(*B2.1*) $BrO_2^{\cdot} + PG \rightarrow HBrO_2 + PG^{\cdot}$

(*B2.2*) $BrO_2^{\cdot} + PG^{\cdot} \rightarrow HBrO_2 + Q$

(*B2.3*) $BrO_2^{\cdot} + Q \rightarrow HBrO_2 + Q^{\cdot}$

(B3) $2HBrO_2 \rightarrow HOBr + BrO_3^- + H^+$
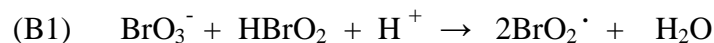
These steps are similar to steps in process B of the classical BZ-reaction. Here, in step B2.1, the role of a metal-ion catalyst is taken over by pyrogallol, i.e. the $BrO_2^{\cdot}$ radical oxidizes the pyrogallol to form a radical PG$^{\cdot}$. This radical can react with another $BrO_2^{\cdot}$ radical (see step B2.2) to form a quinonoid derivative Q [Jwo89, Liu92a, Nag99, Orb95] which can be oxidized again to a quinone radical Q$^{\cdot}$ by another $BrO_2^{\cdot}$ radical.
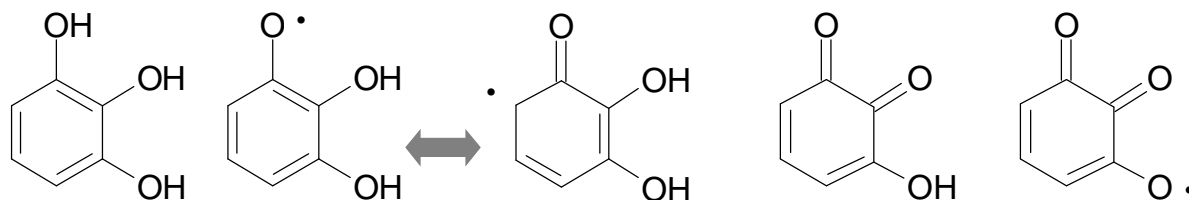
Figure 16: Chemical structures of the intermediates formed in the uncatalyzed BZ reaction with pyrogallol as substrate. From left to right: PG, PG-radical showing two resonance structures [Rap03], Q (3-hydroxy-1,2-benzoquinone [Per06, see also Dictionary of Organic Compounds, 6th Ed., Chapman & Hall , Cambridge, vol. 4, yr. 1996, p. 3588]) and Q-radical.

Furthermore, PG$^{\cdot}$ can also react with HOBr to produce a bromine atom Br$^{\cdot}$, which is rapidly reduced to a bromide ion, as represented in process C.

PROCESS C:

(*C1*) $HOBr + PG^{\cdot} \rightarrow Q + Br^{\cdot} + H_2O$

(*C2*) $Br^{\cdot} + PG^{\cdot} \rightarrow Q + Br^- + H^+$

(*C3*) $Br^{\cdot} + PG \rightarrow PG^{\cdot} + Br^- + H^+$
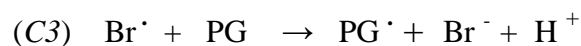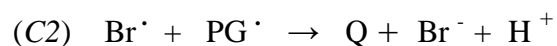
Therefore, process C increases the concentration of bromide ions, so that eventually the rate of process A will increase to the point where it dominates again. This switching back and forth between processes A and C via process B is what leads to the oscillations in the colour of the solution being due to the formation and consumption of Q formed in the reaction (see reaction steps *B2.3* and *C2*), as shown in Fig. 17.
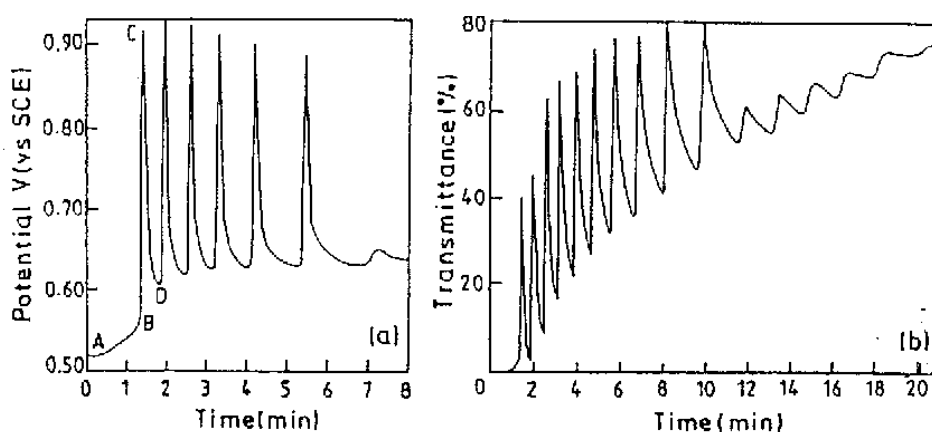
Figure 17: Temporal oscillatory behaviour of the PG-uncatalyzed BZ reaction in a well-stirred batch system at 30.0 $\pm$ 0.1 ^{o}C (from [Sri98b]). [PG] = 25 mM, [H$_2$SO$_4$] = 2.0 M, and [KBrO$_3$] = 0.06 M. During an induction time (from point A to point B), the colour of the solution is dark red-brown of Q. During the oscillatory period, the colour of the solution changes between pale yellow of the brominated and coupled products of Q [Jwo89] at the peak (point C, low [Br $^-$] and [Q]/[PG]) and orange at the base (point D, high [Br $^-$] and [Q]/[PG]).

(a) Potentiometric profile recorded by a Pt-electrode vs. a SCE (Saturated Calomel Electrode) corresponds to different redox couples [Liu92a, Nag99, Orb78] in the solution.

(b) Spectrophotometric profile recorded at 420 nm being due to the light absorption of [Q]/[PG].

Adding silver ions can induce complex - high frequency oscillations in this system arising from bromide ion consumption by silver ions [Var85].

2.4.2 The coupled system: ferroin catalyzed + pyrogallol uncatalyzed

The ferroin is used as a redox indicator, rendering the oscillations between process B and process C visible through oscillations in the colour of the solution. Because ferroin is a one-electron reductant, it can enter the reaction mechanism, and it appears to do so, because the periods and the oscillatory wave forms are more complex [Dut02, Gil92] or even the oscillations can be terminated [Kör80] when ferroin is present. Furthermore, the presence of a catalyst, e.g. ferroin, makes the contours of the waves more clear and pronounced [Orb98]

than in the absence of the catalyst. The mechanism proposed in references [Gil92, Liu92b] of the UBO system with PG including ferroin as the catalyst is given in Table 1. We can see that Q and ferroin are the main reacting species involved in the bromous acid autocatalysis.

Reaction Number (f = forward reaction, b = backward reaction)		Rate Constant
1f	$BrO_3^- + Br^- + 2H^+ \rightarrow HBrO_2 + HOBr$	$2.0 \ dm^9 mol^{-3} s^{-1}$
1b	$HBrO_2 + HOBr \rightarrow BrO_3^- + Br^- + 2H^+$	$3.2 \ dm^3 mol^{-1} s^{-1}$
2f	$HBrO_2 + Br^- + H^+ \rightarrow 2HOBr$	$3.0 \times 10^6 \ dm^6 mol^{-2} s^{-1}$
2b	$2HOBr \rightarrow HBrO_2 + Br^- + H^+$	$2.0 \times 10^{-5} \ dm^3 mol^{-1} s^{-1}$
3f	$BrO_3^- + HBrO_2 + H^+ \rightarrow 2BrO_2^\cdot + H_2O$	$42.0 \ dm^6 mol^{-2} s^{-1}$ (at 20 °C) [Fie86]
3b	$2BrO_2^\cdot + H_2O \rightarrow BrO_3^- + HBrO_2 + H^+$	$4.2 \times 10^7 \ dm^3 mol^{-1} s^{-1}$
4f	$2HBrO_2 \rightarrow HOBr + BrO_3^- + H^+$	$3.0 \times 10^3 \ dm^3 mol^{-1} s^{-1}$
4b	$HOBr + BrO_3^- + H^+ \rightarrow 2HBrO_2$	$1.0 \times 10^{-8} \ dm^6 mol^{-2} s^{-1}$
5	$BrO_2^\cdot + Q \rightarrow HBrO_2 + Q^\cdot$	$5.0 \times 10^6 \ dm^3 mol^{-1} s^{-1}$
6	$2Q^\cdot + H_2O \rightarrow products + Q$	$2.0 \times 10^9 \ dm^3 mol^{-1} s^{-1}$
7	$BrO_3^- + PG + H^+ \rightarrow HBrO_2 + Q + H_2O$ = (B1) + (B2.1) + (B2.2)	$0.15 \ dm^6 mol^{-2} s^{-1}$
8	$HOBr + PG \rightarrow Br^- + Q + H^+ + H_2O$ = (C1) + (C3)	$0.071 \ dm^3 mol^{-1} s^{-1}$
9f	$ferroin^{2+} + BrO_2^\cdot + H^+ \rightarrow HBrO_2 + ferriin^{3+}$	$8.0 \times 10^4 \ dm^6 mol^{-2} s^{-1}$
9b	$HBrO_2 + ferriin^{3+} \rightarrow ferroin^{2+} + BrO_2^\cdot + H^+$	$8.9 \times 10^3 \ dm^3 mol^{-1} s^{-1}$
10	$HOBr \rightarrow products$	$1.0 \times 10^5 \ dm^3 mol^{-1} s^{-1}$
11	$HOBr \rightarrow Br^-$	$10.0 \ dm^{3/2} mol^{-1/2} s^{-1}$
12	$ferriin^{3+} \rightarrow ferroin^{2+}$	$1.0 \times 10^{-3} \ s^{-1}$

Table 1: Mechanism and rate constants with [H$^+$] kept as a constant value of 1 M for coupled UBO with PG as substrate and ferroin as the catalyst (adapted from [Gil92] and [Liu92b]). It should be noted that rate constants of reactions 9f and 9b in the ferroin-catalysed BZ system with MA as substrate are reported to be 1.0×10^9 dm^{6}mol^{-2}s^{-1} and 33 dm^{3}mol^{-1}s^{-1}, respectively [Fie86, Zha93b]. The values given in Table 1 are "actually" valid for the cerium-catalysed BZ system.

The reaction 7 is responsible for the induction period of the uncatalyzed reaction (without ferroin) and the possible mechanism was proposed in [Ada04],

(7.1) $BrO_3^- + 2 H^+ \leftrightarrow H_2BrO_3^+$

(7.2)
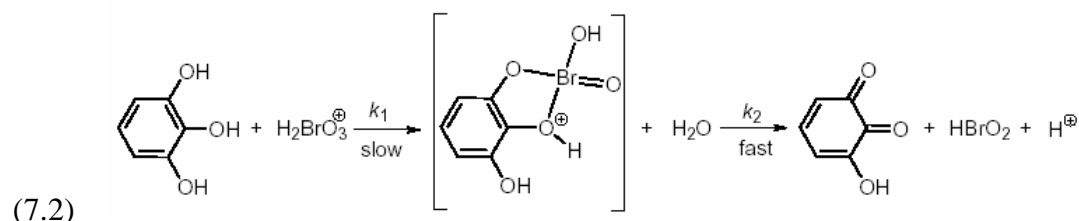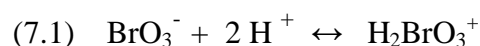
Dutt [Dut02] proposed that complex and aperiodic oscillations in the ferroin catalyzed gallic acid (GA, 3,4,5-trihydroxybenzoic acid) reaction in a CSTR are presumably due to coupling of the uncatalyzed component dominated by gallic acid and the catalyzed component dominated by ferroin that can be described in the same way as that for pyrogallol [Gil92, Sri98b], i.e. the catalyzed step 9f (see Table 1) is coupled to the uncatalyzed step *B2.1* to enhance the autocatalytic production of $HBrO_2$. The stoichiometric reaction [Dut02]:

(E) $6ferriin^{3+} + BrPG$ (from reaction D) $+ 3H_2O \rightarrow 6ferroin^{2+} + Br^- + Q + 7H^+$
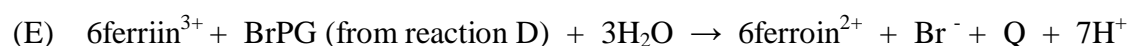
combines with the uncatalyzed steps: 8 (see Table 1), *C2*, and the bromination reaction of PG (the reaction D) to accelerate the regeneration of bromide ions to switch the system from low bromide concentration state (process A) to high bromide concentration state (process C) and thus the oscillatory cycle is then established.

Tlaczala and Bartecki [Tla84] studied effects of Mn^{2+} on chemical oscillations in the closed $PG-BrO_3^- -H_2SO_4$ system. They found that one oscillating system undergoes transformation from pure PG-uncatalyzed system into a Mn^{2+}- catalysed system (see also [Kör80]) via double oscillations that arise from mutual interactions between two oscillators, as shown in Fig. 18. The number of double oscillations decreases with the increasing Mn^{2+} concentration and increases with the increasing PG concentration [Tla83].
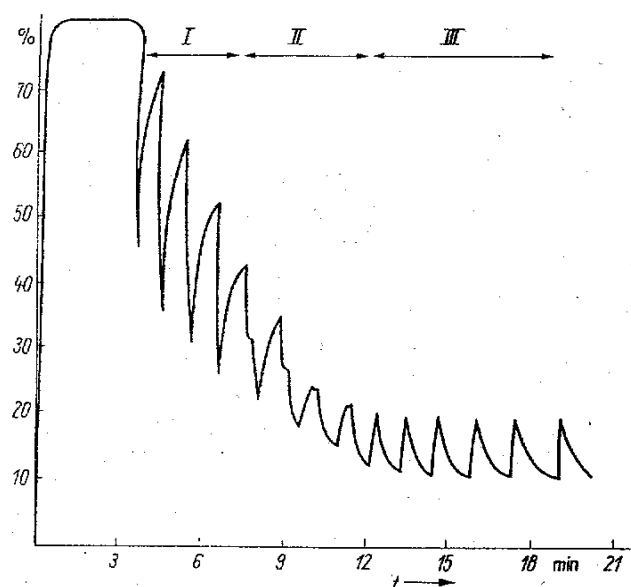
Figure 18: Oscillations observed in the well-stirred batch Mn^{2+}-PG-BrO_3^--H_2SO_4 system at the room temperature (from [Tla84]). [PG] = 0.050 M, [$KBrO_3$] = 0.104 M, [H_2SO_4] = 1.97 M, and [$MnSO_4$] = 2.5 mM. % and t denote the percentage light transmittance at 470 nm being due to the light absorption of Mn^{3+} and time in minute, respectively. Phase I : the uncatalysed system: PG-BrO_3^--H_2SO_4, is characterized by high amplitudes and rather short oscillatory periods, phase II: the coupled uncatalysed and catalysed systems showing double oscillations, and phase III: the catalysed system Mn^{2+}- PG - BrO_3^- -H_2SO_4 having low amplitudes and longer oscillatory periods.

2.4.3 Properties and behaviour of waves in the coupled system

The mechanism of wave propagation can be interpreted analogously as the classical Belousov-Zhabotinsky spatial system [Fie72b]. The development of trigger waves [Ada04, Orb80] is due to the oxidative bromination of pyrogallol coupled with diffusion. When the reagents (pyrogallol, bromate, and sulfuric acid) are mixed, the solution immediately changes to a dark colour (red-brown). This dark colour gradually becomes lighter to yellow. At a certain phase of the colour change light yellow pacemaker centers appear from which chemical waves start to propagate into a region of darker colour (orange-brown). Available color photographs can see in [Ada04]. In the dark region the bromide concentration is above a critical value and here bromate reacts with bromide and the stoichiometry of the reaction is generated by the net reaction U1:

(U1) = (A1)+(A2): $BrO_3^- + 2Br^- + 3H^+ \rightarrow 3HOBr$.
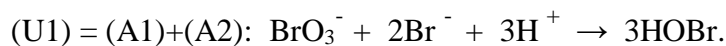
At the front of the moving band the concentration of bromide ion drops below a critical value. The autocatalytic formation of $HBrO_2$ is switched on, and this is realized by the net reaction:

(U2) = 2(B1)+4($B2.1$)+(B3): $BrO_3^- + 4PG + H^+ \rightarrow HOBr + 4PG^{\cdot} + 2H_2O$.

At the boundary of the reducing and the oxidizing zone a sharp concentration gradient exists: the bromide concentration is at its minimum and the $HBrO_2$ is at its maximum. Species formed in reaction U2 undergo further reaction and regenerate bromide ion, the control intermediate in the net reaction U3:

(U3) = ($C1$)+($C2$): $HOBr + 2PG^{\cdot} \rightarrow 2Q + Br^- + H^+ + H_2O$.

By the accumulation of bromide ions, the reaction U1 is switched on again; a new wave can start to propagate from the pacemaker center. The propagation velocity of this trigger wave [Orb80] is 5-6 mm/min for initial compositions: 2.0 M H_2SO_4 , 87 mM $NaBrO_3$, and 52 mM PG at the room temperature of 24-25 ^{o}C. Stationary mosaic pattern was also observed in an unstirred thin film of solution [Ada04, Orb80].

A detailed investigation of the wave behaviour in the PG system with ferroin has been done recently. Sridevi et al. [Sri98a] performed the experiments at 30.0 ± 0.1 ^{o}C and found target waves (the green coloured oxidizing bands move into the bright red coloured reduced medium) and spiral waves in the petri dish.

Depending upon the initial concentrations of reactants, they have the following properties:
1. The whole solution undergoes bulk colour change (red to green and vice versa), these are phase waves.
2. Waves are generated periodically with a constant velocity around a heterogeneous center, these are trigger waves.
3. The medium developed phase waves for the first few minutes and subsequently formed trigger waves brought about by diffusion.

(a)
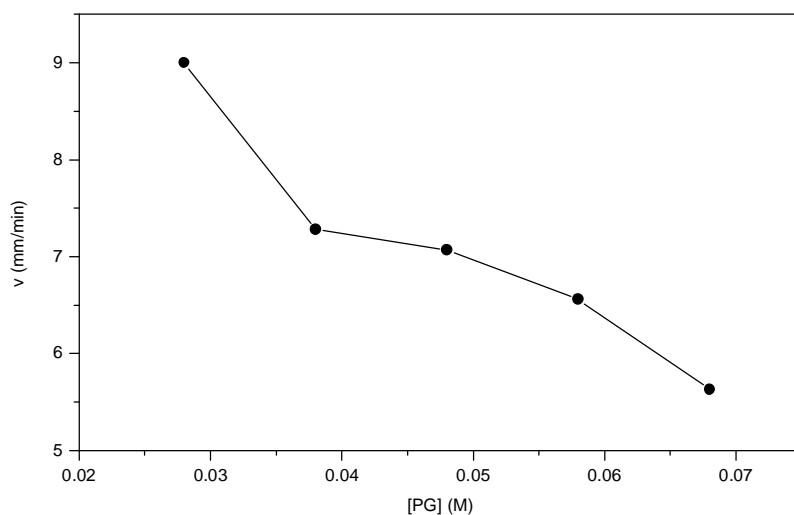
(b)
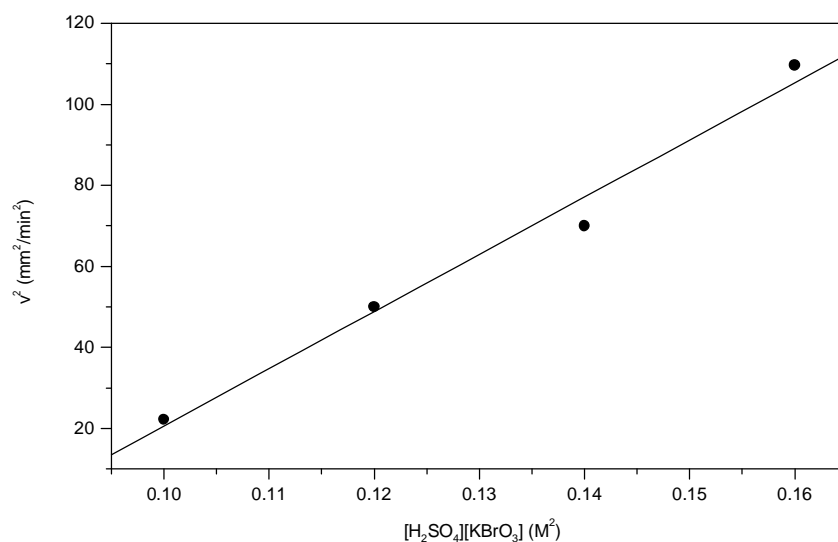
Figure 19: Plots of the wave velocity v dependences on the initial reactant concentrations (extracted and adapted from [Sri98a]). Initial concentrations of reactants: (a) $[H_2SO_4]$ = 1.0 M, [ferroin] = 1.5 mM, $[KBrO_3]$ = 0.12 M, [PG] is varied. v increases as [PG] decreases. (b) $[H_2SO_4]$ = 1.0 M, [PG] = 0.048 M, [ferroin] = 1.5 mM, $[KBrO_3]$ is varied (see details in the text).

4. As in the case of classical malonic acid-ferroin-sulphuric acid-bromate system, the wave velocity depends strongly on the concentration of acid and bromate, and is almost independent of the ferroin concentration [Fie74b, Woo85].

5. The wave velocity depends markedly on the pyrogallol concentration (Fig. 19a), see also in [Ada04] (without ferroin). This is because pyrogallol is also involved in the generation of $HBrO_2$ which is not the case with malonic acid [Fie74b, Nag89a, Woo85].

The kinetics of the classical BZ reaction in solution is reflected by the velocity of circular trigger waves, v, which is mainly determined by the autocatalytic reaction step coupled by diffusion. Based on the slope of the linear dependence in Fig. 19b, the $HBrO_2$ autocatalysis rate constant k of the reaction 3f in Table1 in liquid aqueous solution at 30.0 ± 0.1 ^{o}C, was (49.02 ± 4.65) $M^{-2} s^{-1}$ obtained from $v^2 = 4kD_{HBrO2}[H^+][BrO_3^-]$ (see Eq. 27) by using $D_{HBrO2} = 2 \times 10^{-5}$ $cm^2/s = 0.12$ $mm^2 min^{-1}$.

Recently, Hamik et al. [Ham01] studied in more detail another UBO system with 1,4-cyclohexanedione (1,4-CHD) as substrate including ferroin as the catalyst. They showed that oxidation waves in this modified reaction obey anomalous dispersion relation that is not known from the classical BZ reaction, as shown in Fig. 20. This behaviour could arise from the chemical reactions taking place in the refractory tail of the wave, i.e. the inhibiting action of ferriin in the intermediate vicinity of the $HBrO_2$ pulse and the activating effect of a 1,4-CHD derived intermediate (1,4-dihydroxybenzene) produced continuously but brominated and oxidized to 1,4-benzoquinone in an autocatalytic manner at a farther distance from the $HBrO_2$ pulse.
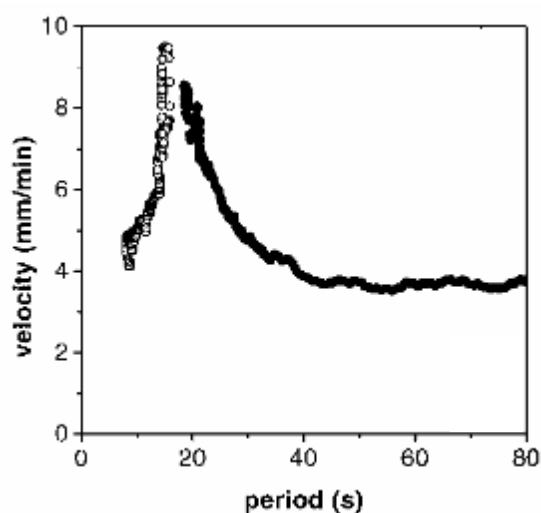
Figure 20: Experimental anomalous dispersion relation curve (non-monotonic non-oscillatory type) observed in the BZ reaction with 1,4-CHD as substrate (from [Ham01]). The velocity of the solitary wave is 4.0 mm/min.

Chapter 3

Experimental procedures

3.1 Capillary reactor

The capillary reactor used in the experiment is made of Plexiglas (see Fig. 21). Its components are the following:

Abbreviation	Description
GC	Rectangular quartz glass (Suprasil) cuvette with inner cross section 0.5×0.5 mm^2, outer cross section 6×6 mm^2, and length 84 mm. Custom made by Hellma® company.
EC	Electrolytic cells with circular diameter of 3 cm and 4.5 cm high.
FC	Filling chambers
SP	Silicone packings
TM	Hydrophobic microporous ion permeable membranes made of Teflon, $(-CF_2-CF_2-)_n$, the electrical conductivity $\kappa = 10^{-11}$ µS/cm at 298 K [Old94]. This membrane prevents possible hydrodynamic flow, the products of electrolysis do not affect the reaction medium inside the cuvette.
PE	Planar platinum electrodes, 3×3 cm^2 and 0.3 mm thick. The distance between two electrodes (d) is 16.0 cm.
ST	Plexiglas stoppers. Their sizes used are about 0.9 cm and 2.9 cm long.
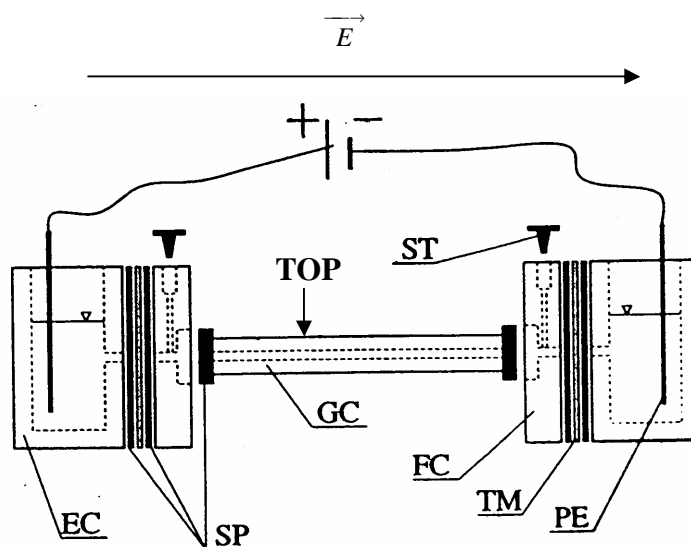
Figure 21: Drawing showing the components of the capillary reactor (adapted from [Šev99], see details in the text). $\overrightarrow{E}$ denote the electric field vector.

A counter-flux of oppositely charged ions which is attained by electrophoresis including diffusion and electro-migration may also create non-equilibrium conditions suitable for instability and non-linear phenomena when the reactant is, for example, the aqueous BZ medium. Application of a voltage between electrolytic cells (EC) can cause charged species to enter the reaction zone in the capillary cuvette (GC) at a constant controlled rate.

One of the practical problems encountered in electro-separations is the generation of heat from dissipation of energy in the resistive medium. The generation of heat (Joule heating) is given by

$$H_J = IU = I^2 R, \tag{31}$$

where H_J is the electrical power in W or J/s, I the electrical current through the medium in Ampere (A), U the electrical potential difference applied in Volt (V), and R the electrical resistance of the medium in Ohm (Ω). The current and the electric field strength $E = U/d$ in V/cm are related via the electrical conductivity κ in S/cm or $\Omega^{-1}cm^{-1}$ of the medium by Ohm's law (U = IR, see also APPENDIX 2B):

$$\kappa = I/E\mathtt{A} \, , \qquad\qquad\qquad\qquad\qquad\qquad\qquad (32)$$

where $\mathtt{A}$ is the inner cross section area of the medium (i.e the capillary cuvette).

The higher the conductivity of the medium, the more difficult capillary electrophoresis becomes because highly conductive solutions mean a higher current density $I/\mathtt{A}$ for a given field strength E (see Eq. 32), and the heat load on the system increases, as there is a square dependence on the current (see Eq. 31). Heating in electrophoresis causes changes in viscosity and density of the medium. The possibility to remove heat from electrophoretic systems by cooling is severely limited, by the maximum capacity of these systems in terms of how large or thick a system can be. In the BZ medium, two important factors exist which act against electrical field effects being observed [Fee81], (a) the high conductivity (and current) of the solution causes the disruption of chemical kinetics of the systems due to heat and evaporation; (b) the relatively high wave velocity compared to a typical ionic drift velocity induced by field of reasonable strength.

The electrodes are typically constructed from platinum. One result for BZ medium is the water electrolysis reactions:

Cathode (-): $2H_2O + 2e^- \rightarrow 2OH^- + H_2$
Anode (+): $H_2O \rightarrow 2H^+ + 0.5O_2 + 2e^-$.
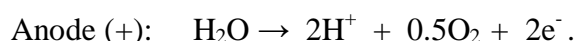
The hydrogen gas produced at the cathode can be hazardous, especially because it is in the vicinity of an electrode that is also producing heat. For this reason, electrode chambers are usually open to the atmosphere so that gases can vent. The negative electrodes produces base OH^- and the positive electrode produces acid H^+ so that there is a possibility of an acidity (and also the temperature) gradient throughout the electrophoresis medium.

3.2 The solution mixtures and their preparation

The following stock solutions were prepared by dissolving weighted amounts of chemicals in 0.75 M H_2SO_4 (diluted from 5.0 M H_2SO_4 Riedel-de Haën standard solution): 1.0 M $NaBrO_3$ (F.W. = 150.90, Fluka; Riedel-de Haën (purity min. 98%)), 1.0 M pyrogallol (PG, M.W. =

126.11, Merck), 0.025 M ferroin (using 0.3712 ± 0.0001 g 1,10-phenanthroline.H_2O (F.W. = 198.23, Fluka) and 0.1738 ± 0.0001 g $FeSO_4.7H_2O$ (F.W. = 278.02, Merck) for a 25 ml solution). All reagents were of the highest commercially available grade (purity above 99 %) and were used without further purification. All stock solutions were freshly prepared in deionized water with an electric conductivity $\kappa = 0.055$ µS cm^{-1} at 22 ± 1 °C.

Solution Mixture Number	[H$_2$SO$_4$] (M)	[NaBrO$_3$] (M)	[PG] (mM)	[ferroin] (mM)	[PG] / [ferroin]
I (*reference*)	0.15	0.10	8	0.5	16
II	0.15	0.10	5	0.5	10
III	0.15	0.10	11	0.5	22
IV	0.15	0.10	14	0.5	28
V	0.15	0.10	8	0.28	28.6
VI	0.15	0.10	8	0.8	10

Table 2: Initial concentrations of chemicals in the solution mixtures used for study.

The concentrations of reactants in all solution mixtures used in this study are given in Table 2. They have the ionic strength $\Gamma \approx 0.55$ M (PG is considered as a non-ionic species) and the conductivity $\kappa \approx 0.11$ S cm^{-1} for the reference solution mixture (see also APPENDIX 2B). They are prepared for each experimental run mostly at room temperature of 22 ± 1 °C from fresh stock solutions. The main purpose of this study is to see how the two catalysts concentrations (PG and ferroin) affect the behaviour of waves with and without an electric field.

Stock Solution	I	II	III	IV	V	VI
(a) 1.0 M NaBrO$_3$ (µl)	5,000	5,000	5,000	5,000	5,000	5,000
(b) 1.0 M PG (µl)	400	250	550	700	400	400
(c) 0.75 M H$_2$SO$_4$ (µl)	3,600	3,750	3,450	3,300	4,040	3,000
(d) 0.025 M ferroin (µl)	1,000	1,000	1,000	1,000	560	1,600
Total (ml)	10	10	10	10	10	10
H$_2$O (ml)	40	40	40	40	40	40

Table 3: Partial volumes of the stock solutions withdrawn by using automatic pipettes (Gilson Pipetman P) for the 50 ml solution mixture.

The general method for the preparation of the solution mixture was as follows (see Table 3): first, required volumes of 1.0 M NaBrO$_3$ and 1.0 M PG were mixed together in a 50 ml volumetric flask. When the colour had changed from dark red-brown to clear yellow (but clear orange for IV) after a time t_1, then required volumes of 0.75 M H$_2$SO$_4$, 0.025 M ferroin,

and the deionized water were added in this order. The colour immediately changed from clear yellow to the colours of oxidized state, i.e. blue (for II, VI) or blue-green (for I and sometimes III also) or green (for III, IV, V) depending on [PG] and [ferroin]. After a time interval t_2, when the colour had changed to red-brown again (reduced state), the solution mixture was immediately put into the well-cleaned capillary reactor. Note that this red-brown colour later can change again to red-orange, when the solution mixture is left for a certain time which, however, was not measured. After putting the whole reactor, including the solution mixture, into the water bath at 15 ^{o}C (the levels of the solution mixture in both electrode chambers should be approximately the same and should be under the level of water in the water bath), the oxidation pulse waves spontaneously generated at both ends of the cuvette, caused by some heterogeneous centers and some surface defects inside the filling chambers, with the initiation time t_3, and then propagated into the cuvette. Times t_1, t_2, and t_3 can be longer or shorter from one batch experiment to another. This strongly depends on many factors, e.g. the room temperature, mixing and aging of the stock solutions, oxygen-sensitivity of the PG solution, the purity of chemicals. Approximate ranges of t_1, t_2, and t_3 for different solution mixtures are given in Table 4.

Solution Mixture Number	I	II	III	IV	V	VI
t_1 (s)	13-17	8-12	16-20	25-30	13-17	13-17
t_2 (min)	4	6-7	2-3	(immediately)	2	3-5
t_3 (min)	10-20	6-14	22-34	35-45	16-24	4-8

Table 4 : Approximate ranges of t_1, t_2, and t_3 of the solution mixtures.

It should be noted how to clean the reactor and activate the Teflon membrane inside. First, rinse the whole reactor with "diethyl ether" 2 times and then with "absolute ethanol" 2 times. Finally, rinse the whole reactor with "the deionised water" 3 times. Let the deionised water stay in the reactor overnight before the experiments to make sure that the membranes are saturated with the water. The glass capillary should be cleaned sometimes by putting it into concentrated sulphuric acid, let it stay in overnight, and rinse it with the deionised water several times before fitting it to the reactor.

3.3 Experimental set-up and methods

The experimental set-up including the capillary reactor (see Section 3.1) is the same as described in [Šev99]. The whole reactor including the solution mixture was bath-thermostated at 15 ^{o}C (Julabo LABORTECHNIK F12-MV Digital Refrigerant).

Figure 22 : Experimental set-up. See details in the text.

The cuvette was illuminated from the bottom of the water bath made of Plexiglas by a light source: Hama 1634 White Light Box (2 x 15 W), illumination area 3 cm x 10 cm. To avoid the disturbance from the external light source, the experiments were always performed in the dark room. Wave propagation in the cuvette was followed from the top (see Figs. 21 and 22) by measuring the difference in the transmitted visible light absorption between ferroin (the reduced part) and ferriin (the oxidized part) of the wave at the wavelength $\lambda = 490$ nm (green , see also APPENDIX 1B) by utilizing optical glass interference filter (SCHOTT 50 mm in circular diameter, 6 mm in thickness, about 47 % transmittance at $\lambda = 490$ nm) providing maximum contrast between the reduced region and the oxidized region of the wave and was monitored by a Charge Coupled Device (CCD) camera (Hamamatsu C3077) with a spatial resolution of about 27 μm per pixel. The recorded images were digitized at rates of either 3 s/frame or 5 s/frame by a frame grabber card (Data Translation, DT 3155) controlled by the LabVIEW (National Instruments Corp., version 5.1) image acquisition software. The images were further processed and analyzed by programs developed in IDL (Interactive Data Language, Research Systems Inc., version 5.2) in order to calculate the propagation velocities and evaluate changes of longitudinal wave profiles in an applied electric field (see also APPENDIX C).

To investigate effects of an electric field on the waves two sets of experiments were performed. In the first set, the wave was allowed to propagate about 3 min without the electric field being switched on. Then a constant voltage was applied to the platinum electrodes immersed in the reaction solution in the electrode chambers, and the propagation of the wave towards either the positive or negative electrode was recorded for another 3 min. From these measurements the dependence of the wave velocity on the electric field intensity was determined. In the second set of experiments, the wave was again allowed to propagate about 3 min without electric field and then the constant voltage was switched on with the positive electrode facing the wave. After the wave was allowed to propagate another 3 min towards the positive electrode, the polarity of the electrode was changed and the wave was further followed. In both sets of experiments, only the first wave entering the cuvette was subject to observation. Voltages up to 150 V were examined.

For the evaluation of the electric field effects the following definitions are used throughout the text (see Fig. 21): a negative field means that the wave propagates towards the positive electrode (in the opposite direction to the electric field vector). A field is positive if the wave propagates towards the negative electrode (in the same direction as that of the electric field vector). The magnitude of the electric field intensity (E) was calculated as $E = U/d$, where U is the applied voltage (in V), and d is the fixed distance between the electrodes, d = 16.0 cm. The current (I in mA) passing through the system was measured (Voltcraft Digital Multimeter MXD-4660A) during each experimental run and was found to be constant at each voltage.

In experiments on multiple reversals (Section 4.3), the same experimental set-up and capillary reactor are used. The reacting media for this study are solution mixtures: I and III to see the role of pyrogallol concentration. At the beginning of each experiment, the propagation velocity at zero field is evaluated. The effects of switching the polarity of the electric field is then investigated as follows: an observation window of size d is applied on the cuvette by selecting the corresponding pixel area for image recording (a frame grabber board 768 pixels (2.07 cm) in width or X-direction and 576 pixels (1.56 cm) in height or Y-direction, area ≈ 3.23 cm^2). When the first wave enters the observation window, an electric field of the chosen magnitude is switched on with the positive electrode facing the first wave. At the same time the grabbing of images starts with a digitization rate of 5 s/frame. When the wave reaches the end of the observation window, the polarity of the electric field is reversed within 2 s by a home-made switch (Moeller easy 618-AC-RC) connected to the power supply (Elektro-Automatik EA-PS 7150-004 A, maximum voltage 150 V and current 400 mA). If the wave reversal occurs, the propagation of the reversed wave is followed further. The reversed wave propagates again towards the positive electrode, and when it reaches the end of the observation window, the polarity of the electric field is again reversed. The changes of the polarity of the electrodes continue until the reversed wave is annihilated upon changing the field polarity. The window sizes d = 0.4, 0.8, 1.2, 1.6, and 2.0 cm are chosen for this study. The voltages used are in the range from 50 to 120 V.

Chapter 4
Experimental results

4.1 Field-free waves

The waves entering the cuvette in the absence of an electric field were observed to have either planar, U-, or V-shaped wave front, as shown in Fig. 23. We will focus in more details on these shaped wave fronts in Section 4.4 of this chapter. The propagation velocities of the planar wave front in zero field for different solution mixtures are given in Table 5.

(a)

(b)

(c)
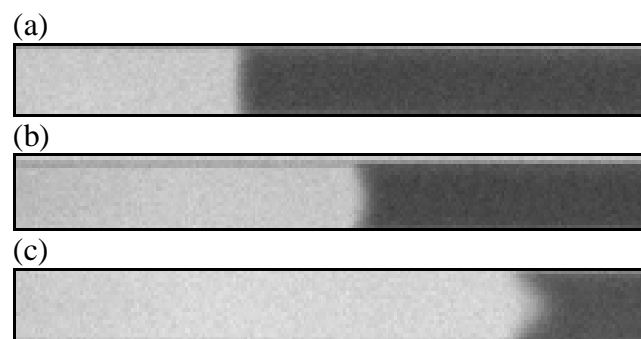
Figure 23: Three different shapes of the wave front observed in the "reference" solution mixture in the absence of an applied electric field : (a) planar, (b) U-shape, (c) V-shape. Waves propagate from left to right. Dark region corresponds to the unreacted reduced medium with low ferriin concentration, light region corresponds to the oxidized region with high concentration of ferriin. The portion of the cuvette shown is 0.6 cm in length.

Data given in Table 5 show that the propagation velocity for a given excitability determined by $[H_2SO_4] = 0.15$ M and $[NaBrO_3] = 0.10$ M is almost independent of the ferroin concentration but depends on the pyrogallol concentration as we can clearly see from the solution mixture I compared to the solution mixtures II and IV.

Solution Mixture Number	[PG] (mM)	[ferroin] (mM)	v_0 (mm/min)
I (*reference*)	8	0.5	0.69 ± 0.09 (79)
II	5	0.5	0.95 ± 0.09 (15)
III	11	0.5	0.62 ± 0.09 (32)
IV	14	0.5	0.34 ± 0.02 (3)
V	8	0.28	0.72 ± 0.06 (13)
VI	8	0.8	0.76 ± 0.07 (8)

Table 5: Average field-free propagation velocities v_0 of the planar wave front in different solution mixtures. The number in parenthesis is the number of experiments done.

Ferriin concentration profiles of the first planar waves without an applied electric field in the solution mixtures of different [PG] and [ferroin] are shown in Fig. 24. The slope of the wave front after excitation (i.e. the sudden growing part of the grey level) does not change significantly with [PG] and [ferroin]. The refractory tail of the wave drops faster (i.e the decaying part of the grey level is steeper) and the wave propagates slower when [PG] is increased. The system with [PG] = 5 mM recovers the slowest and forms the broadest excitation region but still the front propagates faster. The amplitude of the wave increases when [ferroin] is increased. The grey or [ferriin] level of the excitation region of the wave in the solution mixture consisting of [ferroin] = 0.28 mM is slightly higher than the solution mixtures consisting of [ferroin] = 0.5 mM and 0.8 mM and there is no significant difference in the slope of the refractory tail of the wave when [ferroin] is increased.

(a)
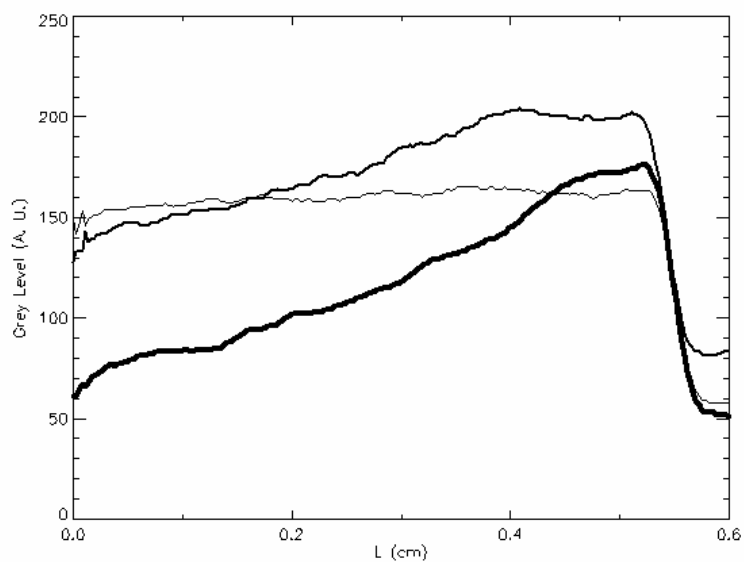
(b)
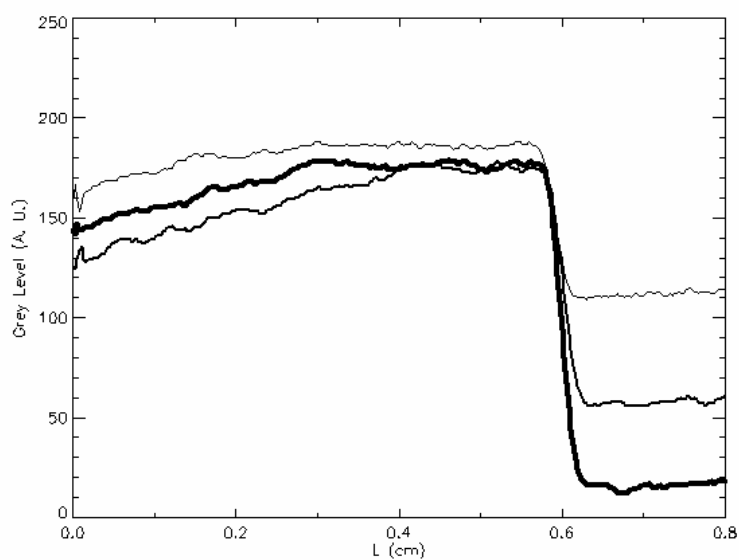
Figure 24: Ferriin concentration profiles represented by grey levels in Arbitrary Units (A. U.) of the field-free planar waves. Solution mixtures consist of $[H_2SO_4] = 0.15$ M, $[NaBrO_3] = 0.10$ M, and varied [PG] and [ferroin]. L denotes the portion of the cuvette in cm.

(a) [ferroin] = 0.5 mM, [PG]: 5 mM (thin line), 11 mM (medium line), and 14 mM (thick line).

(b) [PG] = 8 mM, [ferroin]: 0.28 mM (thin line), 0.5 mM (medium line), and 0.8 mM (thick line).

4.2 The interaction of an electric field with waves

4.2.1 The measured velocity response to the electric field intensity

The effects of applied electric fields on the propagation velocities of the waves for all solution mixtures were investigated in the range of electric field intensities from –9.38 Vcm^{-1} to +1.88 Vcm^{-1}. The data are given in Table 6.

U (V)	E (V/cm)	v_E (mm/min)				
		I (*reference*)	II 5mM PG	III 11mM PG IV {14mM PG}	V 0.28mM ferroin	VI 0.8mM ferroin
+30	+1.88	SA	SA	SA	SA	SA
+15	+0.94	SA	No data	{No data} No data	No data	No data
+10	+0.62	0.5 ± 0.11 (6)	0.86 ± 0.09 (3)	{ No data } 0.48 ± 0.05 (5)	0.52 ± 0.06 (3)	0.64 ± 0.11 (2)
+5	+0.31	0.64 ± 0.1 (4)	No data	{ SA } No data	No data	No data
-5	-0.31	0.88 ± 0.04 (2)	No data	{No data} No data	No data	No data
-10	-0.62	0.87 ± 0.07 (7)	1.02 ± 0.08 (6)	{No data} 0.76 ± 0.07 (6)	0.89 ± 0.02 (4)	0.84 ± 0.09 (4)
-15	-0.94	0.9 ± 0.1 (5)	No data	{0.56 ± 0.01 (2)} No data	No data	No data
-30	-1.88	1.12 ± 0.1 (5)	1.16 ± 0.11 (5)	{No data} 0.97 ± 0.05 (4)	1.14 ± 0.04 (4)	1.02 ± 0.09 (3)
-50	-3.12	1.31 ± 0.1 (5)	1.27 ± 0.12 (5)	{0.84 ± 0.02 (2)} 1.12 ± 0.04 (7)	1.29 ± 0.07 (2)	1.14 ± 0.13 (3)
-70	-4.38	1.24 ± 0.12 (16)	1.39 ± 0.1 (5)	{1.00 ± 0.04 (2)} 1.26 ± 0.03 (7)	1.38 ± 0.06 (2)	1.23 ± 0.11 (3)
-90	-5.62	1.39 ± 0.1 (15)	1.42 ± 0.09 (4)	{1.14 ± 0.06 (2)} 1.4 ± 0.07 (6)	1.47 ± 0.03 (3)	1.28 ± 0.1 (3)
-100	-6.25	1.29 ± 0.17 (9)	1.48 ± 0.1 (4)	{1.22 ± 0.04 (2)} 1.39 ± 0.05 (4)	1.48 ± 0.08 (3)	1.34 ± 0.08 (3)
-120	-7.5	1.5 ± 0.03 (6)	No data	{1.38 ± 0.06 (2)} No data	No data	No data
-150	-9.38	1.62 ± 0.15 (2)	No data	{1.37 (1)} No data {1.56 (1)}	No data	No data

Table 6: Average propagation velocities v_E of the planar wave front under electric field intensities E in different solution mixtures. The number in parenthesis is the number of experiments done. SA means wave Stopping and Annihilation

The average propagation velocities $v_E : X \pm \sigma_{n-1}$ given in Table 6 are calculated from

$$X = \frac{\sum_{i=1}^{n} x_i}{n} \tag{33}$$

$$s_{n-1} = \left[\frac{1}{n-1} \sum_{i=1}^{n} (x_i - X)^2 \right]^{1/2},$$

where X is average or mean, x_i is the ith data point, n is the number of data points or the number of experiments done, and σ_{n-1} is the standard deviation.
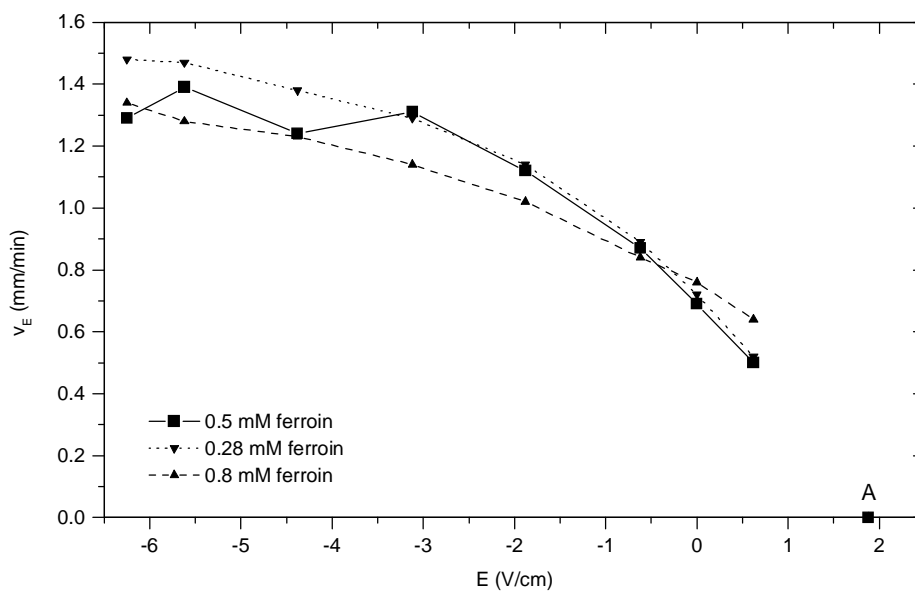
The dependencies of the propagation velocity on the electric field intensity for planar waves shown in Fig. 25 are non-linear. Waves in all solution mixtures are accelerated in the negative field. For field intensities lower than -3 V cm^{-1} the propagation velocities for planar waves in the solution mixture I (reference) reach an approximately constant value, that is 1.31 ± 0.06 mm/min, however, this saturation effect is no longer valid at very high field intensities. For example, in the experiment done at -300 V or -18.75 V/cm ($I \approx 5.8$ mA) we found that the propagation velocity of the wave increased from 0.64 mm/min to 2.55 mm/min. Positive electric fields decelerate the wave propagation and this deceleration is progressive upon increasing the value of the field intensity.

Intensities equal to or higher than 1.88 Vcm^{-1} were found to annihilate the planar waves. The existence of an annihilation field is strong evidence for a true electrical effect on the BZ waves. Feeney et al. [Fee81] proposed that the annihilation field E_A is obtained when ferriin of electrical mobility M is driven by the field at an ionic drift velocity ME_A equal to that of the field-free propagation velocity of the wave v_0. We estimate theoretical E_A ranges by using M calculated from Eq. 7 at 25 ^{o}C and extreme dilution in aqueous solution, i.e. 0.0007041 cm^2 V^{-1}s^{-1}, and using v_0 given in Table 5 we obtain theoretical E_A ranges for solution mixtures, they are **I:** 1.63 ± 0.21 V/cm; **II:** 2.25 ± 0.21 V/cm; **III:** 1.47 ± 0.21 V/cm; **IV:** 0.80 ± 0.05 V/cm; **V:** 1.70 ± 0.14 V/cm; **VI:** 1.80 ± 0.16 V/cm. We can see that experimental values of E_A given in Table 6 lie closely to the theoretical E_A ranges.

(a)
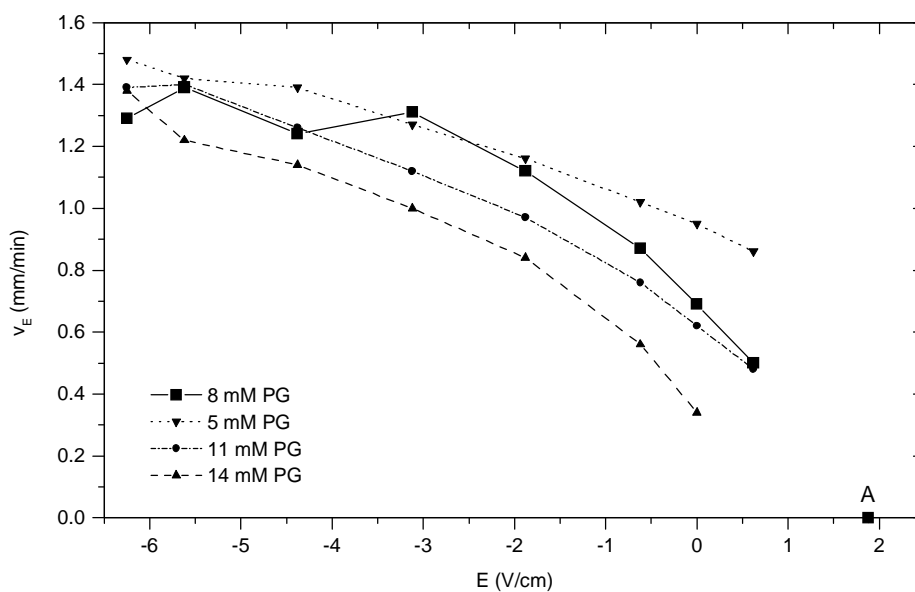
(b)

Figure 25: The dependences of the average propagation velocity v_E on the electric field intensity E plotted from the data in Table 6 for planar waves in different solution mixtures: (a) for [ferroin] = 0.5 mM, different [PG]; (b) for [PG] = 8 mM, different [ferroin]. Point A denotes the annihilation field intensity, beyond which planar waves do not exist. At A = + 0.62 V/cm for solution mixtures IV (14 mM PG) was also observed.

4.2.2 The determination of the mobility of the bromide ion

Following theoretical considerations (see Section 2.2) we approximated the measured dependencies of propagation velocities for planar waves in the reference solution mixture in the range of small electric field intensities from -0.94 V cm^{-1} to $+0.62$ V cm^{-1} by a linear relation $v_E = v_0 + \mu E$, where v_E and v_0 are the wave velocities with and without imposed field, respectively, as shown in Fig. 26. Generally, for a chemical excitable system, the quantity μ plays the role of an "effective mobility" in that the effect of a small field on the wave velocity is the same as if "all ions" had a mobility μ and the field-induced change in the velocity was just shifted by the ionic speed μE [Sch79]. In the work [Góm97, Vié96] the two-variable Oregonator model for the classical BZ reaction was considered to describe the chemistry, and it was shown that the quantity μ can be associated with the mobility of bromide ions. The measurement of the electric field dependence of the propagation velocity was suggested and tested on the BZ waves as a method to determine the mobility of the activator species $HBrO_2$ that is equal to the bromide ion mobility. They found that $\mu = (2.14 \pm 0.08) \times 10^{-4}$ cm^2 V^{-1} s^{-1} [Vié96] in a silica gel medium at 20 ^{o}C with $[H_2SO_4] = 0.17$ M, $[NaBrO_3] = [MA] = 0.15$ M, and $[ferroin] = 8$ mM ($\Gamma = 1.126$ M ≈ 2 times of Γ of the solution mixtures employed for this study) in the field intensity from -1 V/cm to $+1$ V/cm.
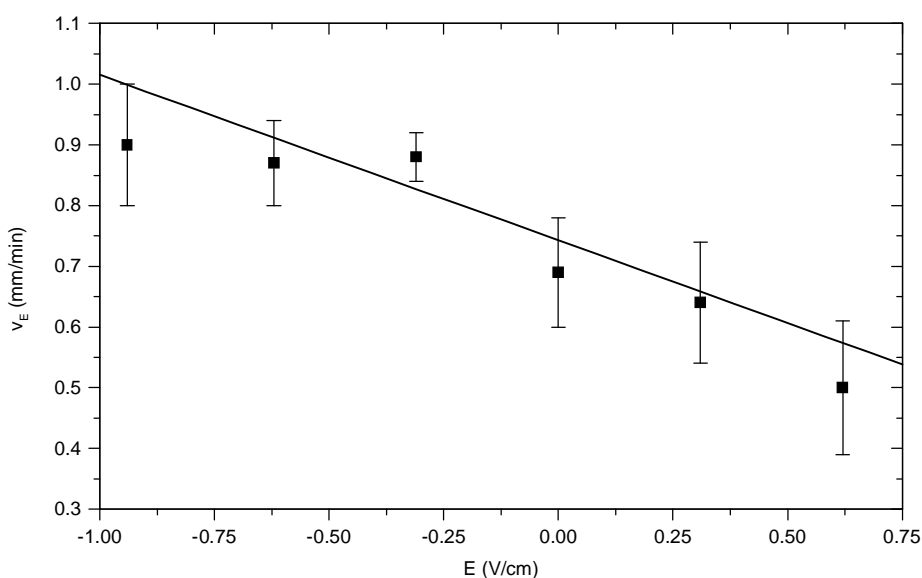
Figure 26: Approximation of the planar wave velocity dependence on small E by the linear relationship $v_E = v_0 + \mu E$. The correlation coefficient of the linear fit is 0.8791 (or linearity is 87.91%). Solution mixture I.

With the linear fit of the above equation to our velocity data for planar waves shown in Fig. 26, the value of bromide mobility in the reference solution mixture is $(4.54 \pm 1.23) \times 10^{-4}$ cm^2 V^{-1} s^{-1} (This value is slightly different from the value given in Table 7 below because of more data points.) and $D_{bromide\ ion} / T = (3.91 \pm 1.06) \times 10^{-8}$ cm^2 s^{-1} K^{-1} (calculated from Eq. 7). The experimentally found value is in the same order of magnitude as the tabulated value of bromide ion mobility in an infinitely diluted aqueous solution at 25 ^{o}C, i.e. 8.09×10^{-4} cm^2 V^{-1} s^{-1} [Atk98]. Considering that the ionic mobilities decrease with increasing concentration of ions (and also viscosity of the medium [Kuh00, Old94]) because the ionic interactions become more important [Ham98], the agreement between experimental and tabulated values is reasonably good.

Solution Mixture Number	[PG] (mM)	[Ferroin] (mM)	v_0 (mm/min)	$\mu_{bromide\ ion}$ (x 10^{-4} cm^2/V.s)	R
I (*reference*)	8	0.5	0.687 ± 0.002	4.954 ± 0.076	0.9999
II	5	0.5	0.943 ± 0.005	2.141 ± 0.149	0.9976
III	11	0.5	0.62	3.764	1
V	8	0.28	0.708 ± 0.006	4.903 ± 0.174	0.9994
VI	8	0.8	0.750 ± 0.01	2.634 ± 0.379	0.9898

Table 7: Bromide ion mobilities in different solution mixtures obtained from slopes of the linear relationship: $v_0 + \mu E = v_E$ in Section 2.2 at E = 0, -0.62, and +0.62 V/cm (data from Table 6). R is the correlation coefficient of linear regression.

Comparison with the reference solution mixture in Table 7 shows that either decreasing [PG] or increasing [ferroin] significantly decreases the bromide ion mobility. Possible causes are not only the ionic interactions but also the increasing viscosity of the solution mixture (however, was not measured) since the Stokes-Einstein relation [Kuh00, Old94] (see also Eq. 7) which accurately describes the behaviour of ions migrating through liquids having the viscosity coefficient η (in kg.m^{-1}s^{-1}) and it is given by

$$m_i = \frac{|z_i|e}{6pha_i} = \frac{s_i}{E},$$

(34)

where a_i is the hydration radius of the ith ion, i.e. the thickness of a sheath of water molecules surrounding the ion and e is the fundamental charge of electron. Calculated $a_{bromide\ ion}$ is ≈ 117 pm for $\eta_{pure\ water} = 8.937 \times 10^{-4}$ kg.m^{-1}s^{-1} [Old94] and the electrical mobility of bromide ion at 25 ^{o}C [Atk98] mentioned above.

4.2.3 Wave behaviour in the electric field

The effects of applied electric fields on the spatial longitudinal profile of the planar wave in terms of the intensity of the light transmitted through the cuvette are illustrated in Fig. 27. The wave propagates from left to right, converting the unreacted medium from the reduced state (low ferriin concentration) to the oxidized or excited state (high ferriin concentration) and then back to the reduced state in the refractory region.
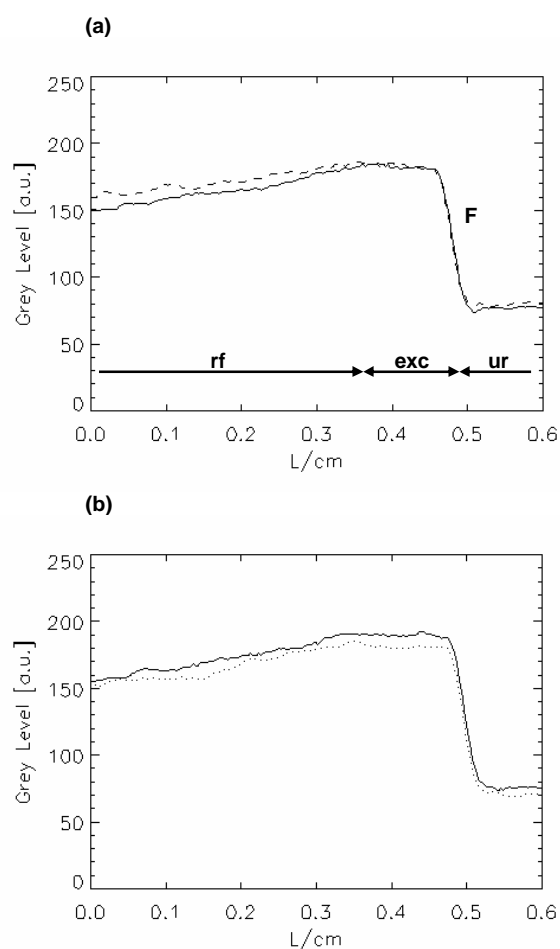
Figure 27: Comparison of the spatial longitudinal profiles of waves in the reference solution mixture propagating (a) in the zero (solid line) and negative (U = -10 V, E = -0.62 V cm^{-1}, I ≈ 0.2 mA, dashed line) and (b) in the zero and positive (U = 10V, E = 0.62 V cm^{-1}, I ≈ 0.2 mA, dotted line) fields. F denotes the wave front, the labels ur, exc, and rf denote the unreacted, excited and refractory regions, respectively. The grey level corresponds to the ferriin concentration.

The maximum of the ferriin concentration in the excited region was observed to be approximately the same for zero and negative fields and a little lower for positive fields. There was no significant difference observed in the slopes of the wave fronts. The most pronounced differences occur in the refractory regions: there the ferriin concentration of the wave propagating in the negative field lies above the ferriin concentrations of the zero and positive field waves. The difference between the level of the ferriin concentration of the zero and the negative field refractory regions was observed to be more significant at larger negative fields.
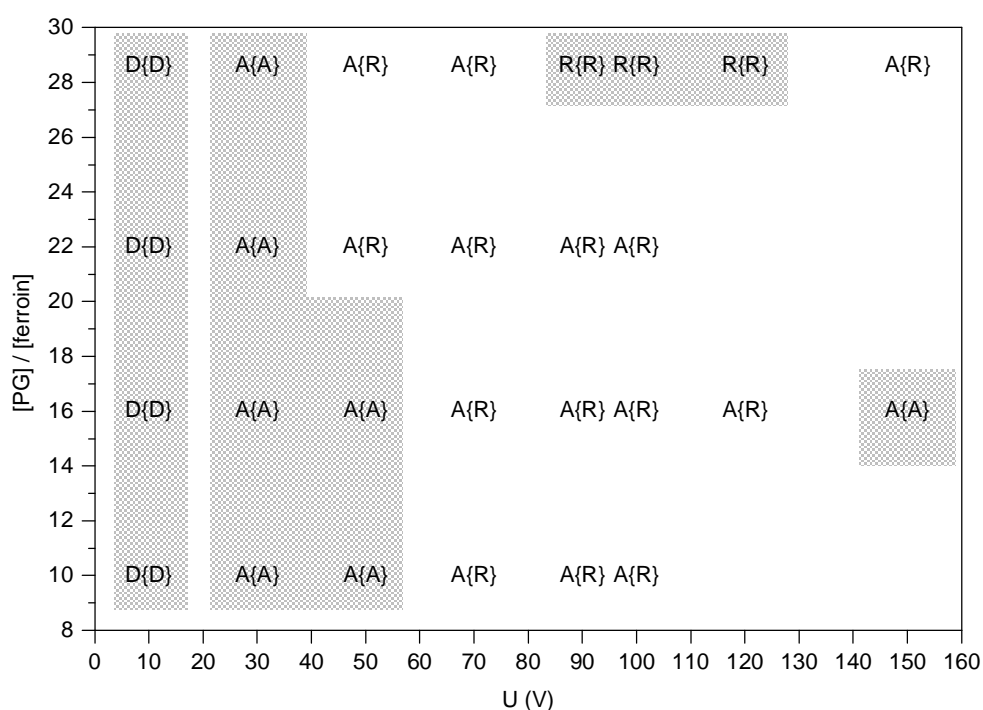
Figure 28: Phase diagram showing the observed dynamical phenomena induced by the positive electric field. D: Deceleration, A: Annihilation, and R: Reversal. Scenario 1: applying the positive field only. Scenario 2 {in brackets}: applying the negative field for the first 3 min and then changing the field polarity.

When a propagating wave is exposed directly to the positive field, one observes its slowing down or its annihilation depending on the magnitude of the electric field intensity. When we first expose the propagating wave to the negative field and then switch the polarity to the positive one then, after changing the polarity, the wave can also undergo a reversal of its direction of propagation. The changing of [PG] or [ferroin] affects the occurrence of the wave reversal in the positive field. As seen in Fig. 28, by increasing [PG] and keeping [ferroin] constant (0.5 mM) at [PG]/ferroin] = 22, the wave reversals can occur at low U (equal to or

higher than 50 V), while at lower U (30 V) the wave always annihilates without a new wave emerging from its refractory tail. By decreasing [ferroin] and keeping [PG] constant (8 mM) at [PG]/[ferroin] = 28.6, the wave reversal can occur without applying the negative field before, but U must be high enough (equal to or higher than 90 V but less than 150 V because we found that the scenarios: A{R} appear again at U = 150 V). Scenarios observed at [PG]/[ferroin] = 10 are the same as scenarios observed at [PG]/[ferroin] = 16 (the reference solution mixture). In addition, we do believe that the scenarios: A{A} would be the last scenarios observed again after the scenarios: A{R} in all solution mixtures at higher U because we observed the scenarios: A{A} in the reference solution mixture at U = 150 V, 200 V, 250 V, and 300 V. (It should be noted that wave annihilation for the scenario 2 has occurred in some cases, in some others wave reversal at an intermediate voltage of 50 V and 150 V occurred.) Positive electric field effects on the waves in the solution mixture IV were not studied in detail.

The process of wave reversal observed at U = 70 V or E = 4.38 V cm^{-1} is illustrated in the series of images of Fig. 29.1a and the corresponding spatial profiles of the wave (Fig. 29.1b). Time t = 0 shows the wave at the moment, when the field polarity was changed from negative to positive. Since the field used is above the annihilation value, the original wave vanishes, i.e. its front becomes more and more dispersed. At the same time the ferriin concentration in the refractory region decreases from the level it had in the negative field to the new level corresponding to the positive field (according to Fig. 27b). During this process, a new wave front emerges (at some time instant between t = 55 s and 155 s) in the refractory tail, close behind the excited region of the original wave. At time t = 155 s the front of a new wave is quite well defined and this new wave adopts progressively a "normal" spatial profile, as it propagates to the left. In fact, we can look at the process of reversing the direction of the wave propagation as a "back firing" of a new wave from the refractory tail of the original one that is simultaneously vanishing. A time-space plot showing reversal of the planar wave in the solution mixture V is illustrated in Fig. 29.2. Reversal occurs by direct application of the positive field intensity of 6.25 V/cm. The reversed wave propagates to the positive electrode , while the original wave annihilates.

(29.1)

(a)

(1) *t* = 0

(2) *t* = 55 s

(+) **(3)** *t* = 155 s **(-)**

(4) *t* = 305 s

(b)

(29.2)

Space (cm)

(+) **(-)**
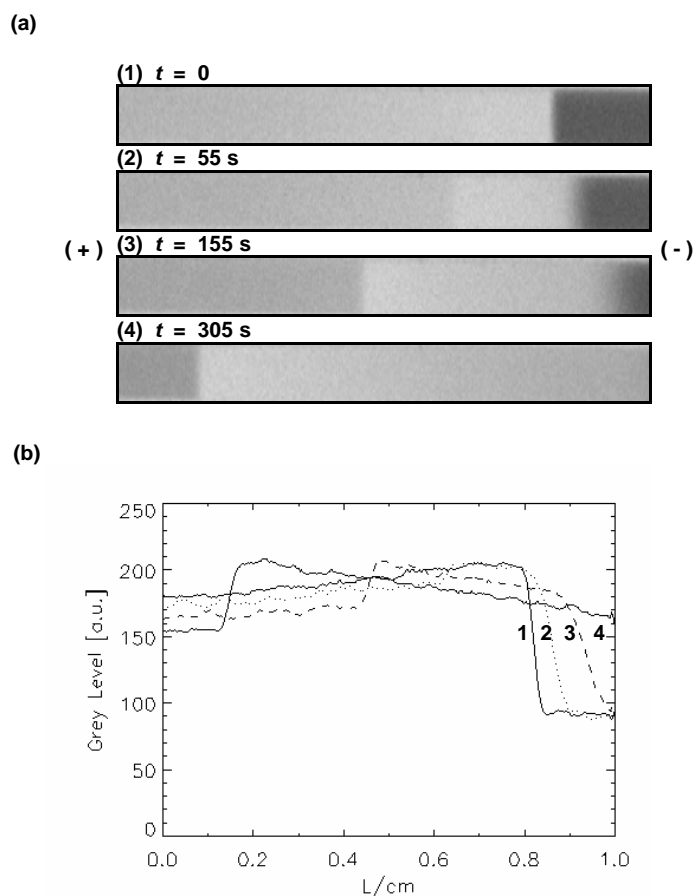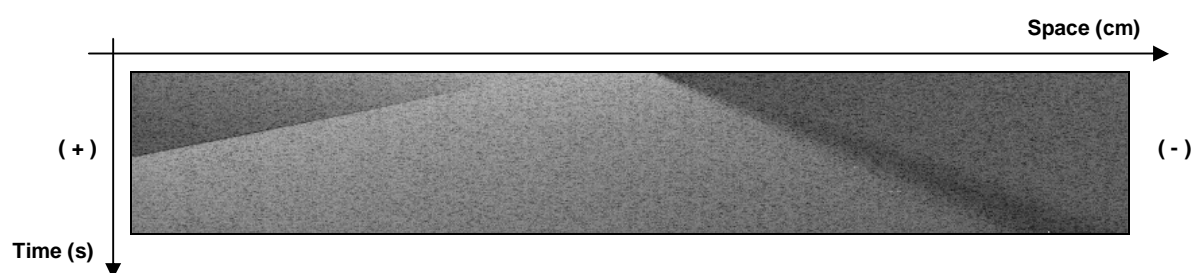
Time (s)

Figure 29: Reversal of the direction of wave propagation of the planar wave.

(29.1) The reference solution mixture at E = 4.38 V cm^{-1} (I $\cong$ 1.2 mA). (a) Time series of images, the portion of the cuvette shown is 1.0 cm. (b) Spatial profiles of ferriin concentration (expressed in grey level) corresponding to the images in (a).

(29.2) The solution mixture V at E = 6.25 V cm^{-1} (I $\cong$ 1.8 mA). Time-space plot is shown. Time runs from the top (0 s) to the bottom (595 s) of the figure. Space runs from the left end (0 cm) to the right end (2.0 cm) of the figure.

4.3 Effect of switching the field polarity: multiple reversals

In this section a perturbation to the planar wave in the form of the alternating electric field of very low frequency by switching the polarity of D.C. electric fields is studied. The summary of our results is given in Fig. 30.
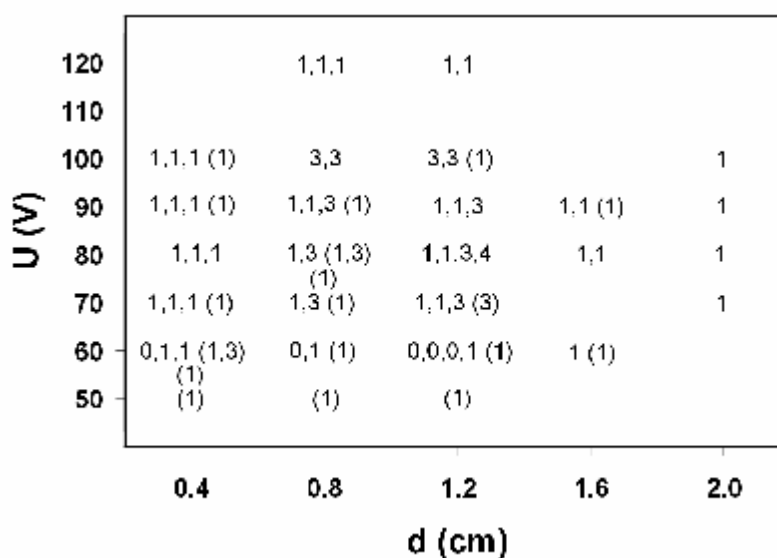
Figure 30: Number of reversed waves as a function of the window size (d) and the applied voltage (U) obtained in each experimental run for 8 mM PG (or 11 mM PG).

We found that multiple reversals of a wave are possible for a limited range of control parameters, i.e. the voltage applied and the size of the observation window. For the 8 mM PG reaction medium, the multiple reversals of a wave occur in observation windows of sizes 0.8 cm and 1.2 cm and in the range of voltages from 70 to 100 V. In either shorter or longer windows and at higher voltages only one reversal has been observed. The voltages $U \leq 50$ V cause the first wave to annihilate upon changing the electric field polarity, but no reversal occurs. The number of reversals is mostly three (10 experiments); in one experiment four reversals were observed. A slightly different range of values of the control parameters was found to be suitable to evoke multiple reversals for the 11 mM PG reaction medium. The range of voltages is narrower (from 60 to 80 V) and shifted towards lower values, whereas the range of observation window sizes is broader including the 0.4 cm window in addition to the 0.8 and 1.2 cm windows.

As we can see from Fig. 30 the number of reversals observed in different experimental runs under the same values of control parameters is not well reproducible, most likely due to the batch experimental arrangement. The consumption of reactants during a batch experiment is probably responsible for the limited number of reversals observed.

U (V)	I (mA)	H_J (mW)	v_U (mm/min)			
			0	1	2	3
0	0	0	0.69 ± 0.09 (57)	-	-	-
			0.60 ± 0.09 (20)	**-**	**-**	**-**
50	0.8	40	**1.11 ± 0.04 (3)**	**1.12 ± 0.15 (3)**	**-**	**-**
60	1.0	60	1.23 ± 0.12 (11)	1.11 ± 0.08 (5)	-	-
			1.18 ± 0.03 (5)	**1.22 ± 0.08 (5)**	**1.09 (1)**	**1.09 (1)**
70	1.2	84	1.19 ± 0.13 (9)	1.30 ± 0.14 (9)	1.14 ± 0.08 (2)	1.32 ± 0.15 (2)
			1.28 ± 0.04 (3)	**1.24 ± 0.10 (3)**	**1.15 (1)**	**1.15 (1)**
80	1.4	112	1.23 ± 0.10 (14)	1.34 ± 0.17 (14)	1.23 ± 0.02 (3)	1.41 ± 0.02 (3)
			1.32 ± 0.04 (2)	**1.36 ± 0.12 (2)**	**1.06 (1)**	**1.14 (1)**
90	1.6	144	1.37 ± 0.09 (13)	1.34 ± 0.15 (13)	1.23 ± 0.21 (2)	1.45 ± 0.23 (2)
			1.37 ± 0.14 (3)	**1.35 ± 0.12 (3)**	**-**	**-**
100	1.8	180	1.27 ± 0.16 (8)	1.37 ± 0.17 (8)	1.2 ± 0.17 (4)	1.5 ± 0.14 (4)
			1.46 ± 0.16 (3)	**1.52 ± 0.19 (3)**	**-**	**-**
120	2.1	252	1.5 ± 0.04 (5)	1.47 ± 0.14 (5)	-	-

Table 8: Average propagation velocities v_U (i.e. v_E) of the first waves (0) and the first (1), second (2), and third (3) reversed waves propagating to the positive electrode (i.e. in the negative field) for different applied voltages U. Medium with 8 mM PG and medium with 11 mM PG (bold numbers). [ferroin] = 0.5 mM. The number in parenthesis is the number of experiments (data) done. The approximate electrical current I is constant during the experiments and H_J denotes the electrical power or Joule heating (see Eq. 31).

(a)
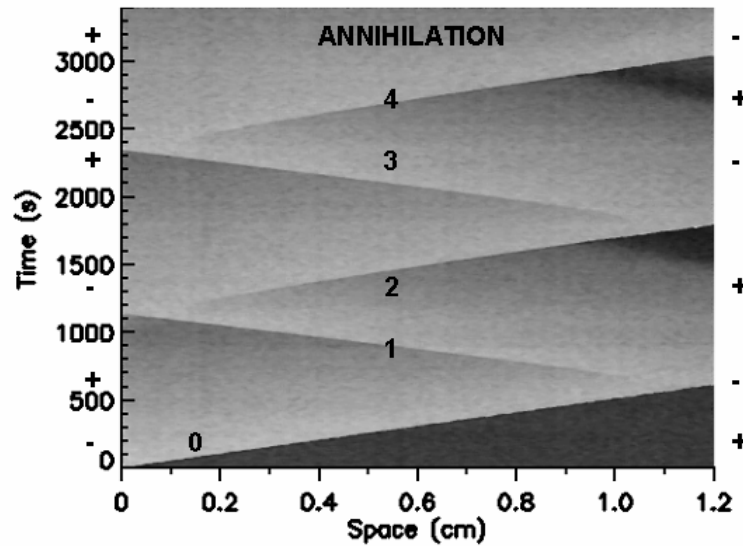
(b)
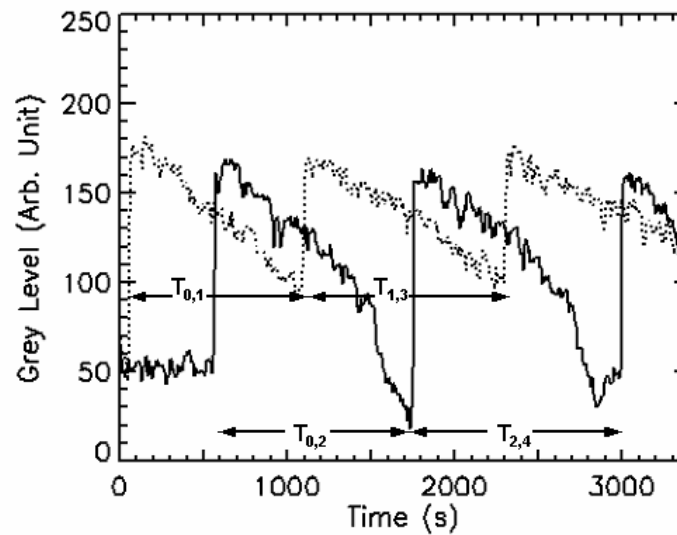
Figure 31: (a) Time-space plot showing zigzag pattern of four reversed waves in the medium with 8 mM PG. U = 80 V (I ≅ 1.4 mA), d = 1.2 cm. The polarities of the electrodes are marked on the time axis. The dark region ahead of the first (0) wave is the unreacted medium with high ferroin concentration. The numbers shown denote the first (0) and four reversed (1-4) waves and their propagation velocities (in mm/min) are 1.18 (0), 1.47 (1), 1.21 (2), 1.39 (3), 0.97 (4), respectively. The zero field propagation velocity of the first wave is 0.68 mm/min.

(b) Profiles of transmitted light intensity represented by grey levels extracted from the time-space plot (a) at the positions: 0.1 cm (dotted line), 1.1 cm (solid line). $T_{0,1}$, $T_{0,2}$, $T_{1,3}$, and $T_{2,4}$ are the excitation periods between two respective waves. $T_{0,1} = 17.1$ min, $T_{0,2} = 19.8$ min, $T_{1,3} = 20.0$ min, and $T_{2,4} = 20.8$ min.

When we investigate closely the course of the experiment with four reversals, illustrated in Fig. 31, we can detect an asymmetry in the system behaviour. First, the propagation velocities of odd reversed waves (propagating to the left) are larger than those of even waves (propagating to the right). This tendency was observed in all cases with multiple reversals of a wave as documented in Table 8. (Note that the propagation velocity of reversed waves was found to be constant throughout the observation window, although the ferroin concentration in front of the wave had been continuously changing in time.)

Second, there is a certain asymmetry in the transmitted light data, corresponding to the concentration of ferriin (and ferroin) in front of the waves propagating to the left and right, as shown in Fig. 31, at locations close to the ends of the observation window. The sharp increase in the grey level corresponds to the excitation of the medium at the chosen location, i.e. to the excitation front of the wave just passing through that location. The recovery of the medium from the excitation (indicated by the slope of the decaying parts of the grey level profiles) begins at both chosen locations with the same rate, but a fast jump downward occurs at 1.1 cm later during the recovery period. Thus, close to the ends of the observation window, the ferroin concentration in front of the even reversed waves is much higher than that in front of the odd reversed waves. This may be due to the electro-migration and diffusion flows of ferroin to the reversed wave fronts.

Third, an asymmetry was also found in the location at which the excitation fronts of reversed waves emerge in the wake of the wave that has arrived at the end of the observation window. The new excitation fronts become visible at a location around 1.0 cm for the reversed waves propagating to the left and at a location around 0.15 cm for those propagating to the right.

The dependence of the excitation periods on the voltages applied to the system in the case of three reversals, is shown in Fig. 32 (see also Table 9). The definition of period $T_{0,1}$ is different from the definition of periods $T_{0,2}$, $T_{1,3}$, and $T_{2,4}$ since $T_{0,1}$ is the period between the first wave passing from the left to the right and the first reversed wave passing from the right to the left, while other periods are measured between reversed waves propagating in the same direction.

U (V)	$T_{0,1}$ (min)	$T_{0,2}$ (min)	$T_{1,3}$ (min)
70	12.0, 16.3	14.7, 18.8	15.2, 19.6
	- , 16.0	**- , 18.8**	**- , 20.0**
80	10.5, 16.1	12.6, 18.7	12.6, 19.5
	9.6 , -	**12.6 , -**	**13.2 , -**
90	8.9, 14.2	10.5, 16.4	11.5, 16.9
100 *1st Experiment*	9.9, 16.4	12.3, 19.3	12.6, 19.8
2nd Experiment	9.9, 15.8	12.3, 17.9	12.6, 18.5

Table 9: Excitation periods of three reversals for 0.8 cm window size, 1.2 cm window size. Periods $T_{0,1}$ and $T_{1,3}$ of both window sizes were evaluated from profiles extracted from the time-space plots at the reversal position: 0.1 cm. $T_{0,2}$ for 0.8 cm and 1.2 cm window sizes were evaluated from profiles extracted from the time-space plots at the reversal positions: 0.7 cm and 1.1 cm, respectively. Medium with 8 mM PG (the reference solution mixture). The bold numbers are the values for medium with 11 mM PG (the solution mixture III).

The tendency: $T_{1,3} > T_{0,2} > T_{0,1}$ is assumed to result from the consumption of reactants in the solution mixture (or aging effect) in the closed system. At a longer period of switching the electric field polarity, as defined by the window sizes, the excitation periods are also longer. The excitation periods drop down to the lowest value at 90 V in both window sizes.
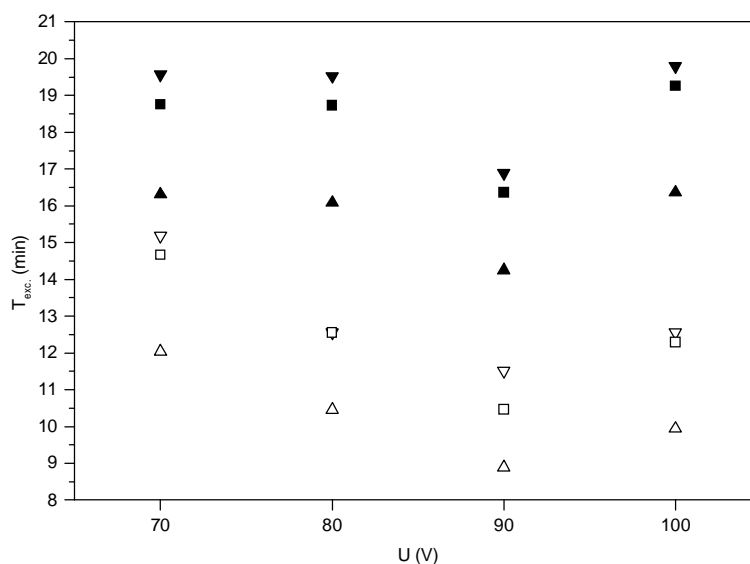
Figure 32: Excitation periods $T_{exc.}$ as a function of the applied voltage U plotted from the data in Table 9 for the medium with 8 mM PG. Open and full symbols are for 0.8 cm and 1.2 cm window sizes, respectively, up triangle: $T_{0,1}$ square: $T_{0,2}$, and down triangle: $T_{1,3}$. Note that excitation periods of the first experiment at 100 V for 1.2 cm-window size are plotted.

The influence of the ferroin concentrations on multiple wave reversals is not studied in detail but in one experiment done at U = 90 V and d = 0.8 cm for the solution mixture V ([ferroin] = 0.28 mM), we found three reversals without previous acceleration of the first wave by the negative field.

4.4 Influence of front shapes

The behaviour of wave fronts with different shapes is very complicated. Here are some of their properties which we observed in the experiments,

1. The generation of shaped waves was random and uncertain and depended on the pyrogallol concentration. When we used short stoppers (see Sections 3.1 and 4.1), V-shaped wave fronts were more often found at 5 mM PG, as shown in Table 10. Planar fronts prevail at higher pyrogallol concentration.

[PG] mM	n	v_0 (mm/min)		
		Planar shape	U-shape	V-shape
5	37	0.75 ± 0.05 (24%)	-	2.99 ± 0.55 (76%)
8 (*reference*)	91	0.67 ± 0.08 (61%)	1.03 ± 0.13 (30%)	1.66 ± 0.29 (9%)
11	34	0.59 ± 0.08 (76%)	-	1.94 ± 0.37 (24%)

Table 10: Percentage found for different shapes of the wave fronts and the average zero-field propagation velocities v_0 related to the pyrogallol concentrations. n denotes the number of experiments done. $[H_2SO_4]$ = 0.15 M, $[NaBrO_3]$ = 0.10 M, and [ferroin] = 0.5 mM.

The influence of ferroin concentrations on the occurrence of the shaped wave fronts is not known in detail, but we found V-shaped wave fronts in the solution mixture VI ([ferroin] = 0.8 mM) in some experiments, too.

2. The refractory part of the V- shaped wave front is shallower than that of the planar wave front (i.e. the system recovers more slowly) and the slope of the wave front (between 0.85 cm and 0.9 cm) is also less steep, as shown in Fig. 33.
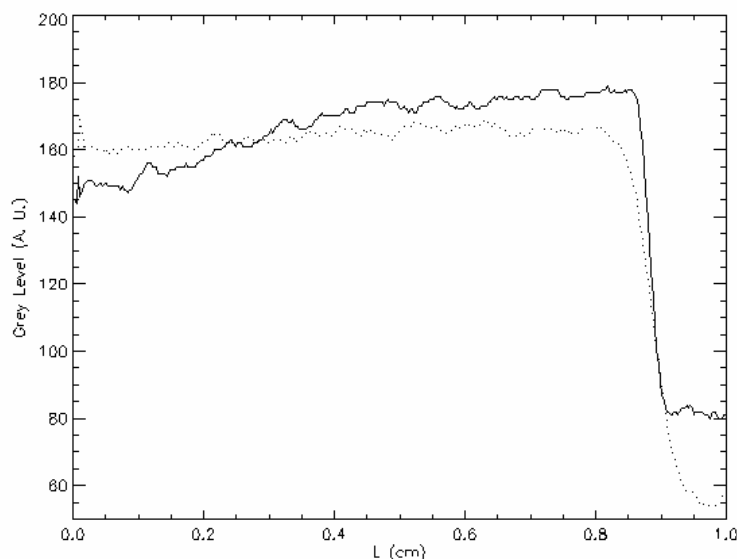
Figure 33: Ferriin concentration profiles represented by grey level of V-shaped wave (v_0 = 3.19 mm/min, dot line) and planar wave (v_0 = 0.77 mm/min, solid line) observed in solution mixture II ([PG] = 5 mM). Short stoppers are used.

3. In some experimental runs, a U- or V-shaped wave can become planar during the propagation, as illustrated in Fig. 34. The change of the shape is accompanied by a pronounced decrease of the propagation velocity. The change to the planar shape was observed both with and without applied electric fields. The opposite phenomenon, the change from a planar to a U- or V-shaped wave, was never observed.
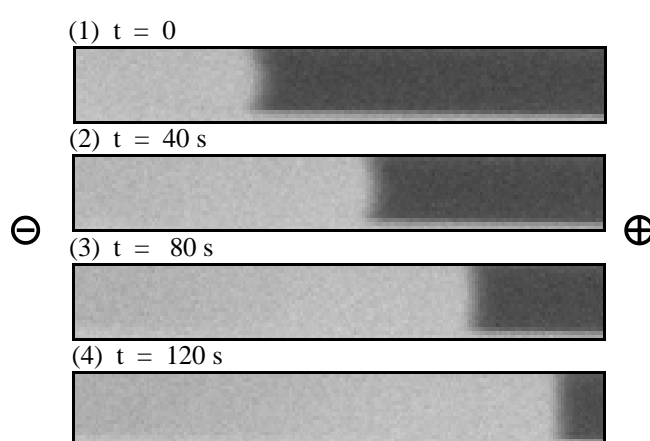
Figure 34: Transformation of the U-shaped wave (t = 0, v_E = 1.82 mm min^{-1}) to the planar wave (t = 120 s, v_E = 1.17 mm min^{-1}) in negative field of intensity E = - 4.38 V cm^{-1}, I ≈ 1.2 mA. The portion of the cuvette shown is 0.4 cm in length.

4. These shaped wave fronts behave the same way as the planar wave front both in the negative and the positive field, and the propagation velocity for a given electric field and without an electric field vary in a very broad range. It is rather difficult to identify the exact relationship between the propagation velocity and the electric field intensity (especially the V-shaped wave front observed in the solution mixture II ([PG] = 5 mM)). However, the saturation-type relationship was observed for the U-shaped wave front as shown in Fig. 35. Propagation velocity is almost constant at 1.63 ± 0.12 mm/min for $E < -3$ V/cm and the annihilation field (point A) occurs at $E = +0.94$ V/cm (the same as planar waves, see Table 6).
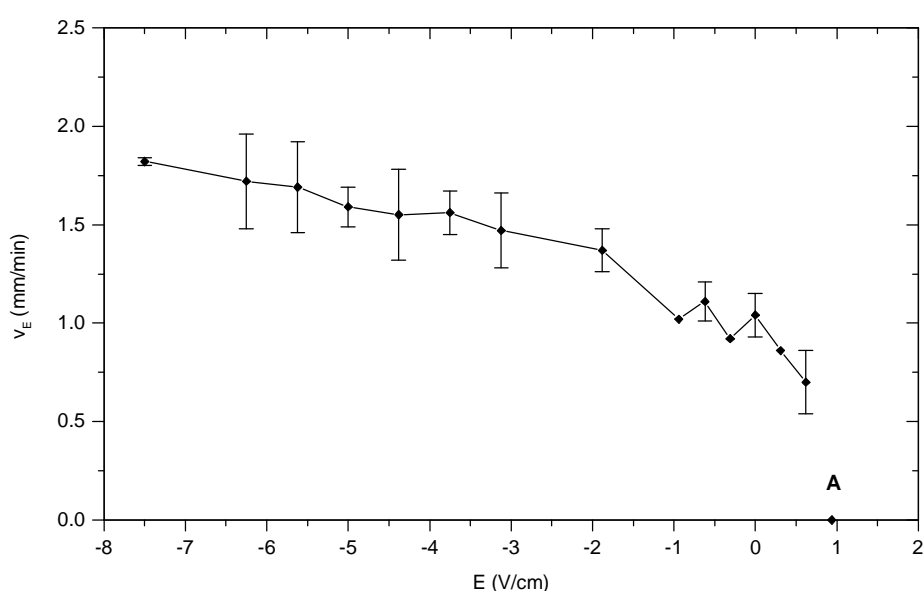
Figure 35: The dependence of the propagation velocity on the electric field intensity of the U-shaped wave front .

5. The reversal of the V-shaped wave front is also very complicated. At $t = 1$ min, the V-shaped wave partially annihilates at its wings [Góm97, see also Fig. 11] but it continues propagating and therefore it looks like splitting phenomenon, as illustrated in Fig. 36. The V-shaped reversed wave is obtained after changing the field polarity (see also Fig. 29.1). In some experiments this reversed wave was found to be transformed again to the planar wave with increasing its velocity when the field was applied long enough.

⊕ ⊖

(1) t = 0 min

(2) t = 1 min

(3) t = 3 min

(4) t = 5 min

(5) t = 7 min (*original figure*)

(5) t = 7 min (after adjusting contrast and brightness)

Figure 36: The reversal of the V-shaped wave in the positive field of intensity E = 4.38 V cm^{-1} , I ≈ 1.2 mA. Solution mixture II ([PG] = 5 mM). The portion of the cuvette shown is 1.0 cm in length. The propagation velocities of the original V-shaped wave and the reversed V-shaped wave to the positive electrode are 3.84 mm/min and 0.47 mm/min, respectively.

6. Multiple reversals of these shaped wave fronts observed in the reference solution mixture vary from 2 to 5 reversals. At 90 V, U-shaped wave and V –shaped wave were transformed to the planar waves in the negative field (see Fig. 34) and then performed 6 reversals in 1.2 cm window size (see also APPPENDIX C) and 5 reversals in 0.4 cm window size, respectively.

7. No U and V-shaped wave fronts were observed, if the long stoppers (see Sections 3.1 and 4.1) were used.

Chapter 5
Discussion

At first of experimental results, we measured the dependence of the wave velocity on the concentrations of pyrogallol and ferroin. As in the case of the classical BZ system with malonic acid as organic substrate [Fie74b, Woo85], the propagation velocity for a given excitability determined by $[H_2SO_4] = 0.15$ M and $[NaBrO_3] = 0.10$ M, is almost independent of the ferroin concentration but depends on the pyrogallol concentration [Sri98a, cf. Table 5], because pyrogallol is involved in the generation of $HBrO_2$ also, which is not the case with malonic acid in the classical BZ system. The qualitative properties of the waves in the pyrogallol system, such as dependence of the amplitude on the ferroin concentration and dependence of the degree of recovery behind the excitation region on the pyrogallol concentration (see Fig. 24) appear to be the same as in the classical BZ system, when either [MA] or [catalyst] is varied and other reactant concentrations are kept constant [Mor91, Nag89b]. The investigated system with pyrogallol substrate forms a medium of very low excitability, in which a pulse wave is characterized by the flat maximum of ferriin concentration [Mor91, Zha93b] in the oxidized region and the very slow decay back to the reduced state (cf. Fig. 27).

Before turning to the discussion of the major electric field-induced effects on the waves in the pyrogallol system, we wish to comment on intriguing features of wave fronts of different shapes: planar, U-, and V-shapes (cf. Fig. 23) which they were observed in the experiments with long and short stoppers, and it is suggested that the global convection in the capillary tube plays an important role and that the electric field can overcome the convective effect in the sense that the qualitative influences of the field on U and V shaped waves (see Section 4.4) are the same as the qualitative influences of the field on planar waves. U and V shaped waves are caused by the gradient of hydrostatic pressure P_h behind the wave front. This pressure P_h (in N/cm^2) $= \rho_C(gh)$ comes from the average density ρ_C of the solution caused by the chemical composition of the reaction solution below the short stopper at both vertical filling chambers (see Fig. 21), where g is the standard acceleration of free fall under gravity,

980 cm.s^{-2} , and h is the solution height ($\approx$ 2.0 cm). Generally, the ferroin catalysed BZ solution in the oxidized state has a higher density than that of the reduced state in order of 10^{-5} g/ml [Poj90], because of differences in the molar volumes of intermediates, catalysts, and products formed in the solution. Furthermore, a periodic change of the viscosity and the density of the BZ solution was also recently found [Yos04]. It was shown that the viscosity of the BZ solution containing high ferriin concentration is also high [Yos04], because the change of the electric charge of the catalyst induces the variation of the interaction between the catalyst and its surrounding water on the molecular scale and this change is then propagated to the bulk scale. The average convective flux density $<J_{C,i}>$ of the ith chemical species in the capillary is given by Poiseuille 's Law [Old94]:

$$\left\langle J_{C,i} \right\rangle = v_x C_i = \frac{-A C_i}{8 p h} \frac{dP_h}{dx}, \tag{35}$$

where v_x is the fluid flow velocity along the x-coordinate; it is usually negative, C_i is the concentration of the ith chemical species, A (or A mentioned in the former text) is the inner cross section of the capillary = 0.5 x 0.5 mm^2, and η is the viscosity coefficient of the solution. dP_h/dx is the pressure gradient causing the global hydrodynamic convective flow in the capillary tube. Poiseuille 's Law is obeyed only if dP_h/dx is sufficiently small that so-called "laminar flow" (or streaming flow) occurs [Old94], see also [Lec03]. The slope of the wave front shown in Fig. 33 of the V-shaped wave that appears to be lower than that of the planar wave, is one clue showing that there is a force or a pressure exerting on the solution behind the wave front and thus the wave front is deformed to V-shape and the propagation velocity is higher. When we decrease [PG] (see Table 10), this effect is more pronounced. The U-shaped wave may be somewhat lying between the V-shaped and the planar wave (depending on the magnitude of dP_h/dx ?). Numerical simulations also show that convection always plays a role in increasing the speed of BZ waves propagating in a horizontal slab of 0.5 mm width [Wu95].

Another possibility is that the V-shaped wave is a kind of phase wave or phase-diffusion wave [Ros88], because of its very rapid propagation and the fact that the ferriin concentration gradient behind the wave front is shallower than in the case of the planar trigger wave (cf. Fig. 33). However, the arguments in this work referring to the effects of the substrate on the electric field-induced phenomena on propagating waves are not predominantly affected by

these different shapes of the wave front, but should be considered as a major topic for further research.

The effects of applied electric fields on the propagation velocity of PG waves account for acceleration in the negative field and deceleration in the positive field which can be explained, as in classical BZ system, by the crucial role of bromide ions [Dut02, Gil92, Orb78, Orb79] in switching between oxidizing and reducing reaction steps. In the negative field the Br^- is removed from the region ahead of the wave, which enhances the wave propagation, whereas in the positive field the bromide migrates from the unreacted region to the medium just ahead of the wave front. Thus, the start of autocatalysis is suppressed and hence the propagation speed is lowered. When the migration flow of the Br^- exceeds the critical value (at the critical positive field intensity), the onset of autocatalysis is suppressed completely and the wave annihilates.

From a qualitative point of view, the effects of imposed electric fields on the propagation velocities are principally similar to what has been observed in the classical BZ reaction [Fee81, Šev83]. A difference arises in that for the classical BZ waves the propagation velocity increases progressively with increasing negative field [Šev83], while in the PG system the propagation velocity reaches a constant value (cf. Fig. 25). Such a saturation effect as observed in the PG system was already proposed by Ortoleva, who associated different possible effects of applied fields to the differences in reaction mechanisms [Ort92].

We can also notice the remarkable differences in the effects of positive fields both on the propagation velocity and other electric field-induced properties of BZ and PG waves. While positive fields were observed to affect the propagation velocity of BZ waves only slightly in a quite large range of magnitudes of intensities (up to 20 V cm^{-1} when the wave annihilates) [Šev83], the velocity of PG wave propagation is very sensitive to positive fields and annihilation occurs at very low fields (cf. Table 6 and Figs. 25, 28).

Numerical results of scenarios observed under direct application of the increasing positive electric field intensity in the ZBKE model [Šev96a] are the same as scenarios observed in our PG system (cf. Fig. 28), i.e. they are the transitions: Deceleration $\rightarrow$ Annihilation for j = 0.50 and Deceleration $\rightarrow$ Annihilation $\rightarrow$ Reversal for j = 0.40 and 0.45, where j is the number of moles of bromide ions produced (see also Section 2.3.1). A wave reversal in the

PG system was observed, when the wave was first accelerated in the negative field and then exposed to the positive field. The wave reversal was observed for relatively high values of the field intensities, while for small intensities wave annihilation occurred (cf. Fig. 28). In the classical BZ system with malonic acid and ferroin, single wave reversal (and the wave splitting and wave annihilation) was also observed under the condition that a wave was first accelerated in the negative field and then exposed to the positive field [Šev92]. However, the occurrence of wave reversal and annihilation, upon increasing the electric field intensity was in opposite order as compared to the PG system: the wave reversal was observed at lower field intensities than the wave annihilation.

Based on the chemical mechanism of the PG-ferroin coupled system shown in Table 1, the important autocatalytic steps of both activating species are

|	
$BrO_2{}^{\cdot} + Q \rightarrow HBrO_2 + Q^{\cdot}$	Rate constant $= 5.0 \times 10^6$ $dm^3mol^{-1}s^{-1}$
$ferroin^{2+} + BrO_2{}^{\cdot} + H^+ \leftrightarrow HBrO_2 + ferriin^{3+}$	Equilibrium constant $= 8.99$ dm^3mol^{-1}.

We can see that Q is a neutral molecule, whereas ferroin is a charged ion. Thus, Q cannot migrate under the influence of an electric field. Furthermore, Q should be dominant in the autocatalytic production of bromous acid because of its irreversible reaction and larger rate constant (cf. Table1). Its concentration (derived from the pyrogallol concentration) is higher than the ferroin concentration used for this study. These differences between both species may play an important role in the electrical field effects which we observed. Since the PG-ferroin coupled system has two annihilation points (see Fig. 28), it is most likely that the system is mainly controlled by the pyrogallol-uncatalyzed kinetics at lower positive electric field intensities, because the first wave annihilation point occurs after wave deceleration. There is also a question, whether the PG-ferroin coupled system is mainly controlled by the ferroin-catalyzed kinetics at higher electric field intensities, because the second wave annihilation occurs after wave reversal (as in the classical BZ system with MA as substrate). Therefore, we can conclude that the waves in the solution mixtures I, II, III, and VI show dominantly the character of the pure PG-uncatalyzed system. The applied negative field shifts the system to the new system showing more the character of the pure ferroin-catalyzed system by speeding up bromous acid autocatalysis of ferroin. The waves in the solution mixture V show a character having equally features of the uncatalyzed system and the catalyzed system (see also Fig. 18).

The reaction medium used in this study belongs to the class of "internally" or "chemically" coupled systems composed of a "classical" BZ system and of a so-called uncatalyzed bromate oscillator (UBO) [Dut02, Gil92]. The system as a whole is still controlled by the concentration of bromide that acts as an inhibitor of the excitation and must be reactively removed during the recovery phase to make the medium receptive to another excitation. Other than in the classical BZ system there are two components activating the autocatalysis in the excitation phase - ferroin (as in the classical BZ system) and an intermediate of the quinone structure Q [Jwo89, Liu92a, Nag99, Orb95] arising from oxidation of pyrogallol. During the refractory phase, both ferroin and the quinone–like intermediate must be recovered [Dut02, Gil92] (cf. Table1).

When an electric field is applied, the voltage used and the duration of the field application control the extent of differential mass flow of ionic reaction species by electro-migration and, consequently, the spatial redistribution of concentrations of these species. The altered local species concentrations change the local course of the reaction and thus can facilitate the recovery of the medium and the onset of a new excitation in the wake of an existing wave. The difference between the conditions of the occurrence of one wave reversal in the classical and in the PG-containing BZ reaction can result from the interplay between the two activating species in the latter medium. The coexistence of the same two activating species was assumed to be the reason for the anomalous dispersion curves measured in an UBO system with 1,4 – cyclohexanedione [Ham01] (see Fig. 20). Since the shape of dispersion curve resides also in the state of the refractory phase, it is reasonable to conclude that the quinone-like intermediate Q plays an important role in the wave reversal, too. During the wave reversal, as it occurs in the classical BZ-system with MA as substrate, the electro-migration of bromide ions from behind the excited region towards the positive electrode helps to speed up the recovery of the reaction medium behind the excited region by reactions: 8 (cf. Table1) and E (see Sections 2.4.1 and 2.4.2), favour the conditions (reaction 2f, cf. Table 1) for the onset of autocatalysis (reactions: 5 and 9f, cf. Table 1) and formation of a new excited front in the wake of the propagating wave (see also Section 2.3.4). The supply of bromide ions to the excited region of the original wave from the medium in front of it stops the autocatalysis by reaction: 2f (cf. Table 1), and causes the excitation front of the original wave to annihilate.

In this experimental study we have also shown that a planar wave in the pyrogallol variant of the BZ reaction can be reversed multiple times by switching repeatedly the polarity of an applied electric field. Multiple reversals were observed in a limited range of the values of control parameters: the applied voltage and the size of observation window (cf. Fig. 30). They could arise in a similar way as single wave reversal, but the multiple activating actions are controlled by Q as well as ferroin recovered repeatedly (see reactions: 6 and 8 (cf. Table 1), E) at certain distances in the refractory tail of the wave.
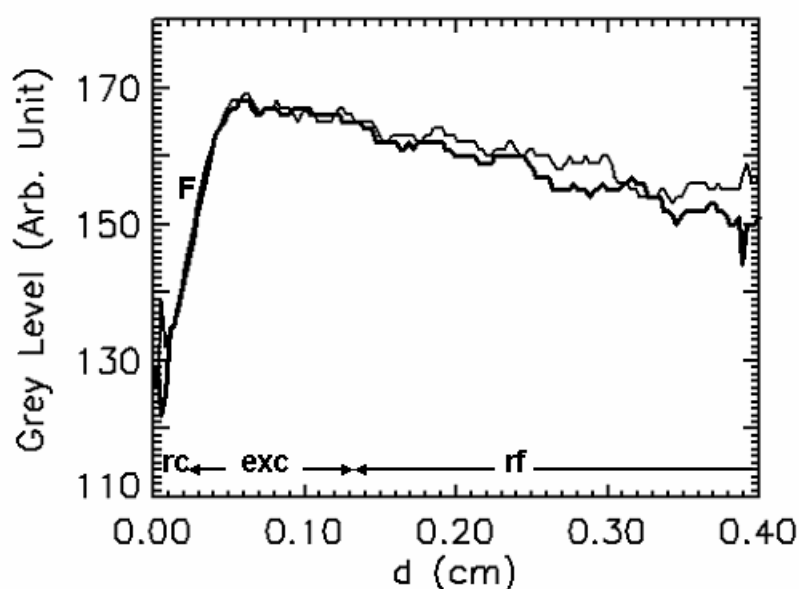
Figure 37: Spatial profiles of the first reversed waves propagating to the positive electrode. U = 60 V, d = 0.4 cm, thin line - 8 mM PG, bold line - 11 mM PG. F denotes the wave front; rc, exc, and rf denote recovered, excited, and refractory regions, respectively.

The initial amount of PG (and, consequently, the amount of quinone-like intermediate) affects also the range of the control parameters, in which the multiple reversals of a wave can occur. This suggests that a fine tuning of the redistribution of reaction species has to be achieved in the refractory zone by applying an electric field of both polarities. The spatial profiles of the first reversed waves for two different concentrations of PG (see Fig. 37, cf. Fig. 24a) indicate that the system with 11 mM PG recovers faster than the system with 8 mM PG. Thus, under these experimental conditions, three reversals could occur in the 11 mM PG system, while in the 8 mM PG system the first reversed wave annihilated upon changing the field polarity (cf. Fig. 30).

Chapter 6
Conclusion and perspectives

Although the main, general tendencies of electric field effects on waves, such as speeding up wave propagation by negative fields and slowing down or annihilating waves by positive fields, remain the same for both the classical BZ system with malonic acid as a substrate and the PG system studied in this thesis, some details in the differences of the dependencies of the propagation velocity and of the occurrence of complex behaviour (wave reversal, splitting and annihilation) induced by positive electric fields point to the importance of details in the reaction mechanisms involved [Ort92].

In the PG system the catalytic pathway of the classical BZ reaction mediated by ferroin is coupled with the „uncatalyzed" pathway, mediated by pyrogallol. These pathways compete not only for the autocatalytic production of $HBrO_2$ but also for the bromide production and the relaxation processes acting behind the oxidized region [Gil92, Liu92a, Orb79]. The effects of this type of competitive processes in the refractory tail of the wave were assumed to give rise to the anomalous dispersion relation in the system with ferroin and the 1,4-CHD as organic substrate [Ham01]. Since wave reversal and splitting in applied electric fields occur in the refractory region, it is reasonable to assume that the competition between catalytic and „uncatalyzed" pathways can also play a significant role in the different manifestation of these phenomena, when comparing the classical BZ reaction with the PG system investigated here. It is interesting to ask, whether this competition for autocatalysis can have an effect on the dependence of the propagation velocity on the electric field intensity. These mechanistic details should be further investigated by changing appropriately the concentrations of either ferroin or pyrogallol, which could shift the system either to the one controlled by ferroin (like in the classical BZ system with malonic acid) or to the one fully controlled by the UBO mechanism. A first step in this direction has been done (see Discussion).

One can conclude from this study that this coupled system has two oscillators, i.e. the PG-uncatalyzed system and the ferroin-catalysed system. These two existing systems interact independently and sometimes mutually, depending on the concentrations of both species and the electric field intensity applied to the system.

This study also shows that multiple reversals by switching the polarity of d.c. electric fields appear to be similar to the reflection of a reaction-diffusion wave [Ei02, Mid93, Pet94], as demonstrated in Section 2.1.2. This finding is interesting not only from a scientific point of view but also as a new perspective model for the design of electronic systems controlling the direction of signal transmission [Tót94]. It is tentative to speculate about any application also in other fields of data transmission and data processing [Ger00, Was03]. Although the system employed for this study is closed, relatively easily set up, transported, and operated, the reactant consumption, however, limits the reproducibilty of the system. During the course of each oscillation in the intermediate concentrations, small but nonzero amounts of the reactants are consumed, thus providing the overall driving force for the reaction. Therefore, each oscillation occurs against a slightly different background concentration of reactants, i.e each oscillation is inevitably slightly different from its predecessor and from subsequent excursions. It would be worth to design an open (CFUR) [Eps98] capillary reactor [Stö95], since we do conjecture that waves arising from this system can keep moving back and forth between the ends of the observation window, where the polarity is changed, as long as the fresh reactants are fed into the reactor.

Experimental findings on multiple reversals of pulse waves in the BZ system with pyrogallol as substrate suggest that dissipative systems of the reaction-diffusion type may behave like particles under proper conditions. This behaviour reminds properties of solitons in conservative systems, but on the other hand, dissipation is crucial for stabilization; we would call them "dissipative solitons" [Bod02]. They are supposed to be a practical importance in biology as nerve impulses [Asl99, deF97, Fer85].

BIBLIOGRAPHY

Following references cited in the text are sorted in alphabetical and chronological order selected from the first three letters of the first author's surname and the published year.

[Ada02] Ĺ. Adamčíková, Z. Farbulová and P. Ševčík, Pattern formation in uncatalyzed bromate oscillator with catechol, *React. Kinet. Catal. Lett.* **75** (2002), 335-341.

[Ada04] Ĺ. Adamčíková, R. Bielik and P. Ševčík, Pattern formation in uncatalyzed bromate oscillator with pyrogallol, *Coll. Czech. Chem. Comm.* **69** (2004), 1553-1565.

[Asl99] O. V. Aslanidi and O. A. Mornev, Soliton-like regimes and excitation pulse reflection (echo) in homogeneous cardiac purkinje fibers: Results of numerical simulations, *J. Bio. Phys.* **25** (1999), 149-164.

[Atk98] P. W. Atkins, *Physical Chemistry*, Oxford University Press, New York, 6th Edn., 1998, p. 948.

[Bab86] A. Babloyantz, *Molecules, Dynamics, and Life: An Introduction to Self-Organization of Matter*, John Wiley & Sons, New York, 1986.

[Bel95] A. Belmonte and J.-M. Flesselles, Non-steady behaviour of a spiral under a constant current, *Europhys. Lett.* **32** (1995), 267-272.

[Bod02] M. Bode, A. W. Liehr, C. P. Schenk and H.-G. Purwins, Interaction of dissipative solitons: Particle-like behaviour of localized structures in a three-component reaction-diffusion system, *Physica D* **161** (2002), 45-66.

[Bra99a] P. Brazhnik, V. Davydov, V. Pérez-Muńuzuri, M. Gómez-Gesteira, A. P. Muńuzuri and V. Pérez-Villar, V-waves of excitation, *Chaos, Solitons & Fractals* **10** (1999), 99-118.

[Bra99b] P. K. Brazhnik and J. J. Tyson, Velocity-curvature dependence for chemical waves in the Belousov-Zhabotinsky reaction: Theoretical explanation of experimental observations, *Phys. Rev. E* **59** (1999), 3920-3925.

[Cro93] M. C. Cross and P. C. Hohenberg, Pattern formation outside of equilibrium, *Rev. Mod. Phys.* **65** (1993), 851-1112.

[DeF97] L. J. DeFelice, *Electrical Properties of Cells: Patch Clamp for Biologists*, Plenum Press, New York, 1997.

[Dra89] P. G. Drazin and R. S. John, *Solitons: An Introduction*, Cambridge University Press, Cambridge, 1989.

[Dut02] A. K. Dutt, Complex dynamical behavior from coupling between a catalyzed Belousov-Zhabotinskii-like reaction and its uncatalyzed oscillatory component in a flow reactor, *J. Phys. Chem. B* **106** (2002), 11069-11072.

[Ei02] S.-I. Ei, M. Mimura and M. Nagayama, Pulse-pulse interaction in reaction-diffusion systems, *Physica D* **165** (2002), 176-198.

[Eng96] H. Engel, F.-J. Niedernostheide, H.-G. Purwins and E. Schöll (Eds.), *Self-Organization in Activator-Inhibitor-Systems: Semiconductors, Gas-Discharge, and Chemical Active Media*, Wissenschaft und Technik Verlag, Berlin, 1996.

[Eps98] I. R. Epstein and J. A. Pojman, *An Introduction to Non-linear Chemical Dynamics*, Oxford University Press, New York, 1998.

[Eva04] R. Evans, C. R. Timmel, P. J. Hore and M. M. Britton, Magnetic resonance imaging of a magnetic field-dependent chemical wave, *Chem. Phys. Lett.* **397** (2004), 67-72.

[Fee81] R. Feeney, S. L. Schmidt and P. Ortoleva, Experiments on electric field-BZ chemical wave interactions: Annihilation and the crescent wave, *Physica D* **2** (1981), 536-544.

[Fer85] H. G. Ferreira and M.W. Marshall, *The Biophysical Basis of Excitability*, Cambridge University Press, Cambridge, 1985.

[Fie72a] R. J. Field, E. Körös and R. M. Noyes, Oscillations in chemical systems. II. Thorough analysis of temporal oscillations in the bromate-cerium-malonic acid system, *J. Am. Chem. Soc.* **94** (1972), 8649-8664.

[Fie72b] R. J. Field and R. M. Noyes, Explanation of spatial band propagation in the Belousov reaction, *Nature* **237** (1972), 390-392.

[Fie74a] R. J. Field and R. M. Noyes, Oscillations in chemical systems. IV. Limit cycle behavior in a model of a real chemical reaction, *J. Chem. Phys.* **60** (1974) 1877-1884.

[Fie74b] R. J. Field and R. M. Noyes, Oscillations in chemical systems. V. Quantitative explanation of band migration in the Belousov-Zhabotinskii reaction, *J. Am. Chem. Soc.* **96** (1974), 2001-2006.

[Fie75] R. J. Field, Limit cycle oscillations in the reversible Oregonator, *J. Chem. Phys.* **63** (1975), 2289-2296.

[Fie85] R. J. Field and M. Burger (Eds.), *Oscillations and Travelling Waves in Chemical Systems*, John Wiley & Sons, New York, 1985.

[Fie86] R. J. Field and H.-D. Försterling, On the oxybromine chemistry rate constants with cerium ions in the Field-Körös-Noyes mechanism of the Belousov-Zhabotinskii reaction: The equilibrium $BrO_3^- + HBrO_2 + H^+ \leftrightarrow 2BrO_2{}^\cdot + H_2O$, *J. Phys. Chem.* **90** (1986), 5400-5407.

[Fil00] A. T. Filippov, *The Versatile Soliton*, Birkhäuser, Boston, 2000.

[Fle98] J.-M. Flesselles, A. Belmonte and V. Gáspár, Dispersion relation for waves in the Belousov-Zhabotinsky reaction, *J. Chem. Soc. Faraday Trans.* **94** (1998), 851-855.

[Foe89] P. Foerster, S. C. Müller and B. Hess, Critical size and curvature of wave formation in an excitable chemical medium, *Proc. Natl. Acad. Sci. USA* **86** (1989), 6831-6834.

[Fuj01] S. Fujieda, Y. Mori, A. Nakazawa and Y. Mogami, Effect of gravity field on the nonequilibrium /nonlinear chemical oscillation reactions, *Adv. Space Res.* **28** (2001), 537-543.

[Ger00] N. Gershenfeld, *The Physics of Information Technology*, Cambridge University Press, Cambridge, 2000.

[Gil92] C.C.D. Giles, P. Ibison, J. Liu and S.K. Scott, Uncatalysed Belousov-Zhabotinskii reaction with pyrogallol: Experimental behaviour in a flow reactor and the influence of ferroin as catalyst, *J. Chem. Soc. Faraday Trans.* **88** (1992), 917-924.

[Góm97] M. Gómez-Gesteira, J. Mosquera, V.A.Davydov, V. Pérez-Muńuzuri, A.P. Muńuzuri, V.G. Morozov and V. Pérez-Villar, Link between the effect of an electric field on wave propagation and the curvature-velocity relation, *Phys. Lett. A* **231** (1997), 389-394.

[Ham98] C.H. Hamann, A. Hamnett and W. Vielstich, *Electrochemistry*, Wiley-VCH, Weinheim, 1998, p. 35.

[Ham01] C. T. Hamik, N. Manz and O. Steinbock, Anomalous dispersion and attractive pulse interaction in the 1,4-cyclohexanedione Belousov-Zhabotinsky reaction, *J. Phys. Chem. A* **105** (2001), 6144-6153.

[Has97] P. Hasal, V. Nevoral, I. Schreiber, H. Ševčíková, D. Šnita and M. Marek, Waves in ionic reaction-diffusion-migration systems, in *Nonlinear Dynamics, Chaotic and Complex Systems* (E. Infeld, R. Zelanzny, and A. Galkowski (Eds.)), Cambridge University Press, Cambridge, 1997, pp. 72-98.

[Jor74] J. Jorné, The effects of ionic migration on oscillations and pattern formation in chemical systems, *J. Theor. Biol.* **43** (1974), 375-380.

[Jwo89] J.-J. Jwo and E.-F. Chang, Kinetic study of the initial phase of the uncatalyzed oscillatory reaction of potassium bromate and gallic acid, *J. Phys. Chem.* **93** (1989), 2388-2392.

[Kap95] R. Kapral and K. Showalter (Eds.), *Chemical Waves and Patterns*, Kluwer Academic Publishers, Dordrecht, 1995.

[Kaš95] P. Kaštánek, J. Kosek, D. Šnita, I. Schreiber and M. Marek, Reduction waves in the BZ reaction: Circles, Spirals and effects of electric field, *Physica D* **84** (1995), 79-94.

[Kör80] E. Körös, M. Orbán and I. Habon, Chemical oscillations during the uncatalyzed reaction of aromatic compounds with bromate 3: Effect of one-electron redox couples on uncatalyzed bromate oscillators, *J. Phys. Chem.* **84** (1980), 559-560.

[Kos95] J. Kosek and M. Marek, Collision-stable waves in excitable reaction-diffusion systems, *Phys. Rev. Lett.* **74** (1995), 2134-2137.

[Kuh85] L. Kuhnert, H.-J. Krug and L. Pohlmann, Velocity of trigger waves and temperature dependence of autowave processes in the Belousov-Zhabotinsky reaction, *J. Phys. Chem.* **89** (1985), 2022-2026.

[Kuh00] H. Kuhn and H.-D. Försterling, *Principles of Physical Chemistry*, John Wiley & Sons, Chichester, 2000.

[Kur97] K. Kurin-Csörgei, A. M. Zhabotinsky, M. Orbán and I. R. Epstein, Photosensitive, bubble-free, bromate-1,4-cyclohexanedione oscillating reactions. Illumination control of pattern formation, *J. Phys. Chem. A* **101** (1997), 6827-6829.

[Lec03] M. Leconte, J. Martin, N. Rakotomalala and D. Salin, Pattern of reaction diffusion fronts in laminar flows, *Phys. Rev. Lett.* **90** (2003), 128302.

[Lee94] K.-J. Lee, W. D. McCormick, J. E. Pearson and H. L. Swinney, Experimental observation of self-replicating spots in a reaction-diffusion system, *Nature* **369** (1994), 215-218.

[Liu92a] J. Liu and S.K. Scott, Mechanism for the uncatalysed Belousov-Zhabotinskii reaction in open systems, *J. Chem. Soc. Faraday Trans.* **88** (1992), 909-916.

[Liu92b] J. Liu and S.K. Scott, Reduced models for the uncatalyzed Belousov-Zhabotinskii reaction, *J . Phys. Chem.* **96** (1992), 9870-9875.

[Mai97] P. K. Maini, K. J. Painter and H. N. P. Chau, Spatial pattern formation in chemical and biological systems, *J. Chem. Soc. Faraday Trans.* **93** (1997), 3601-3610.

[Mer92] E. Meron, Pattern formation in excitable media, *Physics Reports* **218** (1992), 1-66.

[Mid93] U. Middya, M. Sheintuch, M. D. Graham and D. Luss, Patterns of temperature pulses on electrically heated catalytic ribbons, *Physica D* **63** (1993), 393-409.

[Mor91] E. Mori, I. Schreiber and J. Ross, Profiles of chemical waves in the ferroin-catalyzed Belousov-Zhabotinskii reaction, *J. Phys. Chem.* **95** (1991), 9359-9366.

[Mur89] J. D. Murray, *Mathematical Biology*, Springer-Verlag, Berlin, 1989.

[Nag88a] Z. Nagy-Ungvarai, S. C. Müller, T. Plesser and B. Hess, Wave propagation in the Belousov-Zhabotinskii reaction depends on the nature of the catalyst, *Naturwissenschaften* **75** (1988), 87-89.

[Nag88b] Z. Nagy-Ungvarai, S. C. Müller and B. Hess, Wave propagation in the Belousov-Zhabotinskii reaction involving different catalysts, in *Chemical Reactivity in Liquids: Fundamental Aspects* (M. Moreau and P. Turq (Eds.)), Plenum Publishing Corporation, New York, 1988, pp. 489-493.

[Nag89a] Z. Nagy-Ungvarai, J. J. Tyson and B. Hess, Experimental study of the chemical waves in the cerium-catalyzed Belousov-Zhabotinskii reaction. 1. Velocity of trigger waves, *J. Phys. Chem.* **93** (1989), 707-713.

[Nag89b] Z. Nagy-Ungvarai, S. C. Müller, J. J. Tyson and B. Hess, Experimental study of the chemical waves in the Ce-catalyzed Belousov-Zhabotinskii reaction. 2. Concentration profiles, *J. Phys. Chem.* **93** (1989), 2760-2764.

[Nag99] G. Nagy, E. Körös and I. Lamprecht, Simultaneous calorimetric and potentiometric investigations on some uncatalyzed bromate oscillators (UBOs), *J. Therm. Anal. Cal.* **57** (1999), 209-223.

[Oer98] A. v. Oertzen, A. S. Mikhailov, H. H. Rotermund and G. Ertl, Subsurface oxygen in the CO oxidation reaction on Pt (110): Experiments and modeling of pattern formation, *J. Phys. Chem. B* **102** (1998), 4966-4981.

[Old94] K. B. Oldham and J. C. Myland, *Fundamentals of Electrochemical Science*, Academic Press, San Diego, 1994.

[Orb78] M. Orbán and E. Körös, Chemical oscillations during the uncatalyzed reaction of aromatic compounds with bromate 1: Search for chemical oscillators, *J. Phys. Chem.* **82** (1978), 1672-1674.

[Orb79] M. Orbán, E. Körös and R.M. Noyes, Chemical oscillations during the uncatalyzed reaction of aromatic compounds with bromate 2: A plausible skeleton mechanism, *J. Phys. Chem.* **83** (1979), 3056-3057.

[Orb80] M. Orbán, Stationary and moving structures in uncatalyzed oscillatory chemical reactions, *J. Am. Chem. Soc.* **102** (1980), 4311-4314.

[Orb95] M. Orbán and G. Szókán, Intermediates and products formed during the periodic reaction between phenol and bromate, *ACH-Models in Chemistry* **132** (1995), 179-189.

[Orb98] M. Orbán, K. Kurin-Csörgei, A. M. Zhabotinsky and I. R. Epstein, New indicators for visualizing pattern formation in uncatalyzed bromate oscillatory systems, *J. Am. Chem. Soc.* **120** (1998), 1146-1150.

[Ort92] P. J. Ortoleva, *Nonlinear Chemical Waves*, John Wiley & Sons, Chichester, 1992, Chapter 10.

[Pan97] A. V. Panfilov and A.V. Holden (Eds.), *Computational Biology of the Heart*, John Wiley & Sons, Sussex, 1997.

[Per06] A. G. Perkin and A. B. Steven, A product of the action of isoamyl nitrite on pyrogallol, *J. Chem. Soc.* **89** (1906), 802-808.

[Pér93] V. Pérez-Muńuzuri, M. Gómez-Gesteira, A. P. Muńuzuri and V. Pérez-Villar, Control of spiral waves dynamics in electrochemical reactor, *Bull. Electrochem.* **9** (1993), 192-200.

[Pet94] V. Petrov, S. K. Scott and K. Showalter, Excitability, wave reflection, and wave splitting in a cubic autocatalysis reaction-diffusion system, *Philos. Trans. R. Soc. London A* **347** (1994), 631-642.

[Poj90] J. A. Pojman and I. R. Epstein, Convective effects on chemical waves. 1. Mechanisms and stability criteria, *J. Phys. Chem.* **94** (1990), 4966-4972.

[Pót98] G. Póta, Chemical waves and spatial structures in reaction-diffusion systems, *ACH-Models in Chemistry* **5** (1998), 677-748.

[Rap03] Z. Rappoport (Ed.), *The Chemistry of Phenols* (2 parts), John Wiley & Sons, Chichester, 2003.

[Ros88] J. Ross, S.C. Müller and C. Vidal, Chemical waves, *Science* **240** (1988), 460-465.

[Sag03] F. Sagués and I. R. Epstein, Nonlinear chemical dynamics, *Dalton Trans.* **7** (2003), 1201-1217.

[Sch77] S. Schmidt and P. Ortoleva, A new chemical wave equation for ionic systems, *J. Chem. Phys.* **67** (1977), 3771-3776.

[Sch79] S. Schmidt and P. Ortoleva, Multiple chemical waves induced by applied electric fields, *J. Chem. Phys.* **71** (1979), 1010-1015.

[Sch81] S. Schmidt and P. Ortoleva, Electrical field effects on propagating BZ waves: Predictions of an Oregonator and new pulse supporting models, *J. Chem. Phys.* **74** (1981), 4488-4500.

[Sch83] S. L. Schmidt, Electric field effects on BZ chemical waves: Wave annihilation at negative fields, *J. Chem. Phys.* **79** (1983), 5939-5944.

[Sch92] J. Schütze, O. Steinbock and S.C. Müller, Forced vortex interaction and annihilation in an active medium, *Nature* (London) **356** (1992), 45-46.

[Sch03] B. Schmidt, P. De Kepper and S. C. Müller, Destabilization of Turing structures by electric fields, *Phys. Rev. Lett.* **90** (2003), 118302.

[Sei01] M. Seipel, M. Zierhut and A. F. Münster, Complex behaviour of spiral waves induced by an alternating electric field, *Chem. Phys. Chem.* **2** (2001), 613-616.

[Šev83] H. Ševčíková and M. Marek, Chemical waves in electric field, *Physica D* **9** (1983), 140-156.

[Šev84] H. Ševčíková and M. Marek, Concentration pulses and fronts in electric fields, *J. Phys. Chem.* **88** (1984), 2181-2183.

[Šev92] H. Ševčíková, M. Marek and S.C. Müller, The reversal and splitting of waves in an excitable medium caused by an electrical field, *Science* **257** (1992), 951-954.

[Šev96a] H. Ševčíková, I. Schreiber and M. Marek, Dynamics of oxidation Belousov-Zhabotinsky waves in an electric field, *J. Phys. Chem.* **100** (1996), 19153-19164.

[Šev96b] H. Ševčíková, J. Kosek and M. Marek, Splitting of 2D waves of excitation in a direct current electric field, *J. Phys. Chem.* **100** (1996), 1666-1675.

[Šev99] H. Ševčíková and S. C. Müller, Electric-field-induced front deformation of Belousov- Zhabotinsky waves, *Phys. Rev. E* **60** (1999), 532-538.

[Sha85] B. Z. Shakhashiri**,** *Chemical Demonstration: A Handbook for Teachers of Chemistry Vol. 2*, The University of Wisconsin Press, 1985, pp. 289-293.

[Sho87] K. Showalter and J. J. Tyson, Luther's 1906 discovery and analysis of chemical waves, *J. Chem. Educ.* **64** (1987), 742-744.

[Šni98] D. Šnita, H. Ševčíková, J. Lindner, M. Marek and J. H. Merkin, Capillary electrophoresis with chemical reactions: The effect of ionic strength, *J. Chem. Soc. Faraday Trans.* **94** (1998), 213-222.

[Sri98a] V. Sridevi and R. Ramaswamy, Propagating waves and pattern formation in a reaction-diffusion system with pyrogallol as substrate, *Chem. Lett.* (the Chem. Soc. of Japan) **5** (May 1998), 459-460.

[Sri98b] V. Sridevi and R. Ramaswamy, Potential response in the uncatalyzed bromate oscillatory system, *React. Kinet. Catal. Lett.* **65** (1998), 93-100.

[Ste92] O. Steinbock, J. Schütze and S.C. Müller, Electric-field-induced drift and deformation of spiral waves in an excitable medium, *Phys. Rev. Lett.* **68** (1992), 248-251.

[Stö95] R. Stössel and A. F. Münster, Periodic and irregular wave patterns in an open tubular gel reactor, *Chem. Phys. Lett.* **239** (1995), 354-360.

[Tab94] J. J. Taboada, A. P. Muńuzuri, V. Pérez-Muńuzuri, M. Gómez-Gesteira and V. Pérez-Villar, Spiral breakup induced by an electric current in a Belousov-Zhabotinsky medium, *Chaos* **4** (1994), 519-524.

[Til74] J. Tilden, On the velocity of spatial wave propagation in the Belousov reaction, *J. Chem. Phys.* **60** (1974), 3349-3350.

[Tla83] T. Tlaczala and A. Bartecki, Double oscillations in the system: Gallic acid-$KBrO_3$-$MnSO_4$ –H_2SO_4, *Z. Phys. Chem.* (Leipzig) **264** (1983), 507-512.

[Tla84] T. Tlaczala and A. Bartecki, Effect of catalyst ion on the course of oscillation reactions in the system: Pyrogallol-$KBrO_3$-H_2SO_4, *Z. Phys. Chem.* (Leipzig) **265** (1984), 96-100.

[Tót94] Á. Tóth, V. Gáspár and K. Showalter, Signal transmission in chemical systems: Propagation of chemical waves through capillary tubes, *J. Phys. Chem.* **98** (1994), 522-531.

[Tur52] A. M. Turing, The chemical basis of morphogenesis, *Philos. Trans. R. Soc. London B* **237** (1952), 37-72.

[Tys88] J. J. Tyson and J. P. Keener, Singular perturbation theory of traveling waves in excitable media (a Review), *Physica D* **32** (1988), 327-361.

[Ung97] J. Ungvarai, Z. Nagy-Ungvarai, J. Enderlein and S. C. Müller, Effective rate constant of ferriin reduction in the Belousov-Zhabotinsky reaction, *J. Chem. Soc. Faraday Trans.* **93** (1997), 69-71.

[Var85] M. Varga and E. Körös, Various dynamic behavior of Ag^+-induced oscillations in uncatalyzed bromate oscillators, *React. Kinet. Catal. Lett.* **28** (1985), 259-268.

[Vid86] C. Vidal and P. Hanusse, Non-equilibrium behaviour in isothermal liquid chemical system, *Int. Rev. Phys. Chem.* **5** (1986), 1-55.

[Vié96] E. R. Viéitez, J. Mosquera, C. Souto, A.P. Muńuzuri, M. Gómez-Gesteira, V. Pérez-Muńuzuri, V.A.Davydov and V. Pérez-Villar, Electric field influence on a reaction-diffusion system: Determination of ionic mobilities, in *Proceedings of the Workshop*: *Complex Systems in Natural and Economic Sciences* (K. Martinás and M. Moreau (Eds.)), ELFT, Budapest, 1996, pp. 57-69.

[Wal00] J.Walleczek (Ed.), *Self-Organized Biological Dynamics & Nonlinear Control*, Cambridge University Press, Cambridge, 2000.

[Was03] R. Waser (Ed.), *Nanoelectronics and Information Technology: Advanced Electronic Materials and Novel Devices*, Wiley-VCH, Weinheim, 2003.

[Win74] A. T. Winfree, Two kinds of wave in an oscillating chemical solution, *Faraday Symp. Chem. Soc.* **9** (1974), 38-46.

[Win84] A. T. Winfree, Wavefront geometry in excitable media, *Physica D* **12** (1984), 321-332.

[Woo85] P. M. Wood and J. Ross, A quantitative study of chemical waves in the Belousov-Zhabotinsky reaction, *J. Chem. Phys.* **82** (1985), 1924-1936.

[Wu95] Y. Wu, D. A. Vasquez, B. F. Edwards and J. W. Wilder, Convective chemical-wave propagation in the Belousov-Zhabotinsky reaction, *Phys. Rev. E* **51** (1995), 1119-1127.

[Yos04] M. Yoshimoto, H. Shirahama, S. Kurosawa and M. Naito, Periodic change of viscosity and density in an oscillating chemical reaction, *J. Chem. Phys.* **120** (2004), 7067-7070.

[Zha93a] A. M. Zhabotinsky, M. D. Eager and I. R. Epstein, Refraction and reflection of chemical waves, *Phys. Rev. Lett.* **71** (1993), 1526-1529.

[Zha93b] A. M. Zhabotinsky, F. Buchholtz, A.B. Kiyatkin and I. R. Epstein, Oscillations and waves in metal-ion-catalyzed bromate oscillating reactions in highly oxidized state, *J. Phys. Chem.* **97** (1993), 7578-7584.

[Zyk87] V. S. Zykov, *Simulation of Wave Processes in Excitable Media*, Manchester University Press, New York, 1987.
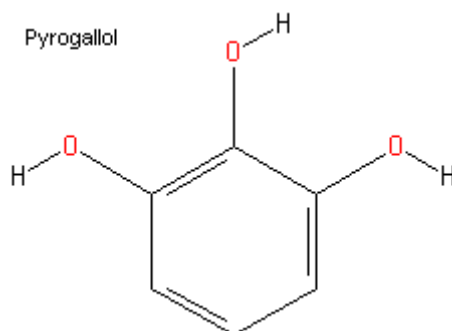
<u>APPENDIX A</u> : Some Properties of Pyrogallol and Ferroin

Pyrogallol (Pyrogallic Acid, PG) [1]

IUPAC Chemical Name: 1,2,3-trihydroxybenzene

**Molecular Formula:** $C_6H_6O_3$

Structural Formula:

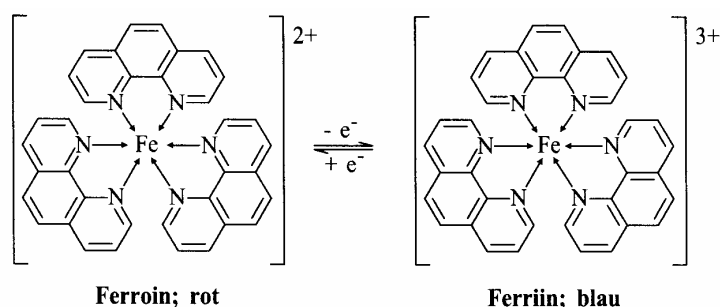

Molecular Weight: 126.11 g/mole

Properties: White, odorless crystals, melting point 131-133 ^{o}C, boiling point 309 ^{o}C. Becomes grayish on exposure to air and light. Poisonous. Density 1.45 g/ml at 20 ^{o}C. Sublimes when slowly heated. Solubility in water: 0.4 g/ml (20 ^{o}C) [2], 0.6 g/ml (25 ^{o}C). Strong reducing agent. The aqueous solution darkens or is oxidized on exposure to air, quite rapidly when alkaline[*] [10]. Pyrogallol has 3 acidic protons [3,4] at 3 hydroxyl groups with dissociation constants k_a, Pk_a = -log(k_a), in aqueous solution at 25 ^{o}C : $C_6H_3(OH)_3 \leftrightarrow C_6H_3(OH)_2O^- + H^+$, Pk_{a1} = 8.94; $C_6H_3(OH)_2O^- \leftrightarrow C_6H_3(OH)O_2^{2-} + H^+$, Pk_{a2} = 11.08; $C_6H_3(OH)O_2^{2-} \leftrightarrow C_6H_3O_3^{3-} + H^+$, Pk_{a3} = 14 (less reliable). λ_{max} = 240 nm (molar absorptivity (ε_{max}) = 907.52 $M^{-1}cm^{-1}$ (0.638 mM in ethanol or methanol)) [5]. Diffusion coefficient D_{PG} at infinite dilution in water [6] follows this relation: log $[D_{PG} (cm²/s)]$ = -1.5655 – (1,068.441/T), where T is the absolute temperature in K. D_{PG}(25 ^{o}C) = 0.709 x 10^{-5} cm^2/s, D_{PG}(15 ^{o}C) = 0.533 x 10^{-5} cm^2/s. P^H of 5% solution or 0.4 M in water = 4-5 at 20 ^{o}C [2].

Note [3,4] **:** Phenol $C_6H_5(OH)$, Pk_a = 9.89; Catechol (1,2-dihydroxybenzene, $C_6H_4(OH)_2$), Pk_{a1} = 9.40, Pk_{a2} = 12.8; MA, Pk_{a1} = 2.847, Pk_{a2} = 5.696.
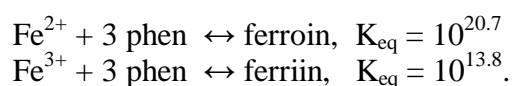
[*]It has been found that the solution of PG in distilled water becomes darkened (yellow-brown) faster than in aqueous sulphuric acid when let the solution stayed overnight.

Ferroin [7]

IUPAC Chemical Name: tris(1,10-phenanthroline)iron(II) ion

Molecular Formula: $[C_{36}H_{24}FeN_6]^{2+}$ (or $Fe(phen)_3^{2+}$)

Structural Formula:
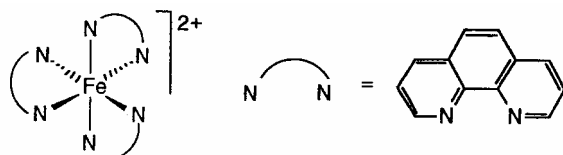
Molecular Weight: 596.4 g/mole

Properties: Red coloured aqueous solution. This complex is difficult to be extracted by using organic solvents. The standard reduction potentials [4,7,8] for $FeL_3^{3+} + e^- \leftrightarrow FeL_3^{2+}$, where L is 1,10-phenanthroline (ortho-phenanthroline) in 1.0 M H_2SO_4 solution and in aqueous solution at 25 °C, are reported to be 1.06 V and 1.18 V, respectively.

Ferroin; rot   Ferriin; blau

The equilibrium constant K_{eq} at 25 °C in aqueous solution [8]:

$Fe^{2+} + 3$ phen $\leftrightarrow$ ferroin, $K_{eq} = 10^{20.7}$
$Fe^{3+} + 3$ phen $\leftrightarrow$ ferriin, $K_{eq} = 10^{13.8}$.

Diffusion coefficients at infinite dilution in water at 25 °C [Šev96a, Šev96b]:

Ferroin: 0.718 x 10^{-5} cm^2/s; Ferriin: 0.603 x 10^{-5} cm^2/s.

Corresponding ionic mobility from the Nernst-Einstein relation (see Eq. 7 in Section 2.2):

Ferroin: 5.589 x 10^{-4} cm^2/Vs; Ferriin: 7.041 x 10^{-4} cm^2/Vs.

Ferroin: $\lambda_{max} = 510$ nm in water, molar absorptivity $\varepsilon_{max} = 11,100$ cm^2/mol [9].

Ferriin: $\lambda_{max} = 602$ nm in concentrated sulphuric acid, $\varepsilon_{max} = 870$ cm^2/mol [9].

References

[1] S. Budavari (Eds.), The Merck Index 12th Edition, Merck & Co. Inc., New York ,1996, pp. 1375-1376.

[2] E. Merck Chemical Catalogue, 2003.

[3] E. P. Sergeant and B. Dempsey, Ionization Constants of Organic Acids in Aqueous Solution, Pergamon Press, Oxford, 1979.

[4] D. C. Harris, Exploring Chemical Analysis, W.H. Freeman and Company, New York, 2001, pp. 546-557.

[5] L. Láng (Ed.), Absorption Spectra in the Ultraviolet and Visibile Region Vol. X, Akadémiai Kiadó, Budapest, 1968, pp. 1706-1707.

[6] C. L. Yaws, Handbook of Transport Property Data: Viscosity, Thermal Conductivity, and Diffusion Coefficients of Liquids and Gases, Gulf Publishing Company, Texas, 1995, pp. 141-143, p.153.

[7] J. E. Macintyre (Eds.), Dictionary of Inorganic Compounds Vol. 2, Chapman & Hall, London, 1992, pp. 2250-2251.

[8] G. H. Aylward and T. J. V. Findlay, SI Chemical Data, John Wiley & Sons, Milton, 5th ed., 2002, p. 134.

[9] M. H. Ford-Smith and N. Sutin, The kinetics of the reactions of substituted 1,10-phenanthroline, 2,2-dipyridine and 2,2,2-tripyridine complexes of iron(III) with iron(II) ions, J. Am. Chem. Soc. **83** (1961), 1830-1834.

[10] H. I. Abrash, D. Shih, W. Elias and F. Malekmehr, A kinetic study of the air oxidation of pyrogallol and purpurogallin, Int. J. Chem. Kinet. **21** (1989), 465-476.

APPENDIX 1B :

UV-VIS (200-700 nm) Absorption Spectra and Temporal Oscillation Profiles

Spectra shown are given for the solution mixture I (reference). Absorbance (Abs) is shown in Arbitrary Units (AU). 0.15 M H_2SO_4 is blank.

0.15 M H_2SO_4, 8 mM PG

$$\lambda_{max} = 280 \text{ nm, Abs}_{max.} = 0.67954 = \varepsilon_{max}bc$$
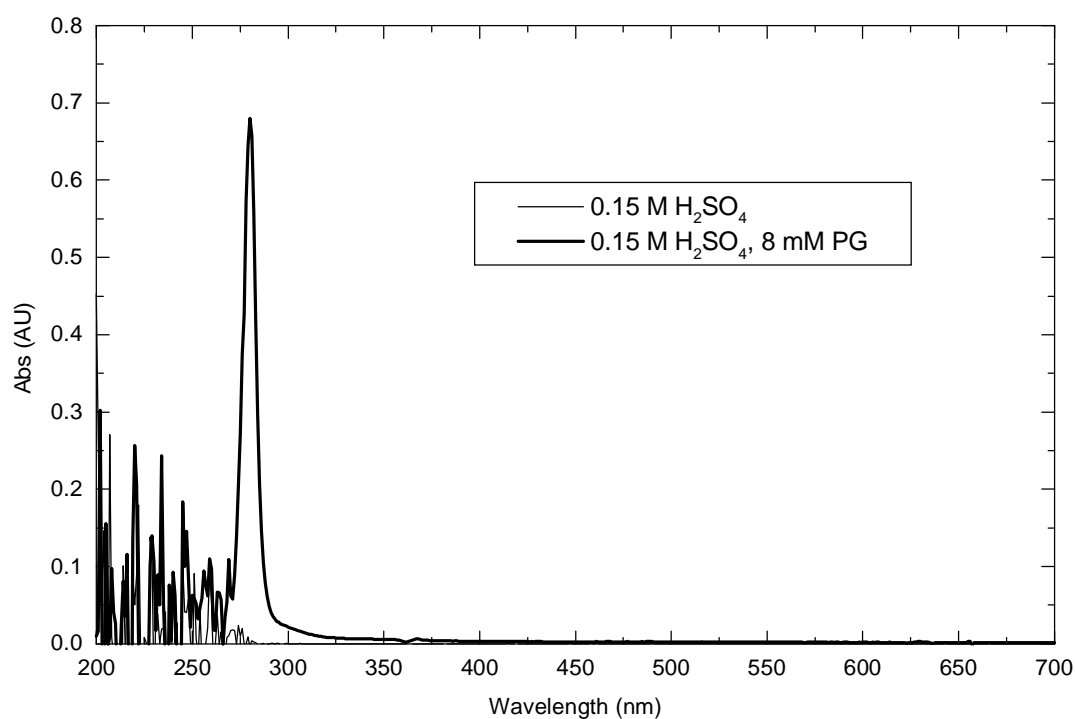
$$\varepsilon_{max} = 0.67954/(1\text{cm x } 0.008 \text{ M}) = 84.94 \text{ M}^{-1}\text{cm}^{-1}$$
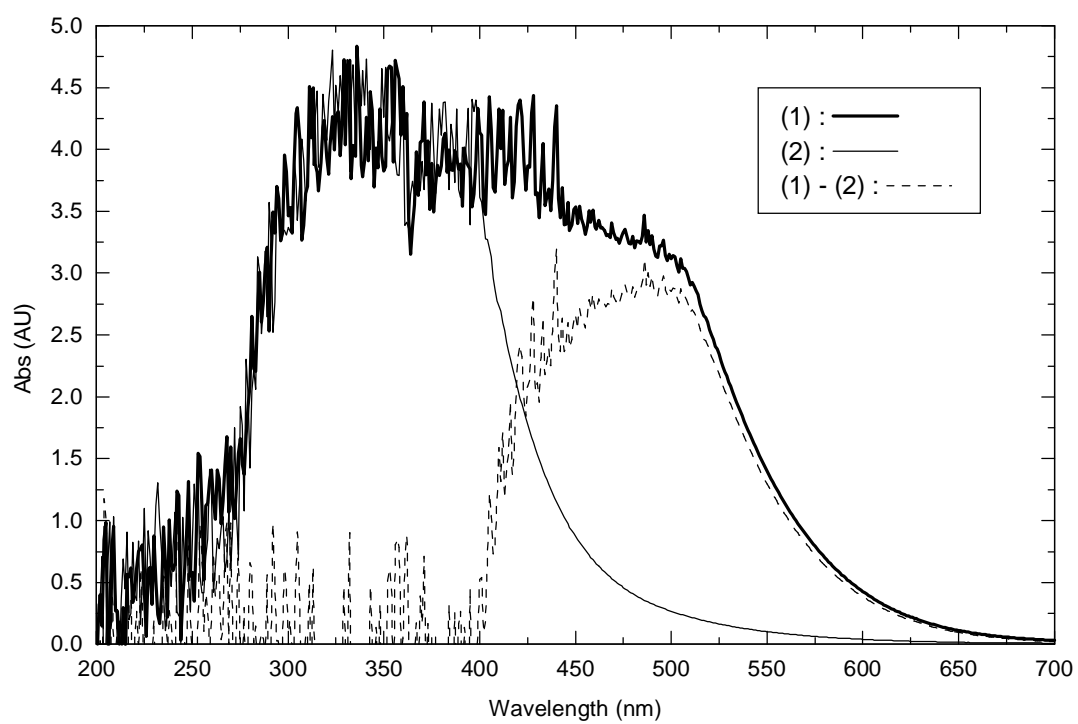
0.15 M H$_2$SO$_4$, 0.10 M NaBrO$_3$, 8 mM PG

(1) : Dark red-brown state.

(2) : Clear pale yellow state.
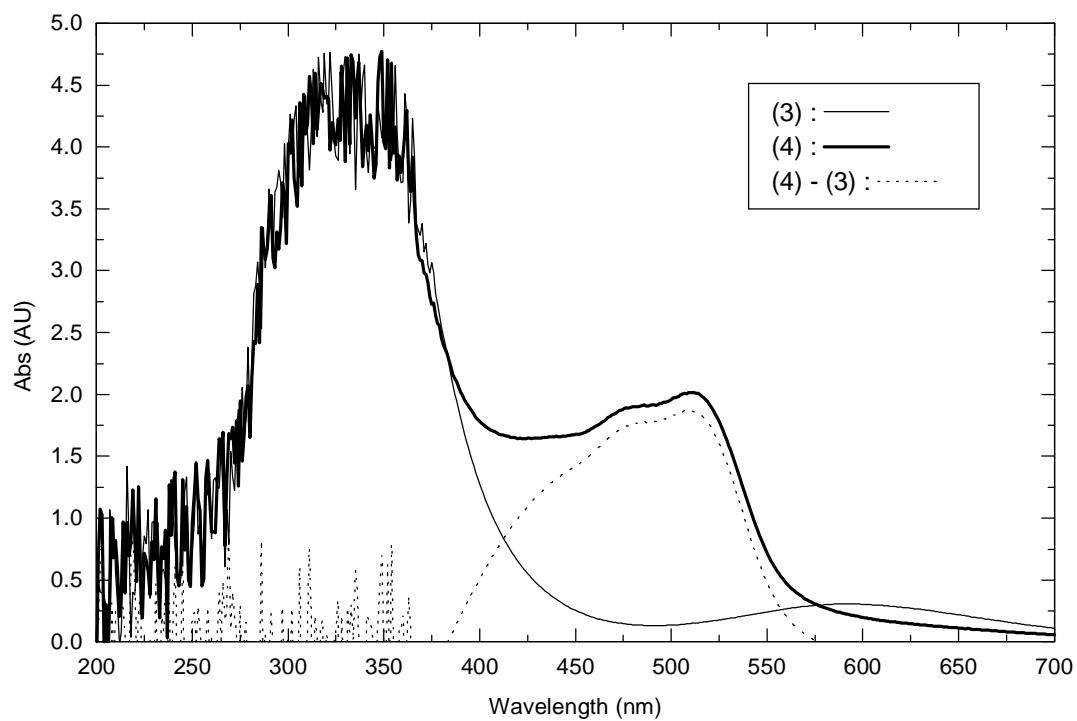
(1) – (2) : Absorbance difference.

0.15 M H$_2$SO$_4$, 0.10 M NaBrO$_3$, 8 mM PG, 0.5 mM ferroin

(3) : Clear blue-green oxidized state. The absorption peak of ferriin is maximum at around 600 nm.

(4) : Clear red-orange reduced state changed from clear red-brown reduced state at the beginning. The absorption peak of ferroin is maximum at around 510 nm.

(4) – (3) : Absorbance difference.

The reference solution mixture used in the capillary experiments does not show temporal oscillations, i.e it is excitable. We detected spectrophotometrically (A) [Q]/[PG] at the violet light 420 nm [Sri98b], (B) [ferroin] at the green light 490 nm, and (C) [ferriin] at the orange light 600 nm in a 2.5 ml well-stirred batch system (using PMMA cuvette, 1.25 cm light path length) at 15.1 $\pm$ 0.1 $^{\circ}$C without open surface to the air. Typical temporal oscillatory profiles (in time, t (s)) of the modified solution mixture with the same value of [PG]/[ferroin] = 16 consisting of 1.0 M H$_2$SO$_4$, 0.10 M NaBrO$_3$, 28 mM PG, and 1.75 mM ferroin are given below. The average induction time and the first three oscillatory periods obtained from 2 experiments are 14.12 $\pm$ 0.64 min and 3.68 $\pm$ 0.08 min, respectively.
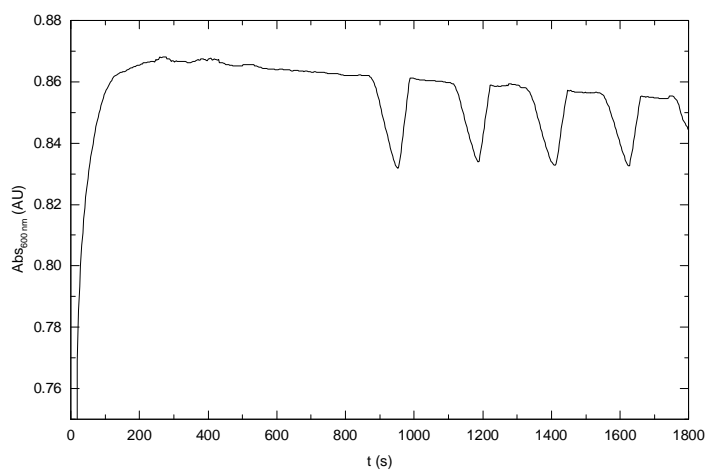
(A)
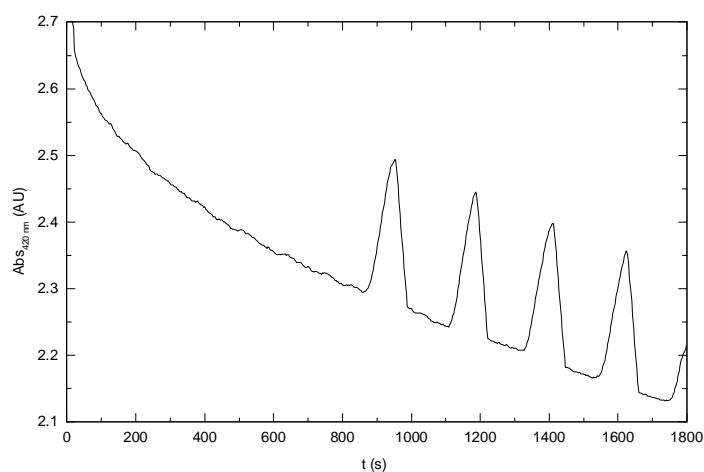
(B)
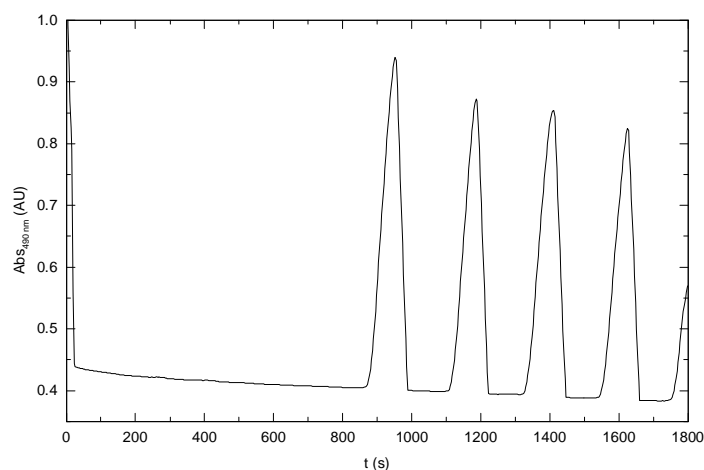
(C)

We can see from these profiles that 1) ferriin concentration profiles in space (cf. Fig. 24b) and time (the profile (C)) are approximately the same shape characterized by the broad band of excited region and 2) the dynamic of ferroin and Q are the same during the recovery period (see profiles (A) and (B)), supporting the chemical mechanism in Section 2.4.2. In addition, [Q]/[PG] oscillates and decreases continuously in time, corresponding to the aging and the consumption of reactant in the solution mixture, as seen in the base line of the profile (A), see also Fig. 17b.

APPENDIX 2B : **Determination of the Electrical Conductivity**
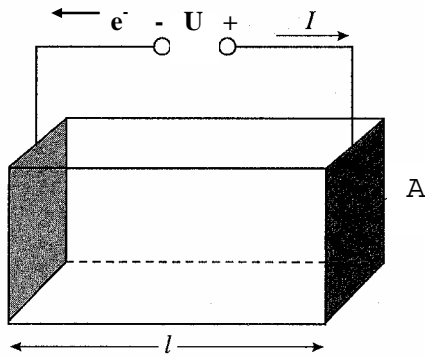
Electrical conductivity of a material [Ham98, Kuh00, Old94] measures the ability of a material to carry an electrical current or electrons, when placed between terminals having a difference of electrical potential U in a steady direct-current electric field $E = U/l$ (in V/cm). The amount of current flow I (in A) depends on both the electrical potential U (in V) and the resistance R (in Ω) by Ohm's law,

$$I = U / R .$$ (i)

The resistance of a sample of isotropic (i.e. direction independent) conducting material is dependent on both the geometry and the intrinsic resistivity of the material to conduction of current. For a conductor of resistivity ρ, the resistance will increase as the length l (or d), of the current path increases, and the resistance will fall as the cross sectional area, A, of the conductor increases, i.e.

$$R = \rho(l) / A .$$ (ii)

Alternatively, the reciprocal of resistivity is a measure of the ease with which current flows in a conducting medium; it is quantitated as conductivity κ (in $\Omega^{-1}cm^{-1}$ or S/cm),

$$\kappa = 1 / \rho = (l) / RA = I(l) / UA = I / EA = \sigma / E .$$ (iii)

σ is the current density or charge transported per unit cross section area of the conductor (in A/cm^2). The existence of a finite resistance means that the energy delivered but the electric field to the current carriers (electrons) is dissipated, being converted to heat (mostly energy from particle vibrations). The rate of dissipation per volume is given by and is called Ohmic heating H_O,

$$H_O = \kappa E^2 = \sigma E .$$ (iv)

In our case, the conductor is the BZ aqueous solution containing mixed electrolytes: 0.15 M H_2SO_4, 0.10 M, $NaBrO_3$, 8 mM PG, and 0.5 mM $Fe(phen)_3SO_4$ in the capillary reactor (l = 16.0 cm, A = 0.05 x 0.05 cm^2, total volume = 0.04 cm^3) bath thermostated at 15 ^{o}C. The solution's density at 15.00 ^{o}C is about 1.02 g/ml. Calculated parameter values from Eqs. iii and iv and the current-voltage plot of the solution mixture are given below. The average electrical conductivity κ of the solution mixture is 0.1144 ± 0.0023 S/cm (κ/F = 1.1855 $\mu mol.cm^{-1}s^{-1} V^{-1}$, see Eq. 16). The linear regression of the current-voltage plot gives I (mA) = -0.01389 + 0.01818 [U (V)] with the correlation coefficient R = 0.9995. Ohm's law yields R = 55 kΩ from the slope.

U (V)	E (V/cm)	I (mA)	σ (mA/cm^2)	κ (S/cm)	H_O (W/cm^3)
10	0.62	0.18	72	0.1152	0.045
15	0.94	0.26	104	0.1109	0.098
20	1.25	0.36	144	0.1152	0.18
25	1.56	0.45	180	0.1152	0.281
30	1.88	0.53	212	0.1131	0.398
40	2.5	0.69	276	0.1104	0.69
50	3.12	0.88	352	0.1126	1.1
60	3.75	1.1	440	0.1173	1.65
65	4.06	1.18	472	0.1162	1.918
70	4.38	1.23	492	0.1125	2.152
80	5	1.45	580	0.116	2.9
90	5.62	1.6	640	0.1138	3.6
100	6.25	1.77	708	0.1133	4.425
120	7.5	2.22	888	0.1184	6.66
150	9.38	2.71	1,084	0.1156	10.162
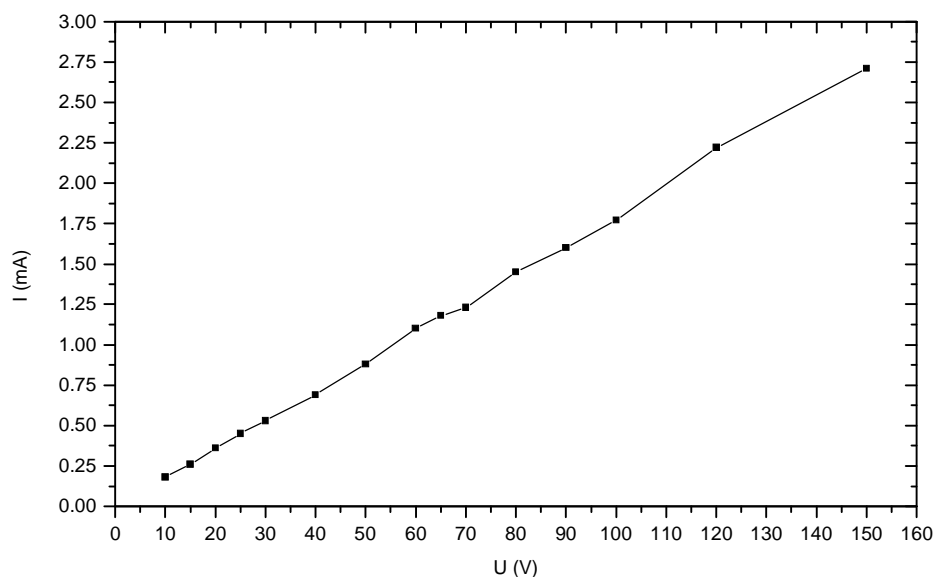
APPENDIX C :

Data Evaluation Procedures from Image Analysis with IDL

IDL Version 5.2 (Win32 x86). Research Systems, Inc.

To contact Research Systems:

Email: info@rsinc.com Web site: http://www.rsinc.com/

To run an overview of IDL's capabilities. To search and run (demo) over 3000 pages of IDL documentation insight.

1) Time-Space Plot

```
;========================================================================
=
;=====
;===== Programm zur Erstellung eines Timespace-Plots
;=====
;========================================================================
=

FUNCTION read_all_lines,unit

      ; Muss man leider so machen in IDL.
      scenes = [""]
      WHILE ( NOT EOF(unit) ) DO BEGIN
            ; Siehe oben, Sonst wird die Zeile zu einer Zahl konvertiert.
         scene = ""
      READF,unit,scene,FORMAT="(A)"
            ; Haenge Zeile an bisherige Zeilen an.
            scenes = [scenes,scene]
      ENDWHILE
      ; Die Kruecke von oben wieder beseitigen.
      nroflines = size(scenes)
      nroflines = nroflines(1)-1
      IF (nroflines GE 1) THEN BEGIN
          scenes = scenes(1:nroflines)
          ; Gelesene Zeilen zurueck an Absender.
          RETURN,scenes
      ENDIF ELSE BEGIN
          RETURN,[""]
      ENDELSE
END

PRO timespace_methasit

dir = 'd:\temp\1.2cm_90V\'    ;directory of the images
timespacenumber = 'tsp'       ;index for the timespaceplot
;framenumber     = 1000        ;number of frames for the timespaceplot

outdir  = strcompress(dir+'_'+timespacenumber+'.tif')

file_in = Pickfile(/READ,FILTER='*.tif', PATH=dir)

bild = READ_TIFF(file_in)

dim    = size(bild, /DIMENSIONS)
```

```
width  = dim[0]
height = dim[1]

CD,dir,CURRENT=old_dir

    ;;;;;;;;;;;;;;;;;;;;;;;;;;;;;;;;;;;;;;;;;;;;;;
    ;; Create list of all TIFF-Movies
    ;;;;;;;;;;;;;;;;;;;;;;;;;;;;;;;;;;;;;;;;;;;;;;
    temppfad = filepath("",/TMP)
    SPAWN,"dir /B /L /ON *.tif > "        +temppfad+"filelist.txt"
    OPENR,unit,temppfad+"filelist.txt",/GET_LUN
    scenes = read_all_lines(unit)
    ; Tifffilenames should be loaded here.
    s=size(scenes)
    CLOSE,unit
    ;SPAWN,"del "+temppfad+"filelist.txt"

    CD,old_dir

framenumber = s[1]
name        = strmid(file_in,strlen(dir),(strlen(file_in)-strlen(dir)-4))
timespace   = FLTARR(width,framenumber)

bild = READ_TIFF(file_in)

WINDOW, 0, XSIZE=width, YSIZE=height, TITLE=name

TVSCL, bild
XYOUTS,10 ,10,'Please select the y-value for the timespace
plot',COLOR=[255,0,0],/DEVICE
CURSOR,x0,ycut,3, /device  ;--- Einlesen der Koordinate
bild(0:width-1,ycut)=0*bild(0:width-1,ycut)
TVSCL, bild

window,1, XPOS = 500, YPOS = 300, xsize=width, ysize = framenumber,
TITLE='timespace plot'

FOR n = 0, framenumber-1 DO BEGIN
   temp1 = STRCOMPRESS(dir+'\'+STRING(scenes(n)),/REMOVE_ALL)
   bild1 = READ_TIFF(temp1)
   bild2 = sobel(bild1)
   timespace(0:width-1,n)=bild1(0:width-1,ycut)-bild2(0:width-1,ycut)
   bild(0:width-1,ycut)=0*bild(0:width-1,ycut)
   frame_num = STRCOMPRESS(STRING(n),/REMOVE_ALL)
   IF (((n+1) MOD 10) EQ 0) THEN BEGIN
   wset,0
   wshow,0
      TVSCL, bild1-sobel(bild1)
      print, n
      XYOUTS,10 ,10,frame_num,COLOR=[255,0,0],/DEVICE
      wset,1
      wshow,1
      tvscl, timespace
   ENDIF
   wset,0
  WSHOW, 1
ENDFOR

wset,1
tvscl, timespace

xshift = 0
yshift = 2
```
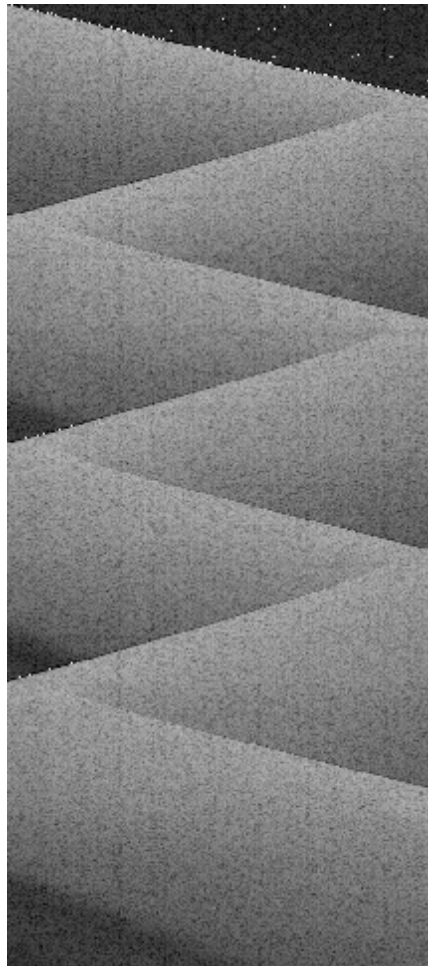
```
timespace1 = timespace-SHIFT(timespace,xshift,yshift)
timespace1 = SMOOTH(timespace1,3)

window,2, XPOS = 500, YPOS = 300+framenumber+30, xsize=width, ysize =
framenumber, TITLE='timespace plot'
tvscl, timespace1
wshow,0
wshow,1
wshow,2
write_tiff, outdir, timespace

END
```

RESULT: 1.2cm_90V_tsp.tif

444 pixels x 1,000 pixels = 1.2 cm x (999 x 5 s) = 1.2 cm x 4,995 s

plotted from 1,000 images: imgs0000.tif -imgs0999.tif obtained from the LabVIEW Image Acquisition

software with a time delay between two images = 5 s.

2) Determination of Propagation Velocity and Profile Plots

IDL commands step by step.

IDL Version 5.2 (Win32 x86). Research Systems, Inc.
For basic information, enter "IDLInfo" at the IDL> prompt.

IDL> a = read_tiff("d:\temp\1.2cm_90V_tsp.tif")
% Loaded DLM: TIFF
IDL> b = median(a,5) [This command is used for smoothing , i.e. noise can be removed from the picture by applying a median filter of 5 x 5 pixels]
IDL> shade_surf, b, shade = bytscl(b), ax = 90, az = 0, background = 255, color = 0, xstyle = 1, ystyle = 1, xticklen = -0.02, yticklen = -0.02, xtitle = 'Space (pixel)', ytitle = 'Time (pixel)', yminor = 10
IDL> !order = 1
IDL> c = tvrd(0)
IDL> tvscl, c
IDL> write_tiff, '1.tif', c

RESULT: 1.tif
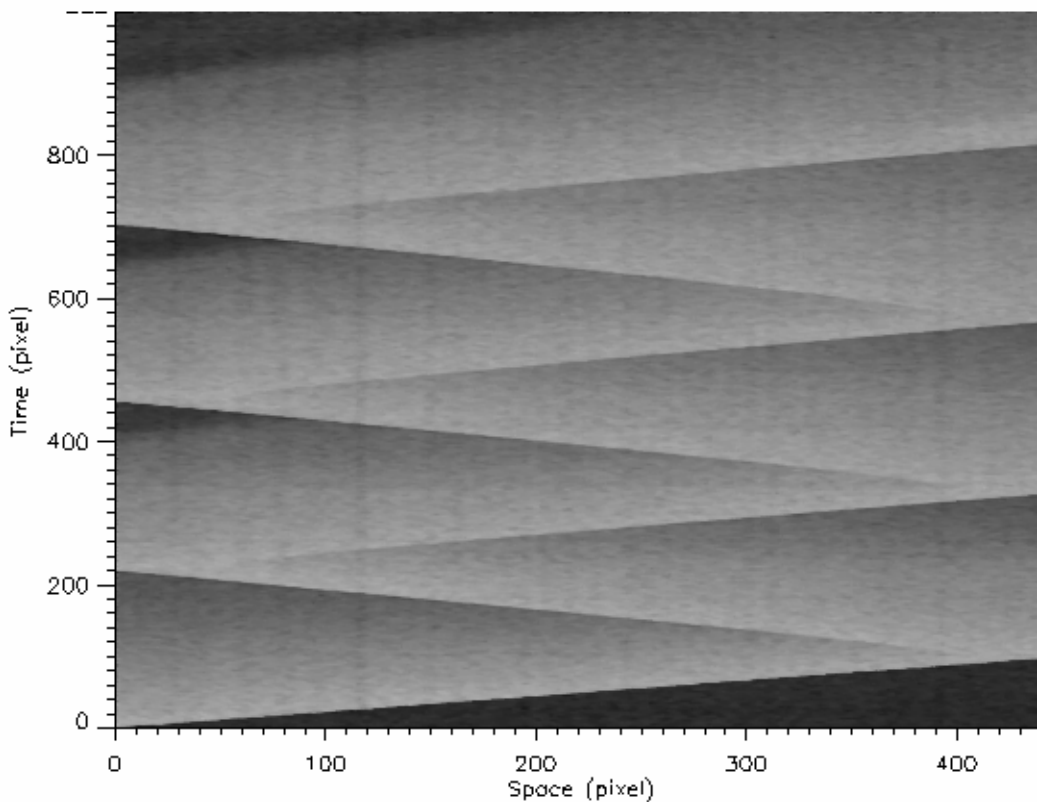
We already know a spatial resolution of 370 pixels/cm and a resolution in time: 1,000 pixels/4,995 s = 0.2 pixels/s. We can approximately evaluate the propagation velocities (Space/Time = $\Delta x/\Delta t$) by linearization with a ruler and calculating the slopes from seven lines in the time-space plot showing 3 wave fronts moving to the left and 4 wave fronts moving to the right, this results in

a) three left lines for three reversed waves: 1st = 1.21 mm/min, 3rd = 5th = 1.18 mm/min.

b) four right lines for an original wave: 1.53 mm/min and three reversed waves: 2nd = 4th = 6th = 1.33 mm/min. Note that 1 cm/s = 600 mm/min = 10,000 μm/s.
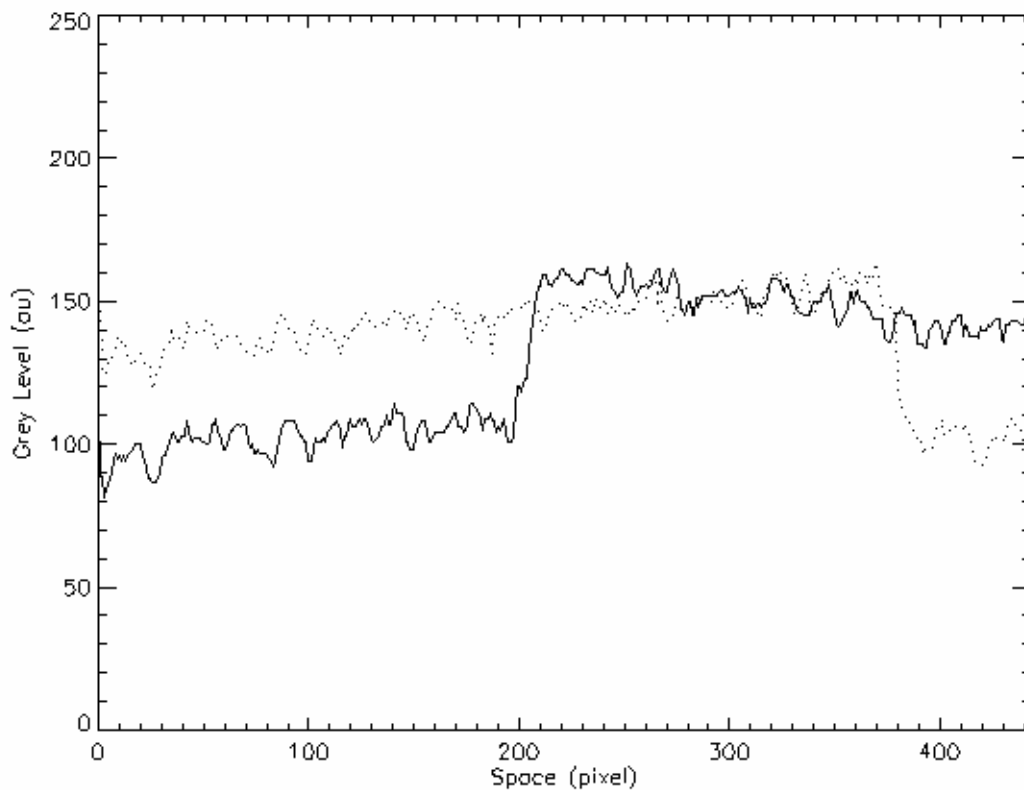
DL> plot, b(*,400), xstyle = 1, xtitle = 'Space (pixel)', ytitle = 'Grey Level (au)', yrange = [0,250]
IDL> oplot, b(*,800), linestyle = 1
IDL> !order = 1
IDL> d = tvrd(0)
IDL> tvscl, d
IDL> write_tiff, '2.tif', d
Changing black colored background image to white colored background image by using a program: IrfanView32 (free download from http://www.irfanview.com/). In the program, open this file 2.tif, choose image and then negative, and save it again.

RESULT: 2.tif

Spatial profiles: Solid profile is taken at 400th pixel or 2,000 s and dotted profile is taken at 800th pixel or 4,000 s.

IDL> plot, b(37,*), xstyle = 1, xtitle = 'Time (pixel)', ytitle = 'Grey Level (au)', yrange = [0,250]
IDL> oplot, b(407,*), linestyle = 1
IDL> !order = 1
IDL> e= tvrd(0)
IDL> tvscl, e
IDL> write_tiff, '3.tif', e
Changing black colored background image to white colored background image by using a program: IrfanView32 (free download from http://www.irfanview.com/). In the program, open this file 3.tif, choose image and then negative, and save it again.

RESULT: 3.tif
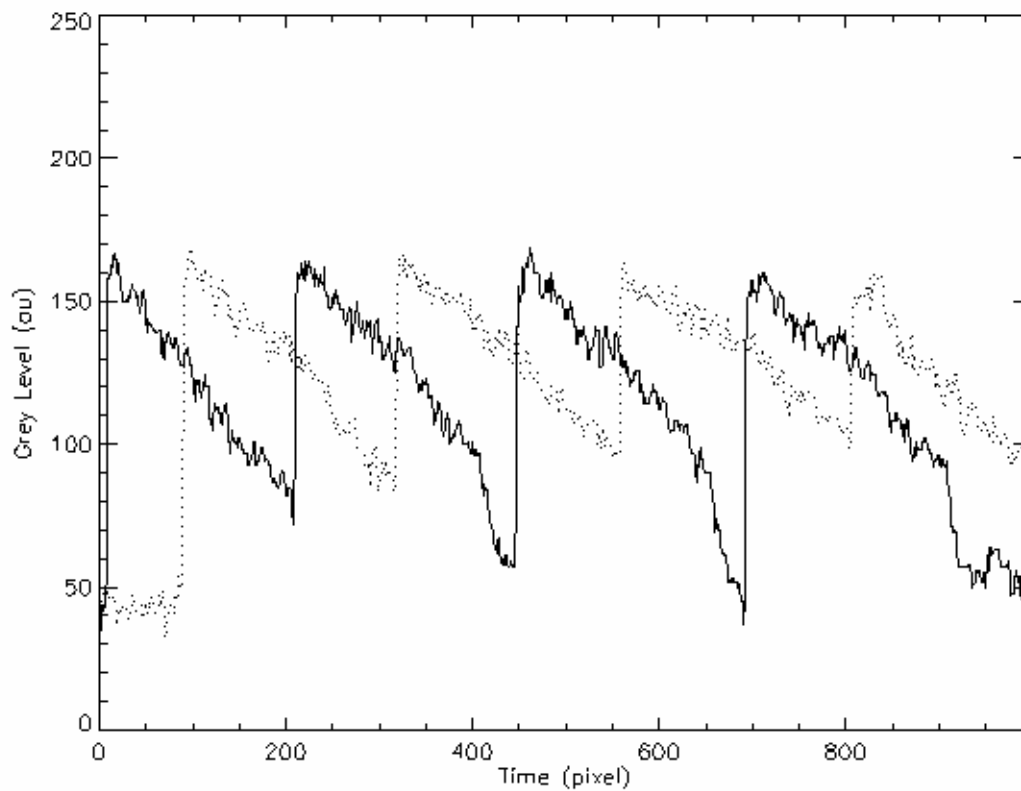
Temporal profiles: Solid profile is taken at 37th pixel or 0.1 cm and dotted profile is taken at 407th pixel or 1.1 cm.

Acknowledgements

This thesis is submitted to the Faculty of Science in partial fulfillment of the requirements for the degree of Doctor rerum naturalium (Dr.rer.nat.) in Physics at Otto-von-Guericke-University of Magdeburg. The research works were carried out at the Department of Biophysics, Institute of Experimental Physics from March 2000 to September 2004.

First, I would like to express my heartfelt thanks to my advisor Dr. Ing. Hana Ševčíková (Center for Nonlinear Dynamics of Chemical and Biological Systems, Prague Institute of Chemical Technology, Czech Republic) for her effective guidances, instructions, constructive ideas, and valuable discussions in this work. I am especially grateful to my supervisor Prof. Dr. rer. nat. habil. Stefan C. Müller who gives me an unique opportunity to live and study in Germany, for his very kind helps for financial supports and insightful comments and recommendations during my stay in Magdeburg. I would like to thank Dr. Vladimir S. Zykov (a former Biophysics group member), Prof. Dr. Miklós Orbán and Prof. Dr. Endré Körös (Department of Inorganic and Analytical Chemistry, Eötvös-Loránd University, Budapest, Hungary) for their fruitful suggestions. I also extend my special thanks to Frau Rosemarie Brandt for literature search, Herrn Gregor Nuglisch and Herrn Jürgen Weißenborn for helpful technical assistances. Many thanks to staff members of the biophysics department for their assistances in doing my research work smoothly during my stay in Magdeburg.

I gratefully acknowledge the financial support by a Stipendium nach dem Graduiertenförderungsgesetz (GradFG) für Promotion des Landes Sachsen-Anhalt (Grant No. 12760/12284) from March 2000 to August 2002. One part of this research work (multiple wave reversals) was internationally presented at the GORDON Research Conference "Oscillations and Dynamic Instabilities in Chemical Systems" (Poster session I / No. 8) at Oxford, England and also granted by the Graduiertenförderung. I also thank the REACTOR research program (Grant No. 62551C G219) of the European Science Foundation (ESF) for giving me a chance to visit the laboratory of Dr. Ševčíková at Prague from 1 to 7 December 2002.

Finally, I would like to dedicate this thesis with endless love to the memories of my parents.

Methasit Pornprompanya
Magdeburg, Federal Republic of Germany.

CURRICULUM VITAE

PERSÖNLICHE DATEN:

Name: Methasit Pornprompanya

Geburtsdatum: 4 Februar 1972

Geburtsort: Chulalongkorn Krankenhaus in Bangkok

Geburtsland: Thailand

Nationalität: thailändisch

Familienstand: ledig

Wohnort: 555/6 Phetkasem 90, Bangkae, Bangkok, Thailand 10160

E-mail: methasith4272@yahoo.com

SCHULISCHE AUSBILDUNG:

1978-1984 Sesawechvitaya Grundschule Bangkok

1984-1990 Paknamvitayakhom Gymnasium Bangkok

STUDIUM:

04.06.1990-05.03.1994

Studium der Chemie an der Universität Kasetsart in Bangkok

Apr. 1993

Praktikum im Bundesministerium für Forschung und Technik in Bangkok

01.06.1994-22.04.1997

Magisterarbeit an der Universität Mahidol in Bangkok im Fach Physikalische Chemie mit dem Titel: *A Study of Complex Chemical Oscillations in the Pseudo- closed System of Belousov-Zhabotinsky Reaction*

1997-2000

Dozent an der Universität Thammasat

WEHRDIENST:

1987-1990

Gesetzliche Zivildienst der Städte Bangkok und Kanchanaburi

Feb. 1996

Abschluss Ableistung des Militärdienstes in Lopburi

PROMOTION:

seit Mär. 2000
Promotionsstudium in der Arbeitsgruppe Biophysik am Institut für
Experimentelle Physik der Otto-von-Guericke-Universität-Magdeburg
Thema der Doktorarbeit: *Durch elektrische Felder induzierte Instabilitäten von Erregungsfronten*
Betreuung durch Prof. S.C. Müller und Dr. H. Sevcikova (Prag)

PROMOTIONSSTIPENDIUM:

Mär. 2000 – Aug. 2002
GradFG-Stipendium des Landes Sachsen-Anhalt
Sep. 2002 – Dez. 2004
wissenschaftliche Hilfskraft(Hiwi)und Mitarbeiter in der Arbeitsgruppe
Biophysik am Institut für Experimentelle Physik
1-7 Dez. 2002
ESF-REACTOR-Stipendium für Forschungsaufenthalt am Prague Institute of
Chemical Technology

PRÄSENTATIONEN:

26-28 Sep. 2001
6th Herbstseminar "Strukturbildung in Chemie und Biophysik", Salzwedel
28 Jul. 2002 - 2 Aug. 2002
GORDON Research Conference "Oscillations and Dynamic Instabilities in
Chemical Systems", Queen's College, Oxford, Großbritannien